



HAL
open science

Experimental Studies of Gas-Phase Reactivity in Relation to Complex Organic Molecules in Star-Forming Regions

Ilsa R. Cooke, Ian R Sims

► **To cite this version:**

Ilsa R. Cooke, Ian R Sims. Experimental Studies of Gas-Phase Reactivity in Relation to Complex Organic Molecules in Star-Forming Regions. ACS Earth and Space Chemistry, 2019, 3 (7), pp.1109-1134. 10.1021/acsearthspacechem.9b00064 . hal-02278042

HAL Id: hal-02278042

<https://univ-rennes.hal.science/hal-02278042>

Submitted on 19 Sep 2019

HAL is a multi-disciplinary open access archive for the deposit and dissemination of scientific research documents, whether they are published or not. The documents may come from teaching and research institutions in France or abroad, or from public or private research centers.

L'archive ouverte pluridisciplinaire **HAL**, est destinée au dépôt et à la diffusion de documents scientifiques de niveau recherche, publiés ou non, émanant des établissements d'enseignement et de recherche français ou étrangers, des laboratoires publics ou privés.

Experimental studies of gas-phase reactivity in relation to complex organic molecules in star-forming regions

Ilsa R. Cooke and Ian R. Sims*

*Université de Rennes 1, CNRS, IPR (Institut de Physique de Rennes) - UMR 6251,
F-35000 Rennes, France*

E-mail: ian.sims@univ-rennes1.fr

Abstract

The field of astrochemistry concerns the formation and abundance of molecules in the interstellar medium, star-forming regions, exoplanets and solar system bodies. These astrophysical objects contain the chemical material from which new planets and solar systems are formed. Around 200 molecules have thus far been observed in the interstellar medium; almost half containing six or more atoms and considered “complex” by astronomical standards. All of these complex molecules consist of at least one carbon atom and thus the term complex organic molecules (COMs) has been coined by the astrochemical community. In order to understand the formation and destruction of these COMs under the extreme conditions of star-forming regions, three kinds of activity are involved: (1) the astronomical identification of complex molecules present in the ISM; (2) the construction of astrochemical models that attempt to explain the formation routes of the observed molecules; and (3) laboratory measurements and theoretical calculations of critical kinetic parameters that are included in the models. In the following review, we present recent laboratory efforts to produce quantitative

1
2
3 kinetic data for gas-phase reactions at low temperatures. We discuss the use of the
4 CRESU technique, a French acronym standing for *Cinétique de Réaction en Ecoule-*
5 *ment Supersonique Uniforme*, which means reaction kinetics in uniform supersonic
6 flow, to measure reactions of astrochemical importance. In particular, we highlight
7 recent and future advances in the measurement of product-specific reaction kinetics at
8 low temperatures.
9
10
11
12
13

14
15
16 Keywords: astrochemistry, chemical kinetics, laboratory astrophysics, low temperatures,
17 interstellar medium
18
19
20
21

22 Introduction

23
24

25 A little over 200 molecules have been observed in the interstellar and circumstellar medium,¹
26 among which are a large number of complex organic molecules that have been found even in
27 very cold (≤ 10 K) environments (e.g. Bacmann et al.²). The detection of complex molecules
28 in cold astrophysical environments poses a challenge to experimentalists and modellers alike.
29
30
31 Currently, two distinct mechanisms are used explain the formation of COMs: their produc-
32 tion in icy mantles condensed onto dust grains or their formation by gas-phase reactions.
33
34 While the formation of some COMs can be explained by their formation in ices, it is un-
35 known how they are delivered to the gas-phase at dust temperatures below that required for
36 their thermal desorption. Experiments are needed to provide quantitative parameters (i.e.
37 rate coefficients, cross sections) for both ice and gas-phase processes to input into theoretical
38 models in order to assess their importance at various stages of star-formation.
39
40
41
42
43
44
45

46
47 This review focuses on the role of laboratory experiments in understanding chemical
48 pathways to complex organic molecules in star-forming regions; in particular, we concentrate
49 on gas-phase reactions at low temperatures. It is organized as follows: in section 1 we present
50 the astrophysical context for this review and classes of reactions expected to take place under
51 astrophysical conditions. We then outline the role of laboratory measurements in elucidating
52
53
54
55
56
57
58
59
60

1
2
3 the chemical kinetics of complex organic molecules in astrophysical regions. In section 2,
4 we discuss laboratory methods for measuring reaction kinetics at low temperatures and
5 present some case studies for different classes of reactions. We then discuss the measurement
6 of products specific reaction kinetics and the implications of such measurements for the
7 understanding of COM formation routes. Finally, we outline future directions in the field of
8 low temperature reaction kinetics.
9
10
11
12
13
14
15
16

17 **Reactions in star-forming regions**

19 The physical conditions under which chemical reactions take place vary dramatically during
20 the sequence of star-formation. In the early stages, gas and dust from old stars collapses
21 inward under the influence of gravity to form diffuse clouds that have temperatures of 50–
22 100 K and gas densities of $10\text{--}10^2\text{ cm}^{-3}$, dominated by atomic hydrogen and other atomic
23 species at lower concentrations.³ Further gravitational collapse leads to the formation of
24 dense clouds with higher gas densities of $10^4\text{--}10^6\text{ cm}^{-3}$ and with temperatures typically 10–
25 20 K.⁴ Here, molecular hydrogen, H_2 , becomes the most abundant species in the cloud due to
26 surface-catalyzed production of H_2 from H atoms adsorbed on dust grains. The H_2 can then
27 undergo cosmic-ray ionization to produce H_2^+ , initiating a network of barrierless ion-neutral
28 reactions that can, at least in part, explain the exotic chemistry that has been observed in
29 dense clouds.⁵
30
31
32
33
34
35
36
37
38
39
40

41 Collapse of the dense cloud core leads to low-mass star formation. A central condensation
42 builds up that is so dense that radiation cannot escape, causing the collapsed area to warm
43 up, eventually reaching temperatures of 100–300 K where it is called a “hot core”. The hot
44 cores host dramatically different chemistry, in particular, high abundances of organic species
45 are observed such as alcohols, aldehydes, esters, acids and ethers commonly found on Earth.⁶
46 To conserve angular momentum, a rotating disk is produced around the protostar forming a
47 nascent protoplanetary disk. Within the disk, dust particles begin to coalesce and aggregate
48 to form the beginnings of meteoritic material and eventually young planets.
49
50
51
52
53
54
55
56
57
58
59
60

1
2
3
4
5
6
7
8
9
10
11
12
13
14
15
16
17
18
19
20
21
22
23
24
25
26
27
28
29
30
31
32
33
34
35
36
37
38
39
40
41
42
43
44
45
46
47
48
49
50
51
52
53
54
55
56
57
58
59
60

Due the wide variety of pressures, temperatures and atomic abundances, a large number of different chemical processes are expected to take place in astrophysical environments. In order to reproduce astronomical observations, networks of reactions must be built that incorporate the many individual reaction rates to solve for the time-dependent molecular abundances. The great majority of bimolecular gas-phase reactions expected to take place in these astrophysical environments can be placed in the following classes: (a) ion-neutral reactions, (b) neutral-neutral reactions (where neutral can also refer to radicals), (c) radiative association reactions, and (d) dissociative recombination reactions.

Ion-neutral reactions involve the reaction of either a positively charged cation with a neutral, $A^+ + B \longrightarrow C^+ + D$, or a negatively charged anion with a neutral, $A^- + B \longrightarrow C^- + D$. Perhaps the most famous astrochemical example is the reaction of H_3^+ with neutrals, initiating a network of ion chemistry in the ISM.⁵ Neutral-neutral reactions involve the reaction of two species that do not possess a charge, but at least one radical possessing unpaired electrons; they can be represented by the chemical equation $A + B \longrightarrow C + D$, or more accurately, $A + B^\bullet \longrightarrow C^\bullet + D$. For example, neutral-neutral reactions of CN with unsaturated hydrocarbons of the form $C_{2n}H_2$ have been shown to provide competitive formation pathways for cyanopolyynes as compared to ion-neutral reaction routes.⁷ Radiative association involves an ion-neutral or neutral-neutral reaction in which the products are stabilized via the emission of a photon, that is, $A + B \longrightarrow AB + h\nu$ or $A^+ + B \longrightarrow AB^+ + h\nu$; for example, the reaction between C^+ and H_2 to produce CH_2^+ , a possible first step in the formation of small hydrocarbons in the ISM.⁸ Dissociative recombination involves the attachment of an electron to a positive ion which causes the ion to dissociate into two or more neutral fragments, i.e. $AB^+ + e^- \longrightarrow A + B$. It is considered a significant process in ISM chemistry as it terminates ion chemistry by leading to stable neutral species. An astrochemically relevant example is the dissociative recombination of N_2H^+ to form $N_2 + H$, which is considered the main destruction route for N_2H^+ in CO poor environments and has

1
2
3 important implications for tracing the CO snowline in protoplanetary disks.^{9,10}
4

5 Often, only overall rate coefficients are measured in laboratory experiments and the
6 branching ratios into different product channels is unknown. This is especially the case for
7 neutral-neutral reactions. The number of these reactions for which rate coefficients have been
8 measured at room temperature is small and even lower at temperatures relevant to the cold
9 ISM. For reactions involving COMs, the branching ratios into the different product channels
10 have not been measured at low temperature. Below, we discuss the role of laboratory meth-
11 ods in understanding observations of astrophysical environments. We also discuss the types
12 of data that laboratory measurements can provide for reactions down to low temperatures
13 relevant to astrophysical conditions, and how this can be input into astrochemical models.
14
15
16
17
18
19
20
21
22
23

24 **The role of laboratory measurements of gas-phase reactions**

25
26
27 Astrochemical observations of star-forming regions rely heavily upon laboratory data; not
28 only for understanding the abundances of molecules that have been detected but also for
29 predicting the detectability of other species in various astrophysical environments. Labora-
30 tory experiments on elementary reaction processes seek to provide two types of information:
31 the first is a quantity that describes the intrinsic efficiency of reaction — the rate coefficient,
32 symbolized by k or by $k(T)$ in order to emphasize that rate coefficients generally depend on
33 temperature. Many formation and destruction pathways involving COMs are bimolecular
34 and can be represented by the chemical equation:
35
36
37
38
39
40
41
42
43
44
45
46



48
49
50
51 The rate of removal of reactant A is then given by:

$$52 \quad -\frac{d[\text{A}]}{dt} = k[\text{A}][\text{B}] \quad (2)$$

where k is the bimolecular rate coefficient for the reaction with standard units of $\text{cm}^3 \text{molecule}^{-1} \text{s}^{-1}$. In order to isolate the bimolecular reaction the laboratory measurement is often conducted in pseudo-first order conditions where the concentration of one reactant, say B, is kept in large excess of the other. Under these conditions the concentration of B remains essentially constant and equation (3) becomes:

$$-\frac{d[\text{A}]}{dt} = k'[\text{A}] \quad (3)$$

where $k' = k[\text{B}]$ is the pseudo-first order rate coefficient.

Laboratory measurements of gas-phase processes generally focus on extracting this rate coefficient as a function of temperature ($k(T)$). These rate coefficients are often expressed by the Arrhenius equation:

$$k(T) = A \exp(-E_A/T) \quad (4)$$

Where A is a pre-exponential factor, E_A is the activation energy (in units of K) and T is the gas kinetic temperature. In astrochemical databases, e.g. the KIDA Home Page: kida.obs.u-bordeaux1.fr/ (accessed March, 2019), a modified Arrhenius equation is used in order to express the temperature dependence of the pre-exponential term:

$$k(T) = \alpha(T/300\text{K})^\beta \exp(-\gamma/T) \quad (5)$$

Here, three parameters (α , β and γ) are used to extrapolate $k(T)$ over various temperatures. Theoretical calculations can also be used to calculate $k(T)$ in some cases; however, the rate coefficients are often sensitive to the presence of small energetic barriers, which can be difficult to determine computationally. In addition, reactions of astrochemical interest often involve ions or radical species with unpaired electrons which can form complexes and intermediates before dissociating to products. The calculation of their low temperature rate coefficients is challenging; in particular, quantum mechanical tunneling through the reac-

1
2
3 tion barrier can become significant at low temperatures due to the quantum behaviour of
4 molecules at low temperature, particularly when the reaction involves the transfer of light
5 atoms. Several methods can be used to determine the reaction rate coefficients ranging
6 from full dimensional quantum dynamics treatment on an ab initio potential energy surface,
7 which is only possible for small systems due to computational demands, to simple statistical
8 methods based on the long-range attractive forces between the reactants.
9

10
11 The second piece of information that laboratory kinetics experiments aim to provide
12 is the nature of the reaction products. If more than one set of products is energetically
13 accessible, the experimental determination of the branching ratios is necessary for input into
14 astrochemical models. The branching ratios are particularly important in large astrochemical
15 networks in which the reaction products can go on to further react; thus even simple reactions
16 may have consequences for the abundances of larger and more complex molecules. Below we
17 describe laboratory methods that can be used to obtain the rate coefficients (both overall
18 and product-channel-specific) at the low temperatures relevant to interstellar space.
19
20
21
22
23
24
25
26
27
28
29
30
31
32

33 **Laboratory methods for measuring low-temperature re-** 34 **action kinetics** 35 36 37 38

39
40 A wide range of experimental methods exist for studying the reactivity of cold molecules
41 relevant to astrochemistry; however, many techniques do not permit the measurement of
42 *absolute* rate coefficients. The determination of absolute rate coefficients requires accurate
43 knowledge of the concentration of the reactant species, or at least one reactant if the ex-
44 periment is conducted under pseudo-first order conditions. Cold gas-phase reactants are
45 typically produced either through collisions with cryogenically cooled walls of a reaction cell
46 or by the expansion of gas from high to low pressure. Cryogenic cells can be used to measure
47 reactions involving species with moderate vapour pressures; however, for species with low
48 vapor pressures at temperatures below ~ 200 K, condensation on the cold cell walls makes
49
50
51
52
53
54
55
56
57
58
59
60

the absolute reactant concentration difficult to determine. The use of cryogenic cells is therefore limited to the measurement of reaction kinetics at temperatures above a few hundred Kelvin — except for reactions involving light species e.g. $\text{CN} + \text{O}_2$ and $\text{CO} + \text{OH}$, which have been measured down to 99 K and 80 K, respectively.^{11,12} This problem motivated the search for “wall-less” experimental techniques that could produce cold molecules at uniform temperatures without interaction with the reaction vessel walls.

Expansion of high-pressure gas through a small aperture to a low-pressure region can be used to produce cold gaseous molecules without the use of cryogenics. Free jet expansions have been used extensively in spectroscopy to produce cold isolated molecules; however, they have limited application to reaction kinetics because their strong temperature and density gradients produce molecules that are not in local thermodynamic equilibrium. Such limitations motivated the development of the CRESU technique, a French acronym standing for *Cinétique de Réaction en Écoulement Supersonique Uniforme*, which means reaction kinetics in uniform supersonic flow. Below we discuss the details of this technique and its application to the study of various reactions at low temperature.

The CRESU technique

The CRESU technique takes advantage of flow properties of gases after expansion through convergent-divergent Laval nozzles. Laval nozzles are a type of axisymmetric nozzle with a convergent section followed by a divergent section and were first described in 1888 by Gustaf de Laval for use in steam turbines. The gas is accelerated in the convergent section of the nozzle, reaching Mach 1 at the throat and higher Mach numbers as it is expanded in the divergent section. Following the isentropic expansion through the nozzle, a flow of gas is produced that is uniform in velocity, temperature and density, and persists for tens of centimetres. The temperature of the flow (T_{flow}) is related to the Mach number by:

$$T_{flow} = T_0 \left(1 + \frac{\gamma - 1}{2} M^2 \right)^{-1} \quad (6)$$

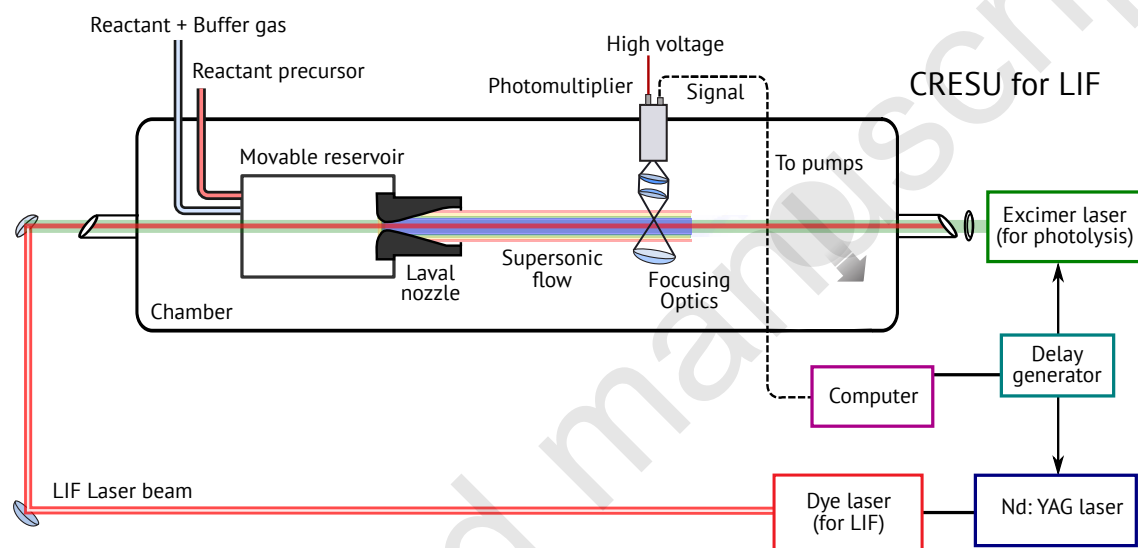


Figure 1: Schematic of a CRESU apparatus configured for the study of neutral-neutral reactions using laser-induced fluorescence, based on the setup at the Université de Rennes. The reactant, buffer gas and radical reactant precursor are delivered to the reservoir via a series of flow controllers. The gas mixture enters the chamber through the Laval nozzle, through which expansion produces a uniform supersonic flow. Radicals are produced in the supersonic beam by photolysis of a precursor using radiation from a fixed frequency pulsed excimer laser and are detected by LIF that is excited using tunable radiation from a dye laser.

1
2
3 where T_0 is the temperature of the gas in the reservoir, $\gamma = C_p/C_v$ is the ratio of the spe-
4 cific heat capacities at constant pressure and volume, and M is the Mach number. Following
5 their passage through the Laval nozzle, the reactants and reactant precursors are delivered
6 to a high-pressure reservoir diluted (typically <1%) in a buffer gas of helium, argon, nitrogen
7 and occasionally hydrogen. The gas mixture passes through the nozzle and the reaction is
8 initiated by crossing the gas flow with an electron beam (to produce ions) or with a UV
9 laser (to produce radicals). Figure 1 shows a schematic of a CRESU experiment configured
10 for laser-induced fluorescence detection. Here, the reaction is initiated when radicals are
11 produced via the photolysis of a radical precursor within the supersonic flow. The reaction
12 is monitored by following the time-dependent LIF of the radical reactant.

13
14
15
16
17
18
19
20
21
22
23 A separate Laval nozzle must be designed and constructed to produce each desired tem-
24 perature and density. The nozzle geometry is calculated by numerically solving the inverse
25 Navier-Stokes flow equations. Construction of the nozzle then requires precise machining,
26 particularly of the inner throat geometry, where any imperfections can perturb the unifor-
27 mity of the flow. Once constructed, the flow produced by each nozzle must be characterized
28 in order to confirm its uniformity. The standard way this is done is by producing a flow
29 under conditions matching the calculated reservoir and chamber pressures and sampling the
30 flow with a Pitot probe. This Pitot measures the impact pressure behind the shock wave that
31 is produced by the impact between the flow and the probe tip. The impact pressure is then
32 used to deduce the Mach number and thus the temperature, density and flow velocity. If the
33 pressure conditions are well met, i.e. the reservoir and chamber pressure are maintained at
34 their calculated values, then the temperature and density conditions are highly reproducible.

35
36
37
38
39
40
41
42
43
44
45
46
47 The lowest temperatures obtainable in the CRESU environment are set first, by the
48 necessity that the reactant concentration is accurately known and secondly, by practical lim-
49 itations of machining of nozzles with narrow throats. At low temperatures, the clustering of
50 reactants in the flow may become significant, such that their concentration becomes uncer-
51 tain. Condensation on the walls of the reservoir or the nozzle also becomes significant for
52
53
54
55
56
57
58
59
60

1
2
3 reactants with low vapour pressures. The lowest temperature achieved so far in a CRESU is
4 6 K,¹³ where the gas was pre-cooled with liquid nitrogen before passing through the Laval
5 nozzle. Without gas pre-cooling, the lowest temperature obtained to date is 12 K.¹⁴
6
7

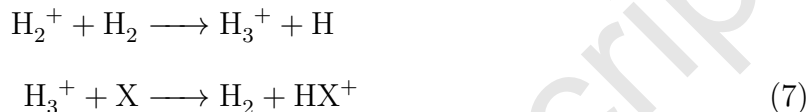
8
9 The CRESU technique was initially developed for continuous gas expansions, with setups
10 built in Rennes,¹⁵ Birmingham¹⁶ and a smaller version operating at higher pressures in
11 Bordeaux.¹⁷ Large flow rates (~ 50 standard litres per minute) are required to maintain the
12 uniformity of the continuous flow for long distances (tens of centimetres). Low pressure in
13 the expansion is also required in order to avoid reactant clustering or three body reactions;
14 therefore, large pumping speeds ($\sim 30,000$ m³/h) are required, especially to obtain the lowest
15 desired temperatures. To overcome this drawback several groups have developed a pulsed
16 version of the CRESU using electromagnetic valves,^{18–21} piezoelectric actuators²² or rotating
17 chopper disks.^{23,24} These pulsed versions significantly reduce the gas consumption and thus
18 the need for large pumps and equipment.
19
20
21
22
23
24
25
26
27
28

29 Versions based on electromagnetic valves supplying gas into the reservoir upstream of
30 the Laval nozzle require very small reservoir volumes (~ 1 cm³) owing to the limited flow
31 rate of such valves. Instead of being essentially at rest, the gas is already moving fast
32 and turbulently in the reservoir, impacting the quality of the uniform supersonic flow and
33 limiting the lowest achievable temperature to 43 K.^{25,26} The use of piezoelectric actuator
34 valves — which allow higher gas flow rates and thus somewhat larger reservoirs, or rotating
35 disk valves — which interrupt the flow close to the Laval throat, enable better quality flows
36 and temperatures as low as 20 K²² and ~ 12 K¹⁴ to be achieved, respectively.
37
38
39
40
41
42
43
44
45
46

47 **Measurements of ion-neutral reactions**

48
49 Early laboratory measurements at low temperatures focused on reactions between neutral
50 species and ions. This was motivated by the assumption at the time that the low tempera-
51 tures of interstellar clouds would reduce the importance of reactions between neutral species
52 and that ion-molecule reactions would dominate the cloud chemistry. In dense clouds, H₂
53
54
55
56
57
58
59
60

1
2
3 becomes the most abundant species in the cloud due to surface-catalyzed production of H_2
4 from atomic H on dust grains. The H_2 can then undergo cosmic-ray ionization to produce
5 H_2^+ , initiating a network of barrierless ion-neutral reactions (equation 7) with other species,
6 X, that can explain some of the exotic chemistry that has been observed in dense clouds.²⁷
7
8
9



10
11
12
13
14
15
16
17
18
19
20
21 The HX^+ ion may then undergo a chain of ion-neutral reactions to produce larger ionic
22 hydrocarbons, which are eventually terminated by dissociative recombination with electrons.
23 Ion-neutral reactions have been invoked, for instance, to explain the high abundance of
24 unsaturated carbon chains in the dense ISM e.g. via reactions between C^+ and neutral
25 hydrocarbons.^{28–30}
26
27
28
29

30
31 Laboratory methods used to study ion-neutral reactions can be placed into two categories:
32 those that utilize ion-trapping and those that inject ions into a gas expansion or flow. Early
33 methods were limited to measurements close to room temperature; though, for many ion-
34 neutral reactions, it is straightforward to predict how the rate coefficient changes as the
35 temperature is decreased using capture theories. The simplest case is the reaction between
36 ions and non-polar neutral species, which can be well predicted by the expression for the
37 Langevin rate coefficient:
38
39
40
41
42
43
44
45

$$k_L = 2\pi e \sqrt{\frac{\alpha}{\mu}} \quad (8)$$

46
47
48
49
50 where e is the charge on an electron, α is the polarizability of the neutral and μ is
51 the reduced mass of ion-neutral pair. The capture models become more complex when the
52 neutral species is polar and in cases where the reactions possess a barrier and more complete
53 theoretical treatments must be used. The potential for polar neutrals is anisotropic and
54
55
56
57
58
59
60

depends on both the distance between the reactants and the orientation of the permanent dipole. One approach that has been used is the classical trajectory method of Su and Chesnavich³¹, in which the long-range potential as a function of distance and orientation is included. This treatment produces a well-known formula for the ion-dipolar rate coefficient, k_D , for linear neutrals, which is expressed relative to the Langevin rate coefficient, k_L :

$$k_D/k_L = \begin{cases} 0.4767x + 0.620 & \text{if } x \leq 2, \\ (x + 0.5090)^2/10 + 526 + 0.9754 & \text{if } x > 2, \end{cases}$$

which relies upon the factor x :

$$x = \frac{\mu_D}{(2\alpha k_B T)^{1/2}} \quad (9)$$

where μ_D is the effective dipole moment of the neutral, α is its polarizability, k_B is the Boltzmann constant and T is the gas temperature.

This treatment is only reliable in the classical regime and temperatures above which rotational motion can be considered classical, typically above 10 K.

Most measurements of ion-neutral reactions up until the 1980s were made using ion cyclotron resonance (ICR) or flowing afterglow (FA) experiments. In the former technique, ions are trapped by electric and magnetic fields and a neutral species is introduced.³² Other trapping methods have been applied at low temperatures, including the Penning trap of Barlow *et. al.*, which has been used to measure the rate coefficient of several reactions with H₂ down to ~ 10 K.³³⁻³⁵ and 22-pole traps, which have made possible the study of ion reactions with H atoms.^{8,36,37} These traps operate at low pressures, giving long trapping times (as long as 1 hour) and thus allowing very slow reaction rates (down to $\sim 10^{-15}$ cm³ molecule⁻¹ s⁻¹) to be measured.

The second category of experiments comprises those based on the use of gas expansion or flow techniques. The flowing afterglow method was first developed in the late 60s and

1
2
3 remains an important technique for the measurement of ion-neutral rate coefficients.³⁸ The
4 apparatus is comprised of a cylindrical flow reactor in which ions are produced and diluted in
5 a buffer gas. Neutral co-reactants are introduced downstream and changes in the ion signal of
6 the gas mixture are detected by a mass spectrometer. The use of cryogenically cooled jackets
7 have allowed reactions to be measured down to around 80 K.³⁹ Several variations to this
8 method have been made, including the addition of a quadrupole mass filter to permit mass
9 selection of the reactant ion.⁴⁰ This technique, known as selective ion flow tube (SIFT), has
10 been used to study a number of ion reactions down to around 90 K as well as their reactions
11 with radical atoms at room temperature.⁴¹

21 Flowing afterglow methods were also developed for the measurement of rate coefficients
22 involving the recombination of ions with electrons to form neutral species. The flowing after
23 glow Langmuir probe (FALP) technique incorporated a movable Langmuir probe (LP) to de-
24 termine the electron density along the FA tube. The FALP method provides no information
25 about the products and thus the branching ratios into the different channels are unknown.
26 In addition, the excited internal states of the ions are neither relaxed nor well defined, and
27 it is difficult to cool the apparatus, though there are some measurements down to ~ 95 K.
28

35 To determine the products of ion-electron recombination reactions, a method was devel-
36 oped in the 1970s known as the merged beam technique.^{42,43} This technique involves two
37 interacting beams of particles that are made to travel along a common axis for some finite
38 distance. Heavy ion storage rings are particularly useful for the study of ion-electron re-
39 actions. They are comprised of a vacuum system, usually >40 m in circumference, with
40 magnetic focusing elements to keep the ions in a closed orbit — producing high intensity ion
41 beams and giving enough time to radiatively cool any vibrationally excited molecules. The
42 ion beam is merged with an electron beam and neutral products are produced. These neutral
43 species are not confined by the magnetic fields and exit the ring to strike a mass-selective
44 detector, giving a complete set of branching ratios. The collision energy can be varied by
45 changing the ion and electron beam velocities, allowing the rate coefficients to be derived
46
47
48
49
50
51
52
53
54
55
56
57
58
59
60

1
2
3 from the cross sections observed as a function of collision energy.
4

5 A major advancement in the measurement of ion-neutral reaction kinetics came with
6 the development of the first CRESU apparatus by Bertrand Rowe and colleagues.⁴⁴ In early
7 experiments, ions were produced by irradiating the gas exiting the Laval nozzle by an electron
8 beam. The rate coefficient for the ion-neutral reaction could then be determined by varying
9 the distance of the sampling port. Later developments incorporated mass selection of the
10 ions.⁴⁵
11
12
13
14
15
16

17 The first reactions studied with the CRESU technique were the reactions of O_2 cations
18 with CH_4 and the association reactions of O_2 and N_2 with their cations.^{44,46} Following
19 this, systematic studies of positive ion reactions with non-polar molecules, polar molecules
20 and molecules with large quadrupoles have been undertaken. A number of ion-neutral bi-
21 molecular reactions involving H_3^+ ,⁴⁷ He^+ ,⁴⁸⁻⁵⁰ N^+ ,⁴⁸ C^{+49-51} or $Ar^+/Ar^{2+52,53}$ ions have
22 been studied, as well as some case studies involving N_2^+ ,⁵⁴ CH^+ ,⁵⁵ O_2^{+46} and O^+ .⁵⁶ Ion-
23 neutral association reactions have also been investigated in CRESU flows for C^+ ,^{45,57} N_2^+ ,⁴⁴
24 O_2^+ ,⁴⁴ CH_3^+ ,⁴⁵ Ar^+ ,⁵⁸ NH_4^+ ,⁵⁹ and H_3O^+ .⁶⁰ The ion-neutral reactions measured to date using
25 CRESU apparatuses are listed in Table 1.
26
27
28
29
30
31
32
33
34

35 Figure 2 shows some example cases displaying the types of temperature dependences that
36 have been observed: the N^+ ion reactions with a non-polar neutral (O_2),⁴⁸ polar neutrals
37 (H_2O and NH_3)⁵¹ and a neutral with a large quadrupole moment (C_6F_6).⁴⁹ In general,
38 the rate coefficients for the reactions of ions with nonpolar molecules match the simple
39 estimate based on the Langevin equation quite well even when the neutral species has a
40 large quadrupole moment, like C_6F_6 . In reactions between ions and polar neutrals, there
41 is an anisotropic attractive force between the charge on the ion and the permanent dipole
42 of the neutral. In this case, the rate coefficients increase as the temperature is lowered, as
43 observed in the reaction between N^+ and H_2O . In the case of N^+ reaction with C_6F_6 , the
44 authors concluded that the existence of a large quadrupole moment did not significantly
45 change in collision rate coefficient or reaction efficiency over a large temperature range.
46
47
48
49
50
51
52
53
54
55
56
57
58
59
60

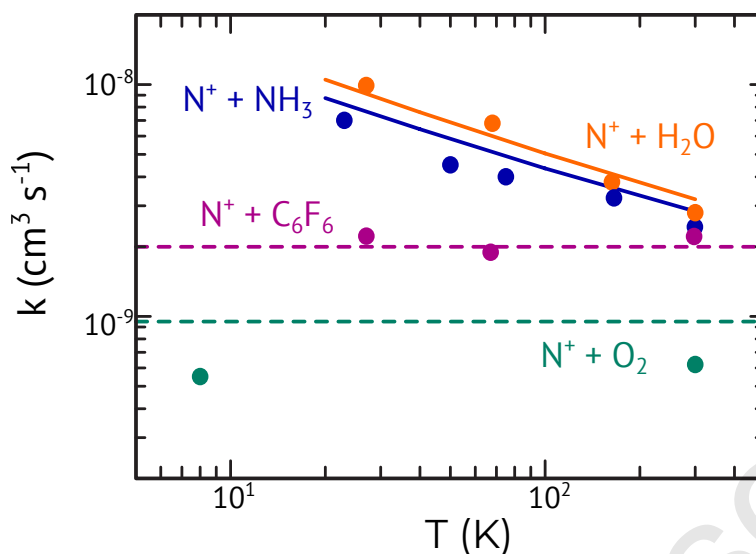


Figure 2: Examples of rate coefficients for some classes of ion-neutral reactions using N^+ ions reactions as examples. The reaction of N^+ with: a non-polar neutral, O_2 (cyan dots),⁴⁸ polar neutrals H_2O (blue dots) and NH_3 (orange dots)⁵¹ and with a neutral with a large quadrupole, C_6F_6 (purple dots).⁴⁹ Predictions using the Langevin formula are shown in dashed lines (for O_2 and C_6F_6) and using the method of Su and Chesnavich in the bold lines (for H_2O and NH_3).

Most of the ion-neutral reactions that have been studied in the laboratory are between singly charged cations and neutral molecules that can be purchased commercially or, in a few cases, synthesized in-house. These molecules comprise only a fraction of the neutral species that could be involved in reactions in dense clouds. A key class of reactions significant in astrophysical environments are the reactions between radicals and ions, which are particularly challenging to study since it is difficult to quantify the concentration of either species. Reactions between several ions and some radical atoms such as $\text{H}(^2\text{S})$, $\text{N}(^4\text{S})$, and $\text{O}(^3\text{P})$ have been studied using the SIFT technique (see the review by Snow and Bierbaum⁴¹), though predominantly at room temperature.

Anion reactions

While a number of reactions between cations and neutral species have been studied down to low temperatures, very few reactions of anions have been measured below 100 K. This is due to a combination of the practical difficulties of producing anions in the laboratory

1
2
3 and assumptions that negative ions would not be present in appreciable quantities in the
4 ISM. While positive ions have been known to exist in the ISM since the discovery of CH^+ in
5 1941,⁶¹ it wasn't until 2006 that the first anion (C_6H^-) was detected.⁶² In the laboratory,
6 the study of anion reactions is more challenging than the study of cation reactions due to
7 the difficulty in producing a stable quantity of the anion reactant species.
8
9
10
11
12

13 The reaction of Cl^- with CH_3Br was studied by Le Garrec et al.⁶³ in 1997, and marks
14 the first study of an anion reaction using the CRESU technique. The reaction was mea-
15 sured between 23–300 K as a classic example of an organic chemistry substitution reaction,
16 rather than in an astrophysical context. Chlorine anions were formed through the dissocia-
17 tive attachment of electrons to CCl_4 by passing a high energy, low intensity electron beam
18 perpendicular to the flow. A dramatic increase in the rate coefficient was found, with the
19 experimental value at 23 K being over two orders of magnitude larger than that observed
20 at 300 K. Motivation to continue laboratory measurements of anion reactions was revived
21 in the mid-2000s with the discovery of negatively charged linear polyynes C_{2n}H^- ^{62,64,65} and
22 cyanopolyynes $\text{C}_{2n+1}\text{N}^-$ ^{66–68} in the ISM.
23
24
25
26
27
28
29
30
31
32

33 Reactions of $\text{C}_{2n+1}\text{N}^-$ (with $n=0, 1$ and 2) cyanopolyynes have recently been studied
34 by the group in Rennes for their application to reactions in Titan's ionosphere and in the
35 ISM.^{69–71} CN^- and C_3N^- and C_5N^- anions were produced by the dissociative electron at-
36 tachment to cyanogen bromide (BrCN), bromocyanoacetylene (BrC_3N) and 5-bromopenta-
37 2,4-diyne nitrile (BrC_5N), the latter two requiring in-house chemical synthesis. Reactions
38 between these small anions and neutral species are predicted to be involved in the growth
39 of anions by initiating a chain of anion reactions.
40
41
42
43
44
45
46

47 Biennier et al.⁶⁹ studied the reaction of CN^- with HC_3N down to ~ 50 K. They found
48 fast rate coefficients for the reaction of $k \geq 4 \times 10^{-9} \text{ cm}^3 \text{ molecule}^{-1} \text{ s}^{-1}$ with a weak negative
49 temperature dependence agreeing with a long-range capture theory. The formation of the
50 C_3N^- anion via the major exit channel $\text{C}_3\text{N}^- + \text{HCN}$ demonstrated that the reaction may be
51 involved in the growth of negative ions in the atmosphere of Titan. In contrast, experiments
52
53
54
55
56
57
58
59
60

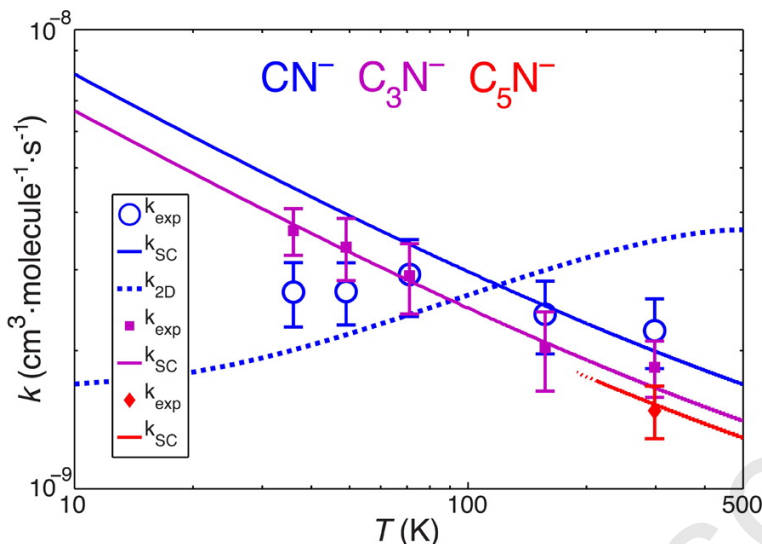


Figure 3: Rate coefficients for the $C_{2n+1}N + HCOOH$ reactions measured between 36 K and room temperature (k_{exp}) and those estimated from the Su and Chesnavich capture model (k_{SC} , solid line). The result of the 2-D quantum model for the $CN^- + HCOOH$ reaction is also shown (k_{2D} , dashed line). Reprinted from Joalland et al.⁷¹

of Bourgalais et al.⁷⁰ showed that in Titan's low-temperature atmosphere the reaction of C_3N^- with HC_3N will not produce anions but instead will lead to the loss of the negative charge.

The kinetics of proton-transfer reactions between these cyanopolyynes anions and formic acid ($HCOOH$) has been studied at 36–300 K.⁷¹ Figure 3 shows the measured rate coefficients for the reactions of CN^- , C_3N^- and C_5N^- with $HCOOH$. They found a negative temperature dependence for the reaction of C_3N^- with $HCOOH$ that could be well reproduced by long-range capture theory using the classical trajectory model of Su and Chesnavich³¹. In contrast, the experiments showed a surprisingly weak temperature dependence for the $CN^- + HCOOH$ reaction, disagreeing with the temperature dependence predicted by capture theories, but agreeing with the temperature dependence predicted by a 2-D time-independent quantum approach.

Comparing the $HCOOH$ reactions to their previous results for HC_3N suggests that dipole-dipole interactions must play an active role in overcoming this limiting effect at low temperatures. The low-temperature reactivity of $HCOOH$ and HC_3N with CN^- and C_3N^- is

similar: the $\text{CN}^- + \text{HC}_3\text{N}$ reaction shows very little temperature dependence, whereas the $\text{C}_3\text{N}^- + \text{HC}_3\text{N}$ reaction exhibits a strong negative temperature dependence. They suggest this behaviour may be due to the factor of 5 difference in the permanent dipole moments of C_3N^- ($\mu = 3.1$ D) and CN^- ($\mu = 0.6$ D) rather than the long-range dipole-dipole interaction.

There is still much to be understood regarding the reactivity of anions with neutral species and their importance in COM formation and destruction in the ISM is yet to be fully explored, both experimentally and computationally.

Table 1: Summary of processes studied in CRESU apparatuses, updated from Smith and Rowe⁷². Reactions studied since the publication of Smith and Rowe⁷² in 2000 are shown in blue.

Process	Reagent	Minimum T (K)	Co-reagent
Ion-neutral reactions			
(i) bimolecular			
	O_2^+	20	CH_4 , ^{45,46,55} CD_4 ⁷⁴
		49	C_2H_6 ⁷⁵
	N_2^+	8	O_2 ⁵⁴
	He^+	8	N_2 , ^{45,48,57} O_2 , ^{48,57} CO ⁴⁸
		23	CH_4 ^{57†}
		27	HCl , ⁵⁰ SO_2 , ⁵⁰ H_2O , ⁵¹ H_2S , ⁵⁰ NH_3 , ⁵¹
			C_6F_6 , ⁴⁹ $\text{c-C}_6\text{H}_{12}$ ⁴⁹
	N^+	8	O_2 , ⁴⁸ CO , ⁴⁸ CH_4 , ^{48,57} H_2 ^{45,51,76}
		20	$p\text{-H}_2$, ⁷⁶ HD ⁷⁶
		23	NH_3 ^{51,57†}
		27	H_2O , ⁵¹ $\text{C}_2\text{H}_2\text{Cl}_2$, ⁷⁷
			C_6F_6 , ⁴⁹ $\text{c-C}_6\text{H}_{12}$ ⁴⁹
		45	D_2 ⁷⁶
	C^+	27	HCl , ⁵⁰ SO_2 , ⁵⁰ H_2O , ⁵¹ H_2S , ⁵⁰ NH_3 , ⁵¹
			C_6F_6 , ⁴⁹ $\text{c-C}_6\text{H}_{12}$ ⁴⁹
	CH^+	23	CO ⁵⁵
	H_3^+	27	$\text{C}_2\text{H}_2\text{Cl}_2$ ⁷⁷
		30	CO , ⁴⁷ N_2 , ⁴⁷ CO_2 , ⁴⁷ NH_3 , ⁴⁷ SO_2 , ⁴⁷
			H_2S , ⁴⁷ CH_4 ^{47†}
	Ar^+	20	N_2 , ⁵² O_2 , ⁵² H_2 , ⁵² CO ⁵²
		23	CH_4 , ⁵⁵ C_2H_6 , ^{55,75} N_2 ^{55,75}
		36	N_2O ⁷⁵
	Ar^{2+}	30	He , ⁵³ Ar , ⁵³ H_2 , ⁵³ O_2 , ⁵³ N_2 , ⁵³ CO_2 ⁵³
	O^+	23	NO , ⁵⁶ N_2 ⁷⁸
	Cl^-	23	CH_3Br ⁶³
	CN^-	36	HCOOH ⁷¹
		49	HC_3N ⁶⁹
	C_3N^-	36	HCOOH ⁷¹
		50	HC_3N ⁷⁰
	C_5N^-	36	HCOOH ⁷¹
(ii) association			

Continued on next page

Table 1 – continued from previous page

Process	Reagent	Minimum T (K)	Co-reagent
	C ⁺	13	H ₂ ^{45,57}
	N ₂ ⁺	20	N ₂ ⁴⁴
	O ₂ ⁺	20	O ₂ ⁴⁴
	CH ₃ ⁺	20	H ₂ , ^{45,55} CO, ⁴⁵ N ₂ ⁴⁵
	Ar ⁺	27	Ar ⁵⁸
	NH ₄ ⁺	15	NH ₃ ⁵⁹
	H ₃ O ⁺	23	H ₂ O ⁶⁰
Neutral-neutral reactions (i) bimolecular			
	CN	13	O ₂ ^{15,79}
		15	CH ₂ CCH ₂ , ⁸⁰ CH ₃ CCH ^{80,81}
		23	C ₃ H ₆ , ⁸² C ₃ H ₈ , ⁸² CH ₃ CH ₂ CCH, ⁸³ C ₄ H ₆ , ⁸² HC ₃ N, ²³ CH ₃ NH ₂ , ⁸⁴ (CH ₃) ₂ NH, ⁸⁵ (CH ₃) ₃ NH ⁸⁵
		25	NH ₃ , ¹⁵ C ₂ H ₂ , ⁸⁶ C ₂ H ₄ , ⁸⁶ C ₂ H ₆ ⁸⁶
		105	c-C ₆ H ₆ , ⁸⁷ c-C ₇ H ₈ ⁸⁷
		123	C ₆ H ₅ CCH ⁸⁸
	OH	12	CH ₃ OH, ^{14,89-91*} CH ₃ COCH ₃ ^{92,93*§}
		21	CH ₃ CH ₂ OH ^{94,95}
		22	HC(O)OCH ₃ , ⁹⁶ H ₂ CO ⁹⁷
		23	HBr, ⁹⁸⁻¹⁰⁰ C ₄ H ₈ , ^{24,101-104}
		39	O(³ P) ¹⁰⁵
		58	CH ₃ CHO, ¹⁰⁶ CH ₃ CH(NH ₂)COOC ₂ H ₅ ^{107,108} C ₂ H ₅ CHO ¹⁰⁹
		63	CH ₃ OCH ₃ ^{92,93*}
		86	(CH ₃) ₃ COOH ²¹
		88	CH ₃ CH(OH)CH ₃ ^{94*}
		93	CH ₃ C(O)CH ₂ CH ₃ ⁹²
		96	H ₂ O ₂ ¹¹⁰
	CH	13	NO, ¹¹¹ O ₂ , ¹¹¹ D ₂ ¹¹²
		23	NH ₃ , ^{111†} CH ₄ , ¹¹³ C ₂ H ₂ , ¹¹³ C ₂ H ₄ , ¹¹³ C ₂ H ₆ , ¹¹³ butenes ¹¹³
		50	H ₂ O ¹¹⁴
		58	c-C ₁₄ H ₁₀ ¹¹⁵
		77	CH ₃ CCH, ¹⁷ CH ₂ CCH ₂ , ¹⁷ C ₃ H ₆ ¹⁷
	C ₂ H [†]	15	O ₂ , ^{73,116,117} C ₂ H ₂ , ^{73,117-119} C ₂ H ₄ , ^{73,120} C ₃ H ₆ ^{73,120}
		63	CH ₃ CCH, ^{80,117} CH ₂ CCH ₂ ^{80,117}
		74	CH ₃ CH ₂ CCH ¹²¹
		79	butenes, ¹²²⁻¹²⁴
		96	C ₂ H ₆ , ¹²⁵ C ₃ H ₈ , ¹²⁵ n-C ₄ H ₁₀ ¹²⁵
		104	C ₄ H ₆ , ¹²³ i-C ₄ H ₁₀ , ¹²³ NH ₃ , ^{126†} ND ₃ ¹²⁶ C ₂ H ₅ CN, ¹²³ C ₃ H ₇ CN ¹²³
		105	c-C ₆ H ₆ ¹²⁷
		165	CH ₃ CN ¹²³
	NH	53	NO, ¹²⁸ CH ₄ , ¹²⁸ C ₂ H ₂ , ¹²⁸ C ₂ H ₄ , ¹²⁸ C ₂ H ₆ , ¹²⁸ C ₃ H ₆ C ₄ H ₂ ¹²⁸
	¹ C ₂	24	NO, ¹²⁹ CH ₄ , ¹³⁰ C ₂ H ₂ , ^{130,131} C ₂ H ₄ ¹³⁰ C ₂ H ₆ , ¹³⁰ C ₃ H ₈ ¹³⁰
		77	CH ₃ CCH, ¹³¹ CH ₂ CCH ₂ , ¹³¹ C ₃ H ₆ ¹³¹

Continued on next page

Table 1 – continued from previous page

Process	Reagent	Minimum T (K)	Co-reagent
		145	O ₂ ¹²⁹
	³ C ₂	24	NO, ¹²⁹ C ₂ H ₂ , ¹³² C ₂ H ₄ ¹³²
		36	C ₃ H ₈ ¹³²
		200	C ₂ H ₆ ¹³²
	C ₄ H	39	C ₂ H ₂ , ^{133,134} C ₂ H ₄ , ^{133,134} C ₂ H ₆ , ^{133,135} CH ₃ CCH ^{133,134} C ₃ H ₆ , ¹³⁴ C ₃ H ₈ , ^{133,135} CH ₂ CCH ₂ , ¹³⁴ CH ₃ CH ₂ CCH, ¹³⁴ C ₄ H ₆ , ¹³⁴ C ₄ H ₈ , ¹³⁴ n-C ₄ H ₁₀ ¹³⁵
		200	CH ₄ ^{133,135}
	¹ CH ₂	43	H ₂ , ²⁵ CH ₄ , ²⁵ C ₂ H ₂ , ²⁶ C ₂ H ₄ , ²⁶ C ₂ H ₆ ²⁶
	C(³ P)	15	NO, ^{136,137} O ₂ , ^{136–138} C ₂ H ₂ , ^{138,139} C ₂ H ₄ , ¹³⁸ C ₃ H ₆ ¹³⁸ CH ₃ CCH, ¹⁴⁰ CH ₂ CCH ₂ ¹⁴⁰
		50	NH ₃ , ^{141,142} H ₂ O, ¹⁴³ D ₂ O, ¹⁴³ CH ₃ OH ¹⁴⁴
	C(¹ D)	50	NO, ¹⁴⁵ O ₂ , ¹⁴⁵ H ₂ ¹⁴⁶ , D ₂ ¹⁴⁷ CO ₂ , ¹⁴⁸ CH ₄ , ¹⁴⁹ C ₂ H ₆ ¹⁴⁹
		127	CH ₃ OH ¹⁴⁴
	Al(² P)	23	O ₂ ¹⁵⁰
	Si(³ P)	15	C ₂ H ₂ , ¹⁵¹ C ₂ H ₄ , ¹⁵¹ NO, ¹⁵² O ₂ ^{152,153}
	B(² P)	23	C ₂ H ₂ , ¹⁵⁴ C ₂ H ₄ ¹⁵⁵
		24	O ₂ ¹⁵⁶
	O(³ P)	23	C ₂ H ₄ , ¹⁵⁷ C ₃ H ₆ , ¹⁵⁷ butenes ¹⁵⁷
	O(¹ D)	50	CH ₄ , ¹⁵⁸ H ₂ , ¹⁵⁹ CO ₂ , ¹⁴⁸ C ₂ H ₆ , ¹⁶⁰ C ₂ H ₂ , ¹⁶⁰ D ₂ ¹⁶¹
	N(⁴ S)	48	NO ¹⁶²
		54	C ₂ N ¹⁶³
		56	OH, ¹⁶⁴ CN, ¹⁶⁵ CH ¹⁶⁶
		57	¹ C ₂ ¹⁶⁷
	N(² D)	50	NO ¹⁶⁸
		75	CH ₄ , ¹⁶⁹ C ₂ H ₆ , ¹⁶⁹ C ₃ H ₈ ¹⁶⁹
	S(¹ D)	6	H ₂ ¹³
		23	CH ₄ , ¹⁷⁰ C ₂ H ₂ , ¹⁷⁰ C ₂ H ₄ ^{171,172}
	Cl(² P)	48	C ₂ H ₆ , ¹⁷³ C ₃ H ₈ ¹⁷³
	F(² P)	11	H ₂ ¹⁷⁴
(ii) association			
	OH	23	NO, ^{175–177} butenes ¹⁰¹
		50	CH ₂ CCH ₂ , ¹⁷⁸ C ₃ H ₆ ^{20,102–104}
		56	O ₂ ^{179–181}
		58	C ₂ H ₂ , ^{21,107} C ₂ H ₄ ^{21,107,110} C ₅ H ₈ ²⁰ C ₁₄ H ₁₀ ¹⁸²
		69	CH ₃ CCH ²¹
	CH	25	C ₆ H ₆ ¹⁸³
		53	H ₂ , ^{112,184} N ₂ , ^{185,186} CO ¹⁸⁵
	CN	23	CH ₃ CN ^{187*}
(iii) dimerization			
	C ₆ H ₆	15	C ₆ H ₆ ¹⁸³
	C ₁₄ H ₁₀	59	C ₁₄ H ₁₀ ¹⁸⁸
	C ₁₆ H ₁₀	59	C ₁₆ H ₁₀ ¹⁸⁹
	H ₂ O	23	H ₂ O ¹⁹⁰

Continued on next page

Table 1 – continued from previous page

Process	Reagent	Minimum T (K)	Co-reagent	
Collisional energy transfer	NO(A ² Σ ⁺ ,v=0)	34	NO, ¹⁹¹ O ₂ ¹⁹¹	
	NO(v=1)	7	NO ¹⁹²	
	NO(v=3,j)	7	He ¹⁹³	
		23	Ar, ¹⁹³ N ₂ ¹⁹³	
	toluene	38	He ¹⁹⁴	
		74	N ₂ ¹⁹⁴	
		112	Ar ¹⁹⁴	
	CO(X ¹ Σ ⁺ ,v=2,j)	15	He ¹⁹⁵	
		30	Ar ¹⁹⁶	
	CH(v=1)	23	H ₂ , ¹⁸⁴ D ₂ , ¹⁸⁴ N ₂ , ¹⁹⁷ CO ¹⁹⁷	
	¹ CH ₂	43	He, ²⁵ N ₂ , ²⁵ O ₂ , ²⁵	
	C ₂ (a ³ Π _u)	24	NO, ¹²⁹ O ₂ ¹²⁹	
	Al(² P _{3/2})	44	Ar ¹⁹⁸	
	C(³ P)	15	He ¹⁹⁹	
	Si(³ P)	15	He ¹⁹⁹	
	O(¹ D)	50	N ₂ , ²⁰⁰ O ₂ , ²⁰⁰ Ar, ²⁰⁰ Kr ²⁰¹	
	C(¹ D)	50	N ₂ ²⁰²	
	S(¹ D)	6	Ar ²⁰³	
	Electron Attachment	electron	48	SF ₆ , ²⁰⁴ CF ₃ Br, ²⁰⁴ CCl ₂ F ₂ , ²⁰⁴ C ₁₄ H ₁₀ ²⁰⁵ CH ₃ I, ²⁰⁶ HI, ²⁰⁷ DI, ²⁰⁷ HBr ²⁰⁸ HCl, ²⁰⁸ POCl ₃ ²⁰⁹

[†] Corrections to Smith and Rowe⁷²: He⁺ + CH₄ was omitted, N⁺ + NH₃ was measured at 23 K, H₃⁺ + CH₄ was measured at 30 K, reactions of C₂H with C₂H₂, C₂H₄ and C₃H₆ by Chastaing et al.⁷³ were measured at 15 K, C₂H + O₂ was omitted, the NH₃ + C₂H was reportedly measured at 25 K but we were unable to source this publication. NH₃ + CH was measured at 23 K

* These reactions may display mixed bimolecular and termolecular mechanisms.

§ Blázquez *et. al.* to be published in this issue.

Measurements of neutral-neutral reactions

Most chemical reactions between stable neutral species grind to a halt at the low temperatures of interstellar clouds because the molecules do not have sufficient thermal energy to overcome activation barriers. However, many reactions involving radicals do not possess barriers and remain rapid or even become more efficient at low temperatures.

In order to study neutral-neutral reactions, pulsed laser photolysis or discharge methods are used to produce radicals. These radicals meet the other more abundant reactant species, and the change in radical concentration is observed as a function of time, typically by laser-induced fluorescence. To our knowledge, rate coefficient data on bimolecular reactions involving 21 different radicals (including different electronic states) and around 50 neutrals

1
2
3 have been published to date, for a total of around 160 neutral-neutral reactions. These
4 reactions are listed in Table 1, as well as those involving three-body collisions.
5
6

7 The first measurement of a rate coefficient for a radical-radical reaction below 100 K was
8 made for $\text{CN} + \text{O}_2$.⁷⁹ This study was motivated by results obtained in a cryogenic cell that
9 displayed a negative temperature dependence consistent with a “capture” by the long-range
10 dipole-quadrupole forces between the reagents and the formation of a transient complex.
11 They found that the reaction rate coefficient increases with decrease in temperature, following
12 a $T^{-1/2}$ dependence. Such negative temperature dependences of the rate coefficient have since
13 been observed for a range of radical-radical reactions, for example reactions of $\text{CH}(X^2\Pi)$ with
14 O_2 and NO ,¹¹¹ $\text{NH}(X^3\Sigma^-)$ with NO ¹²⁸ and $\text{N}(^4\text{S})$ with $\text{C}_2(^1\Sigma_g^+)$.¹⁶⁷
15
16
17
18
19
20
21
22

23 The discovery that the rate coefficients of many neutral-neutral reactions increase as the
24 temperature is lowered was one of the most significant findings of CRESU experiments and
25 has had a large impact in the field of astrochemistry. A surprising aspect of early CRESU
26 studies was the observed diversity in the temperature dependence of the measured rate
27 coefficients. While the rate of many reactions increased with temperature, others possessed
28 a “U” shaped temperature dependence, with a marked minimum typically between 100-200
29 K. This behaviour has been observed for several cases where the reaction passes through an
30 initial weakly bound complex and then over a (submerged) barrier.^{86,89,157}
31
32
33
34
35
36
37
38

39 In order to predict whether a neutral-neutral reaction is expected to remain rapid ($k >$
40 $10^{-10} \text{ cm}^3 \text{ molecule}^{-1} \text{ s}^{-1}$) at 10 K, Smith et al.²¹⁰ proposed two criteria: the rate coefficient
41 must be greater than $\sim 10^{-11}$ at room temperature and the difference between the ionization
42 energy (IE) of the molecule and the electron affinity (EA) of the neutral must be less than
43 8.75 eV. When IE-EA is less than 8.75 eV the reaction will be barrierless or possess barriers
44 below the reactant energy (submerged barriers).
45
46
47
48
49
50

51 The reactions between ground state oxygen atoms, $\text{O}(^3\text{P})$, and unsaturated hydrocarbons
52 provided a good test of this empirical theory, having IE-EA values that straddle 8.75 eV. It
53 was indeed found that the temperature dependences supported the empirical theory proposed
54
55
56
57
58
59
60

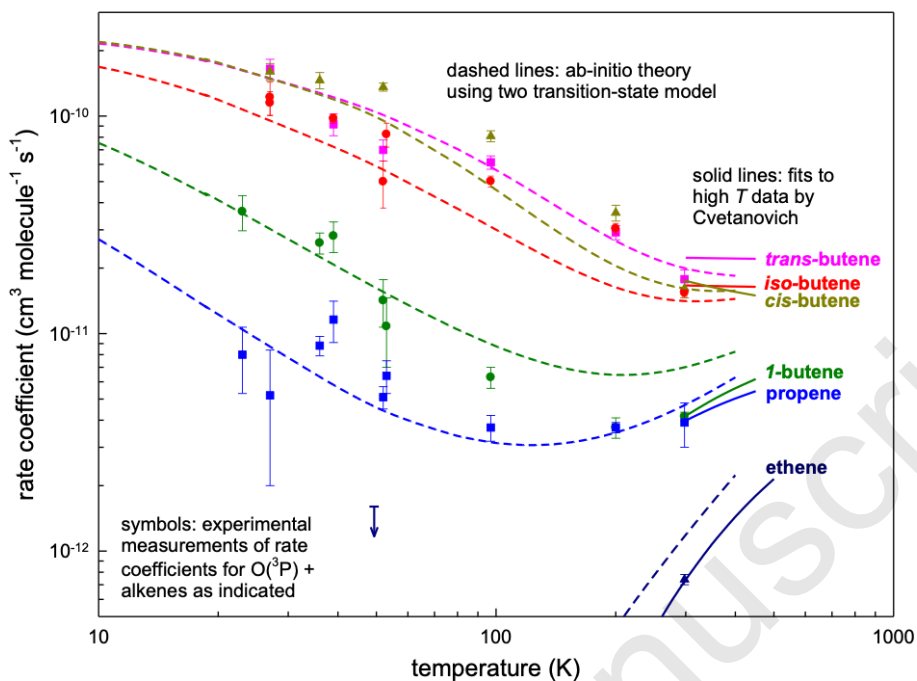


Figure 4: Rate coefficients for the reactions of $O(^3P)$ atoms with alkenes. The dashed lines show theoretical calculations based on a two-transition state model. The solid lines show the recommended fit to the kinetic data from 300–700 K based on the Arrhenius expression. Adapted with permission from Sabbah et al.¹⁵⁷ Copyright (2007) AAAS.

by Smith and co-workers. Figure 4 shows the reaction rate coefficients for the $O(^3P)$ reactions with the unsaturated hydrocarbons ethene, propene and butene isomers. The reaction of oxygen atoms with *cis*-, *trans*- and *iso*-butene isomers, which possess fully submerged barriers and IE-EA values less than 8.75 eV, showed negative temperature dependence. The oxygen reaction with ethane possesses a true barrier and an IE-EA much greater than 8.75 eV, here the reaction rate coefficient is lower than measurable in the CRESU. The IE-EA for 1-butene and propene reactions with $O(^3P)$ are only slightly below the threshold and displayed the characteristic U-shaped temperature dependence consistent with their barely submerged inner barriers. A number of neutral-neutral reactions of relevance to COM reactivity have been studied using the CRESU technique and we outline some interesting cases below.

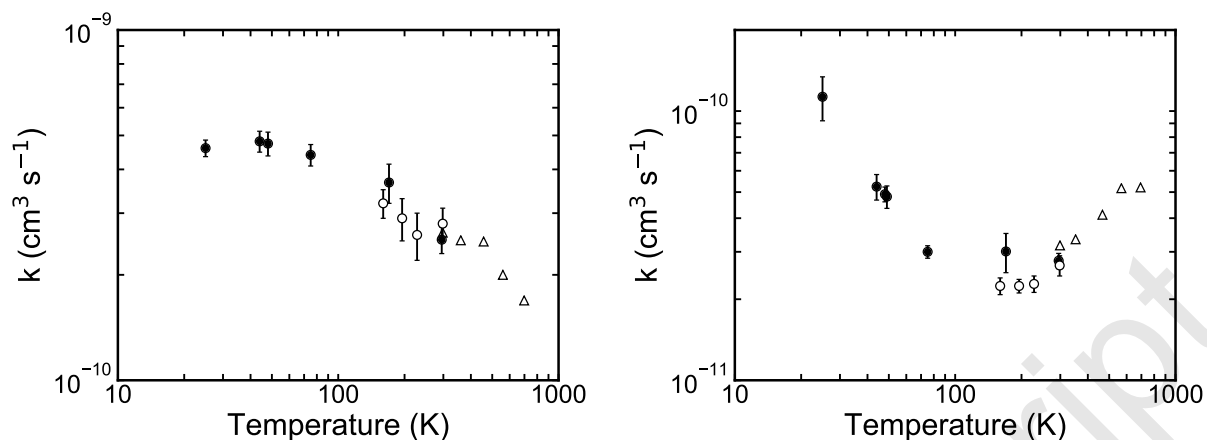


Figure 5: Rate coefficients for the reaction of CN radicals with C_2H_2 (left) and with C_2H_6 (right). The circles show data taken from Sims et al.¹⁵, where the filled circles were measured using a CRESU apparatus and the open circles using a cryogenic cell. The triangles show high temperature data of Herbert et al.²¹¹.

Reactions between CN and hydrocarbons

Some of the earliest neutral-neutral reactions studied using the CRESU technique involved the reactions of the cyanogen (CN) radical with saturated (C_2H_6) and unsaturated (C_2H_2 , C_2H_4) hydrocarbons.⁸⁶ The temperature dependent rate coefficients were measured between room temperature and 160 K in a cryogenic cell and down to 25 K in the CRESU apparatus at Rennes. Similar to the prototypical radical-radical reaction between CN and molecular oxygen, the rate coefficients for reactions between several unsaturated hydrocarbons and CN displayed negative temperature dependences. The reaction between C_2H_6 and CN displayed a remarkable temperature dependence, decreasing as the temperature was lowered to ~ 100 K and then rapidly increasing to a maximum at 25 K. The rate coefficients for CN reactions with C_2H_2 and C_2H_6 are shown in Figure 5 to illustrate the negative temperature dependence ($\text{C}_2\text{H}_2 + \text{CN}$) and the U-shaped temperature dependence ($\text{C}_2\text{H}_6 + \text{CN}$). The authors explained the temperature dependence by the presence of two transition states along the reaction potential: a “loose” transition state, where the reactants are still well separated, and a “tight” one that is lower in energy but with wider spaced energy levels, beyond which products form. A schematic of a representative potential energy surface for such a reaction is

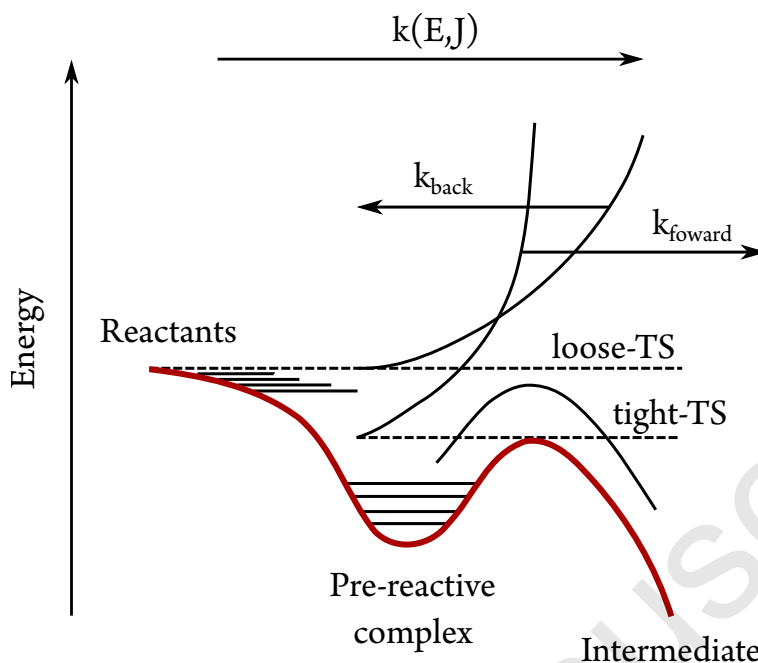


Figure 6: Schematic showing the dynamics of a reaction proceeding through a pre-reactive complex. At low temperatures the reaction rate is dominated by the formation of the pre-reactive complex via the loose transition state whereas at high-temperatures the the rate is dominated by the passage through the tight transition state. Adapted with permission from Hansmann and Abel¹⁰⁷ Copyright (2007) Wiley.

shown in Figure 6. At high temperatures, collisions between the two reactants are direct and there is only one chance for the reaction to occur and k_{back} is dominant. As the temperature is lowered, the proportion of collisions forming pre-reactive complexes is increased and more of the potential surface can be accessed to find a path to products. In other words, at high temperature, passage through the tight transition state governs the reaction rate, while at lower temperatures the loose transition state is rate determining.

Following these early studies, a handful of other reactions between CN and hydrocarbons have been measured. The reaction of CN with allene ($H_2=C=CH_2$) and methyl acetylene (CH_3CCH) were measured by Carty et al.⁸⁰ between 15 K and 295 K. For both reactions, the temperature-dependence is negligible and the authors recommended the use of a temperature independent value $k = (4.1 \pm 0.5) \times 10^{-10} \text{ cm}^3 \text{ molecule}^{-1} \text{ s}^{-1}$. At all temperatures, the rate coefficients approach the collisional limit and thus the reaction is expected to be significant under ISM temperature conditions. The reaction mechanism was predicted to occur in both

1
2
3 cases by a barrierless addition followed by loss of an H atom.^{212,213}
4

5 The reaction of CN with propene, propane, 1-butyne were measured by Morales et al.⁸²
6 between 23-298 K. The reaction between CN and propene displayed a slight negative temper-
7 ature dependence while its the unsaturated counterpart propane followed Arrhenius behavior
8 at high temperatures with a minimum at around 300 K, very similar to that observed for
9 ethane. The reaction between CN and 1-butyne was found to be temperature independent,
10 with an average value of $k = (4.0 \pm 0.7) \times 10^{-10} \text{ cm}^3 \text{ molecule}^{-1} \text{ s}^{-1}$. The reaction of
11 1,3-butadiene with CN was studied soon after and was found to possess a slightly positive
12 temperature dependence following Arrhenius behaviour,⁸³ illustrating the range of temper-
13 ature dependences that can be observed, even for reactions involving isomers.
14
15
16
17
18
19
20
21
22
23

24 **Reactions of the hydroxyl radical with COMs**

25
26 During the last few decades, several reactions between organic molecules and the hydroxyl
27 radical (OH) have been studied, particularly by the group of Dwayne Heard at Leeds. These
28 reactions display a marked increase in the rate coefficient as the temperature is lowered.
29 Such reactions have been shown to proceed via gas-phase hydrogen abstraction reactions,
30 forming weakly bound ($<30 \text{ kJ mol}^{-1}$) hydrogen-bonded complexes with the organic neu-
31 trals. Reactions with OH at low temperatures have thus far been studied for the alcohols
32 methanol,^{14,89-91} ethanol^{94,95} and propan-2-ol,⁹⁴ dimethyl ether,^{92,144} the ketones butanone
33 (methyl-ether-ketone),⁹² acetone,^{92,144} and formaldehyde⁹⁷ and for the esters methyl for-
34 mate⁹⁶ and L-alanine ethyl ester.¹⁰⁸ The reaction between methanol and OH, in particular,
35 has been studied in detail both experimentally^{14,89-91} and theoretically^{14,214-217} by several
36 different groups. The reaction was first studied at low temperature by the Leeds group, who
37 measured the rate coefficient by OH LIF at 63 K and 80 K. They found the rate coefficient
38 for the reaction between OH and methanol was almost two orders of magnitude larger at
39 63 K than previously measured at $\sim 200 \text{ K}$.²¹⁸ Later experimental efforts focused on mea-
40 surements down to lower temperatures (recently, as low as $\sim 12 \text{ K}$) and investigations of the
41
42
43
44
45
46
47
48
49
50
51
52
53
54
55
56
57
58
59
60

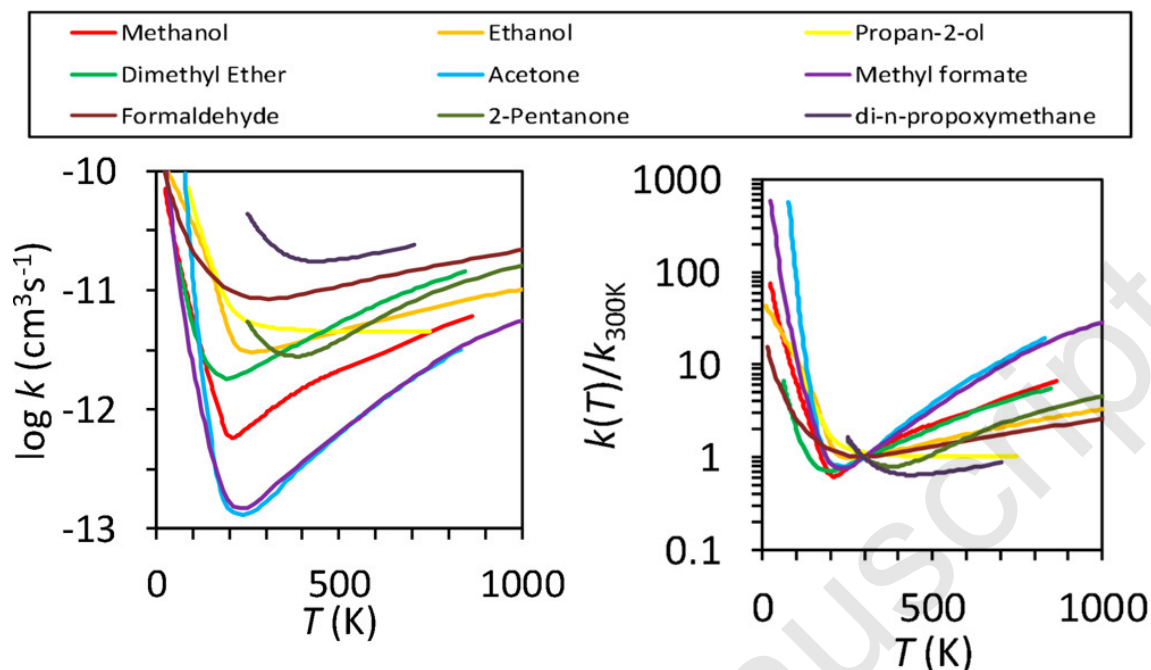


Figure 7: Rate coefficients, k (left), and the ratio, $k(T)/k(300\text{K})$ (right), as a function of temperature for reaction of OH with several organic molecules. The lines are interpolated fits to data in the literature. Reprinted from Heard²¹⁹.

pressure dependence of the reaction rate coefficient.

Figure 7 shows the temperature dependences of the rate coefficients for reactions of OH with several of these organic molecules, interpolated to the experimental data. In accordance with the empirical treatment of Smith *et. al.* a rapid U-shaped temperature dependence is observed resulting in low-temperature rate coefficients up to a thousand times faster than those at room temperature. At low temperatures the lifetime of the van der Waals complex increases and the probability of tunnelling under the reaction barrier to form products becomes much higher.

An important aspect of these measurements is the pressure dependence of the rate coefficients. If the rate coefficient is dependent on the total density in the flow the pre-reactive complex may be stabilized by three-body collisions, and thus the enhanced rate coefficient at low temperature will not be applicable to most astrochemical environments due to their low densities. In the low pressure limit (LPL) the reaction can be considered as a direct H-abstraction process without the formation of a stabilized pre-reactive complex, whereas

1
2
3 in the high-pressure limit (HPL) the pre-reactive complex is fully stabilized with an energy
4 state population following a Boltzmann distribution. For the $\text{CH}_3\text{OH} + \text{OH}$ reaction, the
5 rate coefficients were measured as a function of pressure at 80 K and were found to be inde-
6 pendent of the total density which was explained by the presence of a weakly bound complex
7 that is not fully stabilized by collisions but undergoes quantum mechanical tunnelling to the
8 products.⁸⁹ Tunnelling mechanisms can be verified by checking for kinetic isotope effect; how-
9 ever, experiments with deuterated reagents are more experimentally challenging and costly.
10 Measurement of the rate coefficients from 11.7 K to 177.5 K by Ocaña et al.¹⁴ displayed
11 a pressure dependence between 120–150 K, below which the rate coefficients were pressure
12 independent. Gao et al.²¹⁵ computed the rate coefficients between 30 K and 2000 K using
13 the competitive canonical unified statistical (CCUS) model. Their results indicated that the
14 rate coefficients measured below 100 K are close to the HPL. Roncero et al.²¹⁴ calculated
15 a new full-dimensional potential energy surface and used quasi-classical trajectory methods
16 to determine the rate coefficients as a function of temperature. The rate coefficients were
17 found to be almost temperature independent between 20 K and 300 K and much lower than
18 the experimental measurements. Recently, Nguyen et al.²¹⁶ have used 2-D master equation
19 methods to compute the temperature and pressure dependent rate coefficients. Their results
20 suggest that the low-temperature measurements are approaching the high-pressure limit.
21 However, del Mazo-Sevillano et al.²¹⁷ used a ring-polymer molecular dynamics method and
22 were able to reproduce well the experimental data assuming the zero pressure limit. Thus,
23 even for the reaction between OH and one of the simplest COMs, methanol, there is still
24 debate about the reaction mechanism under interstellar conditions.

25
26
27
28
29
30
31
32
33
34
35
36
37
38
39
40
41
42
43
44
45
46
47
48
49
50
51
52
53
54
55
56
57
58
59
60

OH reactions with larger alcohols ethanol and propan-2-ol and with acetone, methyl-ethyl-ketone, dimethyl ether, methyl formate and H_2CO also displayed distinct upturns in the rate coefficient for H-abstraction towards low temperature. In reactions of OH with acetone, a marked pressure dependence was observed, suggesting the enhanced rate coefficients at low temperature are likely due to collisional stabilization. However, rate calculations in the

low pressure limit predicted that the reaction will remain rapid ($k \sim 10^{-11} \text{ cm}^3 \text{ molecule}^{-1} \text{ s}^{-1}$) under interstellar conditions.⁹³ The lifetime of the pre-reactive complex is determined by the density of vibrational states. Complexes of larger molecules will have long enough lifetimes that the enhancement of the rate coefficient at low temperatures can be enhanced by collisional stabilization. For small molecules, the lifetime of the pre-reactive complex is short and the rate coefficient at low temperature is controlled by tunnelling.

The largest enhancement in the rate coefficient observed to date is that for the OH + methyl formate reaction, increasing by a factor of ~ 600 at 22 K compared to room temperature. The pressure dependence of this reaction has not been investigated and thus the mechanism for the dramatic enhancement in $k(T)$ at low temperatures is unknown.

Product specific reaction kinetics

Reactions involving complex organic molecules often have more than one set of products. In such multichannel reactions, rate coefficients can be defined for each channel and related to overall reaction rate coefficient by their branching ratios. Take, for example, a two-channel reaction between CH_3OH and OH , producing products CH_3O and H_2O (channel a) and CH_2OH and H_2O (channel b):



Here, the overall rate coefficient, $k_1 = k_{1a} + k_{1b}$, is the sum of the product specific rate coefficients, k_{1a} and k_{1b} . The product branching ratios into channels a and b are then defined as $\alpha_a = k_{1a}/k_1$ and $\alpha_b = k_{1b}/k_1$.

It has long been acknowledged that branching ratios between the products in such multichannel reactions are as important as the overall rate coefficient in order to accurately

1
2
3 reproduce complex astrophysical environments.²²⁰ Significant progress has been made in the
4 measurement of overall low-temperature rate coefficients during the last few decades; how-
5 ever, the measurement of reaction products and their branching ratios has lagged behind.
6
7 This is, in part, because there is no universal way of determining reaction branching ratios.
8
9 In order to efficiently probe multichannel reactions, the experimental technique should be
10 universal (i.e. detect all reaction channel products), highly sensitive and multiplexed (i.e.
11 able to detect multiple species at the same time). The sensitivity requirement arises from the
12 need to kinetically isolate the bimolecular reaction of interest and minimize the contribution
13 of side or back reactions. These side reactions are reduced by conducting the experiment
14 under pseudo-first order conditions, such that one reactant species (typically an unstable
15 radical) is kept at much lower concentration than the other. The concentrations of the prod-
16 ucts are then limited by that of the less abundant reactant. Multiplexed detection methods
17 are required in order to detect multiple products simultaneously; thus detection techniques
18 that must be tuned to a specific product are impractical e.g. LIF or other narrow-band
19 spectroscopic techniques. Multiplexed detection also reduces systematic errors that arise
20 from drifts in experimental parameters over time.
21
22
23
24
25
26
27
28
29
30
31
32
33
34

35 In the following sections, we discuss techniques that have been used to determine product
36 branching ratios of elementary reactions and their extension to low-temperature reactions.
37 Only a handful of measurements have been made of product specific reaction kinetics below
38 room temperature, relying on either mass spectrometric or spectroscopic detection methods.
39 We outline these methods and present some key results that have been obtained.
40
41
42
43
44
45
46

47 **Calibrated LIF experiments**

48
49 In addition to measuring the decay of a reactant, LIF measurements can be used to measure
50 the presence and growth kinetics of particular products. These data can be used to check for
51 consistency with the decay kinetics of the reactant and confirm the rate coefficient, as well
52 as to provide some evidence supporting a particular reaction mechanism. The use of LIF
53
54
55
56
57
58
59
60

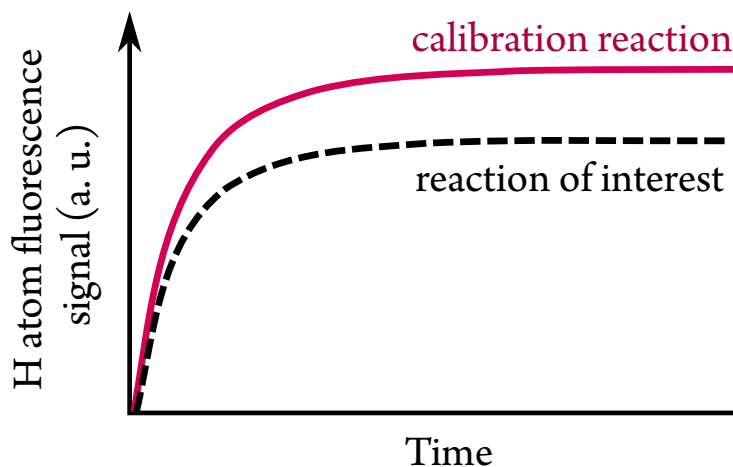


Figure 8: Schematic illustrating a calibration experiment for measurement of H-atom branching ratios. The solid line is the H atom fluorescence from the calibration reaction which has a 100% conversion to the H-atom product channel. The dashed line is the H atom fluorescence from the reaction of interest with an identical initial concentration of the radical reactant. Adapted with permission from Seakins²²⁰ Copyright (2007) RSC.

to measure reaction product branching ratios, however, remains challenging, as it is difficult to relate fluorescence signals to absolute product yields. LIF methods are highly sensitive and often selective, but require calibration to determine absolute concentrations of products. The use of calibration reactions has enabled some determinations of H-atom product yields; however, no direct information is obtained on the identity of the co-product.

The reactions of acetylene and ethylene with CN were studied by this technique at room temperature.²²¹ In this study, the time resolved H atom signal was compared with that from a chosen calibration reaction, $\text{CN} + \text{H}_2 \rightarrow \text{HCN} + \text{H}$. Figure 8 shows a schematic of the calibration technique. The time dependence of the radical removal can be measured in addition to the H atom production to ensure that the observed H is produced from the target reaction and not from secondary or side reactions. In order to detect H atom fluorescence at the Lyman- α transition (121.6 nm), the Lyman- α probe beam was produced by frequency tripling 365.8 nm radiation in a gas cell containing krypton and argon. The 365.8 nm beam was first produced by mixing 1064 nm radiation from a YAG pump laser with dye laser radiation at 554.6 nm. The branching ratio into the H atom channel was determined by:

$$\alpha = \frac{I(\text{reactant}) \times C(\text{reactant})}{I(\text{calibration}) \times C(\text{calibration})} \quad (12)$$

Where I refers to the intensity of the H atom signal and C is a correction factor to account for differences in quenching or absorption by the reactant (here C_2H_2 or C_2H_4) as compared to the calibration reactant (here H_2). Using this method, the authors found room temperature branching ratios to H atom channels of (1.08 ± 0.13) and (1.04 ± 0.11) for the reactions of CN with C_2H_2 and C_2H_4 , respectively.

The H atom calibration technique has been applied to a handful of reactions at $T < 300$ K: by the group of Seakins and co-workers at the University of Leeds, to study reactions of $^1\text{CH}_2$,^{26,222} and by Hickson and co-workers at the Université de Bordeaux for reactions involving $\text{C}(^3\text{P})$,^{139,142,144} $\text{C}(^1\text{D})$,¹⁴⁹ and $\text{O}(^1\text{D})$.^{158,160} In the former set of experiments, the authors found that the H atom branching ratio for the reaction of $^1\text{CH}_2$ with both acetylene and ethene increases with temperature between 195 and 298 K. The temperature range was later extended down to 100 K using a pulsed CRESU apparatus and the H-atom branching ratio was shown to continue to decrease at lower temperatures.²⁶ The removal of $^1\text{CH}_2$ was instead dominated by quenching to $^3\text{CH}_2$ at 100 K. Similar to Choi et al.²²¹, the authors used the reaction with H_2 as a calibration reaction, as they had previously measured the temperature dependent branching ratios for its reaction with $^1\text{CH}_2$ in their laboratory.^{223,224} Douglas et al.²⁵ have also used LIF from OH to determine the branching ratios for quenching of $^1\text{CH}_2$ to $^3\text{CH}_2$ by H_2 and CH_4 versus reaction to other products. In these experiments, $^1\text{CH}_2$ is produced in a bath gas of N_2/He mixed with O_2 . The $^1\text{CH}_2$ is quenched by collisions to $^3\text{CH}_2$, which can then react with O_2 , producing OH. In the presence of H_2 or CH_4 , some of the $^1\text{CH}_2$ is removed in chemical reactions, resulting in less $^3\text{CH}_2$ and therefore less OH LIF signal.

The H-atom product branching ratios have been determined by Hickson and co-workers for a number of reactions involving carbon ($\text{C}(^3\text{P})$, $\text{C}(^1\text{D})$) and oxygen atoms ($\text{O}(^1\text{D})$). In most cases, a suitable reference reaction was chosen in order to extract the absolute H-atom

yields, for example the reaction of C(³P) with C₂H₄, which has a known H-atom branching ratio of 0.92 ± 0.04 at 300K.²²⁵ The H-atom LIF calibration of C(³P) + CH₃OH reaction is more complicated due to a competing reaction with C(¹D) atoms, which are also produced during photodissociation of the carbon atom precursor, CBr₄. The proportion of C(³P) and C(¹D) produced from CBr₄ was first characterized by comparing the H atom yields from the reactions of the photoproduced C with H₂ and with methylacetylene, C₃H₄. C(³P) does not react with H₂, whereas C(¹D) atoms react rapidly with 100% branching into the H atom channel; therefore, adding H₂ to the flow and monitoring the H atom signal could be used to determine whether any C(¹D) was produced. The proportions of C(³P) and C(¹D) were then quantified by comparing the H atom signal produced in the C + C₃H₄ reaction to that from C + H₂, assuming H atom branching fractions of 0.85 and 1 for the two reactions, respectively.

Experiments were then performed in the presence and absence of excess H₂, allowing the authors to determine the H atom yield from the C(¹D) + CH₃OH reaction to be approximately 100%. The H atom signals from the C + CH₃OH and C + C₃H₄ reactions were thus compared to obtain the H atom yield from the C(³P) + CH₃OH reaction. These steps can be summarized as follows:

$$I(\text{C}(\text{}^3\text{P}) + \text{CH}_3\text{OH}) = 0.85 \times \frac{I(\text{C} + \text{CH}_3\text{OH}) - I(\text{C}(\text{}^1\text{D}) + \text{H}_2)}{I(\text{C} + \text{C}_3\text{H}_4) - I(\text{C}(\text{}^1\text{D}) + \text{H}_2)} \quad (13)$$

where $I(\text{C}(\text{}^1\text{D}) + \text{H}_2)$, $I(\text{C} + \text{C}_3\text{H}_4)$ and $I(\text{C} + \text{CH}_3\text{OH})$ are the H atom LIF signals derived from fitting the signals recorded when the C atoms were in the presence of H₂, C₃H₄ and CH₃OH, respectively. At both 296 K and 127 K, the H atom yield of the C(³P) + CH₃OH reaction was seen to represent only ~10% of the total. This result allowed the authors to place constraints on statistical calculations using the MESMER²²⁶ (Master Equation Solver for Multi Energy-well Reactions) code to determine that the only major product channel in the C(³P) + CH₃OH reaction is the formation of HCO + CH₃. Some of the HCO radicals (10-15% at most) fall apart to give H + CO, producing the H atom signal detected by LIF.

1
2
3 While laser induced fluorescence is a particularly valuable product detection method,
4 offering excellent sensitivity and selectivity, it is only able to provide kinetic information
5 about a single product channel during a given experiment. The major weakness of the
6 calibrated LIF technique is the difficulty to directly provide branching ratios into product
7 channels other than the H atom channel. Furthermore, even for channels yielding H atoms
8 that can be quantified, different co-products may exist and the technique would be unable
9 to distinguish between them. In order to do measure branching fractions into other product
10 channels, the LIF system must be tuned to detect a specific (and fluorescent) product and a
11 calibration reaction must be found in order to determine the absolute product concentration.
12
13
14
15
16
17
18
19
20
21
22

23 Ionization techniques

24
25 Many species of interest for astrochemistry do not fluoresce (owing to, for example, predissociation) and, as noted above, it is generally not possible to detect multiple species at the same time by this technique as each molecule requires a specific excitation and detection scheme. In contrast, mass spectrometry is a universal detection method that can be used to detect multiple species during the same experiment. Mass spectrometry coupled to tunable vacuum ultraviolet synchrotron photoionization has been used in a number of kinetics experiments to identify reaction products as well as radical intermediates. The photoionization spectra obtained can be used to distinguish between isomeric reaction products with the same m/z , since each isomer has a distinct ionization threshold and photoionization efficiency (PIE) curve, determined by Franck-Condon overlap between the neutral and the cation. This affords new insights into detailed reaction mechanisms that could not be obtained using mass spectrometry alone.
26
27
28
29
30
31
32
33
34
35
36
37
38
39
40
41
42
43
44
45
46
47
48

49 Osborn and co-workers further developed the photoionization mass spectrometer (PIMS) design of Slagle and Gutman^{228,229} for use with a flow tube reactor.²²⁷ To avoid the significant fragmentation that occurs using conventional electron-bombardment ionization, the instrument used vacuum ultraviolet (VUV) radiation produced in a synchrotron that could
50
51
52
53
54
55
56
57
58
59
60

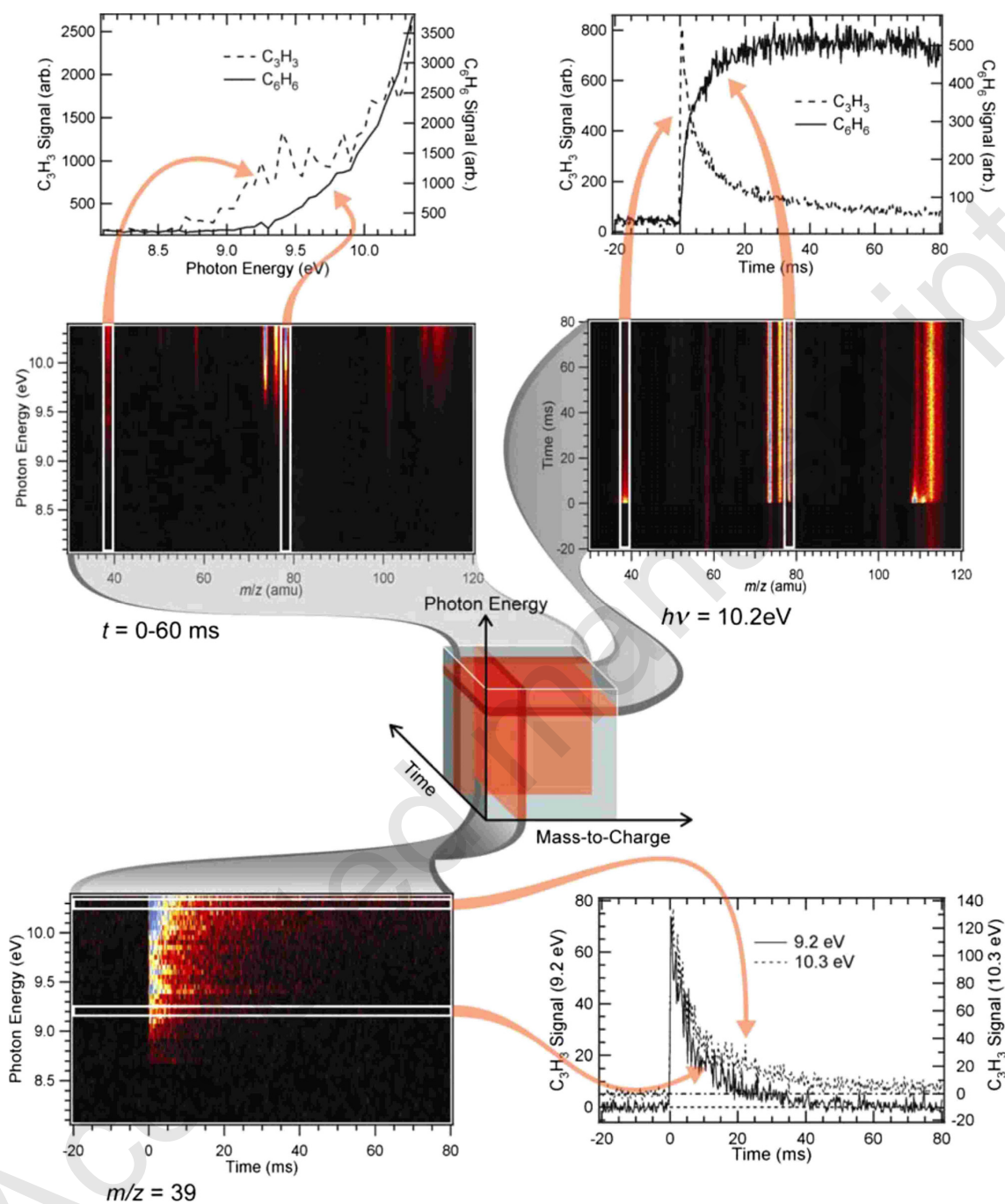


Figure 9: Image representing the 3D data cube that is obtained using photoionization mass spectrometry for measurement of reaction product branching ratios. Both the photon energy and the mass-to-charge ratio are measured as a function of time. The 2D slices show examples of data that can be obtained: The mass spectrum over time at a single photon energy, the photoionization spectrum over time at a single mass-to-charge ratio and the mass-to-charge ratio versus photon energy at a given time. Reprinted with permission from Osborn et al.²²⁷ Copyright (2008) AIP.

1
2
3 be tuned to energies within a few eV of the ionization energy of the species of interest.
4
5 The broad tunability of the synchrotron source provides high selectivity, minimizing frag-
6
7 mentation and allowing one to distinguish between structural isomers due to their different
8
9 ionization energies and PIE curves. The photoionization spectroscopy was coupled to a mul-
10
11 tiplexed mass spectrometer producing a data cube signal, as shown in 9, that is a function
12
13 of time as well as mass (m/z) and VUV energy (E). In the first version of the instrument, a
14
15 multiplexed magnetic sector mass spectrometer was employed²²⁷ but this was subsequently
16
17 replaced by a rapidly pulsed orthogonal time of flight mass spectrometer.^{230,231}
18

19 This technique has enabled significant advances in the measurement of product branching
20
21 ratios for reactions at 300 K and above, with particular significance to atmospheric and
22
23 combustion chemistry.^{232,233} It has also been used to study reactions of astrochemical interest,
24
25 including (at room temperature) the reaction of CN with benzene to produce benzonitrile,⁸⁷
26
27 Here, the authors found that benzonitrile was the only detected product channel, with no
28
29 evidence for a $C_6H_5 + HCN$ channel; however, it remains unclear if the benzonitrile channel
30
31 would remain dominant at the 10 K gas temperature of TMC-1, where it has been recently
32
33 detected.²³⁴ The detection of benzonitrile in the ISM provides a link to the simplest aromatic,
34
35 benzene, which itself cannot be detected by radio astronomy due to its lack of a permanent
36
37 dipole. A potential formation route to benzene, the reaction of C_2H with 1,3-butadiene, was
38
39 also studied using synchrotron photoionization mass spectrometry.²³⁵ The principal reaction
40
41 channel involves addition of the C_2H radical to one of the unsaturated sites of 1,3-butadiene,
42
43 followed by H atom loss to give isomers of C_6H_6 . The photoionization spectra indicated
44
45 that fulvene is the major isomer product, with a branching fraction of $\sim 60\%$. These results
46
47 disagree with the branching fractions found in crossed-beam experiments which found 1,3-
48
49 hexadien-5-yne as the dominant isomer ($70 \pm 10\%$) followed by benzene ($30 \pm 10\%$).²³⁶
50
51 They suggested this discrepancy may be due the high collisional energy of the crossed-
52
53 beam experiment (translating to thermal energy of 5400K), emphasizing the importance of
54
55 studying reactions under both single collision and thermal conditions.
56
57
58
59
60

1
2
3 In a recent development at the Advanced Light Source (ALS) synchrotron in Berke-
4 ley, Wilson, Leone and co-workers combined a pulsed Laval nozzle expansion with syn-
5 chrotron photoionisation and quadrupole mass spectrometric detection to determine the
6 product branching ratios for reactions at ~ 80 K.¹¹⁸ This development implemented sam-
7 pling of the collimated expansion through a small pinhole ($450 \mu\text{m}$) in an airfoil in order
8 to reduce the density of the flow for mass spectrometric detection while minimizing the dis-
9 tance between sampling of the flow and photoionization in order to conserve the kinetic time
10 resolution.²³⁷ They used this technique to study reactions of alkenes: ethene, propene and
11 isomers of butene, with C_2H radicals.^{120,124}

21 In the case of butene, the isomer-specific product branching ratios for the reaction of C_2H
22 radicals with the C_4H_8 isomers (1-butene, *cis*-2-butene, *trans*-2-butene and isobutene) were
23 obtained.¹²⁴ We describe this set of experiments as an illustration of the photoionization mass
24 spectrometry technique for product determination in low temperature reactions. The butene
25 isomers were sequentially introduced into the flow mixed with the C_2H precursor (acetylene)
26 and nitrogen as a buffer gas. The C_2H radicals were produced by pulsed-laser photolysis
27 of acetylene at 193 nm. Following its production, C_2H could react either with the C_4H_8
28 isomer itself, or potentially with one of its photofragments. In order to unravel the origin
29 of the products, the mass spectrum of the butene isomer exposed to the 193 nm photolysis
30 beam is used as a baseline and to identify the butene photolysis products in absence of C_2H .
31 Following subtraction of the photolysed butene mass spectrum, new features were identified
32 at 50, 52 and 66 amu for 1-butene, at 50 and 66 amu for both 2-butene isomers and at 50, 66
33 and (weakly at) 80 amu for isobutene. The mass peak at 50 amu was assigned to diacetylene
34 (C_4H_2), which is a well-known product of the $\text{C}_2\text{H} + \text{C}_2\text{H}_2$ reaction. The masses at 52, 66
35 and 80 correspond to isomers of C_4H_4 , C_5H_6 and C_6H_8 , respectively.

51 In order to determine the isomeric identity of the product species detected at masses 52,
52 66 and 80, photoionization spectra of the products (recorded both as a function of time and
53 m/z) are analyzed at these mass channels. For the 1-butene isomer reaction, the mass 52
54
55
56
57
58
59
60

1
2
3 peak was well fit by vinylacetylene with a predicted upper limit of 5% for the other C₄H₄
4 isomers. The photoionization spectrum at mass 66 displayed a ionization threshold around
5 9.8 eV. This ionization threshold is close to that of 4-penten-1-yne, calculated to fall at 9.9 eV,
6 and far from the thresholds of other possible C₅H₆ isomers. This gave a product branching
7 ratio of (65 ± 10)% C₄H₄ in the form of vinylacetylene and (35 ± 10)% C₅H₆ in the form
8 of 4-penten-1-yne. A similar treatment was applied for the other butene isomers in order to
9 extract the product branching ratios. Both 2-butene reactions produce solely 3-penten-1-yne
10 with no discrimination possible between *cis*- and *trans*-3-penten-1-yne. The reaction with
11 isobutene yields (26 ± 15)% 3-penten-1-yne, (35 ± 15)% 2-methyl-1-buten-3-yne, and (39
12 15)% 4-methyl-3-penten-1-yne.
13
14

15 The reaction rate coefficients were determined under pseudo first-order conditions by
16 measuring the time dependent ion signal at a set product m/z and at a constant ionization
17 energy. The rate coefficients were identical within statistical error for all of the butene
18 isomers with values of (1.9 ± 0.5), (1.7 ± 0.5), (2.1 ± 0.7) and (1.8 ± 0.9) × 10¹⁰ cm³ s⁻¹ for
19 the reaction of C₂H with 1-butene, *cis*-2-butene, *trans*-2-butene, and isobutene, respectively.
20
21

22 This technique remains challenging for the quantification of reactions involving complex
23 polyatomic species as they often require fitting of composite and sometimes incompletely
24 resolved photoionization spectra to determine branching ratios, and clear product signatures
25 are often lacking. The other obvious difficulty is obtaining a tunable soft ionization source
26 requires synchrotron time, which is often not readily available. Despite these challenges,
27 several groups are currently using this technique to constrain product branching ratios for
28 reactions of astrochemical relevance. We discuss the perspectives for this technique further
29 in the conclusions section.
30
31
32
33
34
35
36
37
38
39
40
41
42
43
44
45
46
47
48
49

50 **Crossed-beam experiments**

51 Great advances in our understanding of the dynamics of elementary reactions in the gas-
52 phase have been made possible using crossed molecular beam (CMB) experiments. CMB
53
54
55
56
57

1
2
3 experiments have the particular advantage that they allow reactions to be studied under
4 single collision conditions, guaranteeing that the products formed are not subject to subse-
5 quent reaction. The reactants are confined into distinct beams, with well defined velocities,
6 which cross each other at a defined angle, ensuring that the species of each beam collide only
7 with those of the other beam. Once formed, the reaction products travel to the detector
8 (often a rotatable mass spectrometer i.e. the so-called “universal machine developed by Lee
9 et al.²³⁸) without undergoing secondary collisions, since the reaction chamber is kept under
10 high- or ultra-high vacuum. As a result, the outcome of many identical collisions under
11 well-defined conditions are recorded at the detector. Major advances were made following
12 the implementation of soft ionization sources using low energy electrons or VUV synchrotron
13 radiation in order to eliminate dissociative ionization that occurs in standard hard electron
14 ionization sources. While the CMB in the universal machine setup can be used to study
15 complex reactions with multiple product channels, its resolution is generally insufficient to
16 obtain state-resolved information about the products. Instead, laser spectroscopic methods
17 such as LIF and resonance-enhanced multi-photon ionization (REMPI) can be used to obtain
18 state-resolved differential cross sections. These laser-based techniques have been coupled to
19 a number of sophisticated detection schemes, such Doppler-selected time of flight (TOF),²³⁹
20 ion velocity-map imaging technique,²⁴⁰ and, in the case of H atom forming reactions, high
21 resolution Rydberg H-atom TOF.²⁴¹

22
23
24
25
26
27
28
29
30
31
32
33
34
35
36
37
38
39
40
41 In many cases, the experiments are performed at fixed or at least high collision energies
42 corresponding to temperatures of often several thousands of Kelvin. As the product branch-
43 ing ratios may vary strongly with temperature, there remains room for debate regarding
44 products at intermediate to low temperatures relevant to the cold ISM. Crossed-beam ex-
45 periments thus can produce reaction dynamics data that are complementary to the kinetics
46 data obtained under thermal conditions using, for example, the CRESU technique.

47
48
49
50
51
52
53 The CMB technique has been used to great success for characterizing various elementary
54 reactions involving polyatomics, the details of which can be found in recent reviews articles
55
56
57
58
59
60

1
2
3 e.g. Pan et al.²⁴². Several classes of reactions have been tackled including direct abstraction
4 reactions, indirect insertion reactions and indirect addition elimination reactions. We limit
5 our discussions below to a few measurements made using the universal machine setup.
6
7

8
9 Much can be gained from joint crossed-beam and low-temperature kinetics studies in-
10 vestigating the same reaction. Recently, the reaction between CN and 1,3-butadiene was
11 investigated in a study which independently measured the low-temperature rate coefficients
12 using a CRESU apparatus and the reaction products under single collision conditions using
13 a crossed-beam experiment.⁸³ The low-temperature kinetics demonstrated that the reaction
14 remains fast from room temperature down to 23 K, with rate coefficients close to the gas
15 kinetic limit, indicating that the reaction proceeds potential energy surface that does not
16 have an entrance barrier. The crossed beam studies showed that the reaction proceeds via a
17 long-lived C_5H_6N complex, producing C_5H_5N and atomic hydrogen. Experiments were also
18 conducted with partially deuterated 1,3-butadienes and these indicated that the H atom loss
19 originates from a terminal carbon of 1,3-butadiene. Electronic structure calculations were
20 used to support the crossed-beam experiments and suggested that the thermodynamically
21 less favorable 1-cyano-1,3-butadiene isomer is the dominant reaction product; with less than
22 a few percent from the aromatic pyridine molecule feasible but not confirmed.
23
24
25
26
27
28
29
30
31
32
33
34
35
36

37 The authors compared these results to the reaction between C_2H and 1,3-butadiene,
38 studied by Jones et al.²³⁶. In the reaction of C_2H , benzene was found at significant fractions
39 ($30\% \pm 10\%$) in addition to the thermodynamically less stable isomer, hexa-1,3-dien-5-yne.
40 The authors suggested that, despite similar barriers to ring closure and H-atom migration,
41 the formation of benzene may be significant due to a stabilization of the C_2H addition
42 intermediate (~ 100 kJ mol⁻¹ lower in energy than the CN intermediate) followed by a
43 lower energy transition state. In addition, the addition intermediates pass through barriers
44 to cyclization of -90 kJ mol⁻¹ and -181 kJ mol⁻¹ followed by barriers to hydrogen shift
45 of $+4$ kJ mol⁻¹ and -144 kJ mol⁻¹ for the CN and C_2H reactions, respectively. These
46 results suggested that in the case of isoelectronic CN and C_2H reactions, benzene may be
47
48
49
50
51
52
53
54
55
56
57
58
59
60

1
2
3 formed favourably compared to pyridine in the ISM. This study also serves to highlight that
4 thermodynamics does not necessarily control the reaction products. In the case of CN +
5 1,3-butadiene, the thermodynamically less stable isomer 1-cyano-1,3-butadiene was favoured
6 over pyridine. As mentioned above, products formed in the C₂H + 1,3-butadiene reaction
7 were also probed at room temperature in a separate study using photoionization time-of-
8 flight mass spectrometry.²³⁵ The observation of fulvene as the major reaction product is not
9 in good agreement with the crossed-beam study of Jones *et. al.*, highlighting differences
10 between the two methods (i.e. the collisional environment) for study of reaction products
11 and suggesting the need for further investigation of the C₂H + 1,3-butadiene reaction.
12
13
14
15
16
17
18
19
20

21 Most crossed molecular beam experiments work with the beams at right angles, with
22 collisional energies of a few to a few tens of kcal mol⁻¹, where 1 kcal mol⁻¹ corresponds to
23 ~300 K. Thus most crossed-beam experiments operate at collisional energies much higher
24 than those relevant to the cold ISM. A molecular beam apparatus has been built at the
25 University of Bordeaux that enables the beam intersection angle to be varied between 90
26 and 12.5°, facilitating very low relative translational energies.^{13,243,244} These measurements
27 at low collisional energies are an important step towards understanding the reaction products
28 that can be formed under ISM conditions.
29
30
31
32
33
34
35
36
37
38

39 Microwave spectroscopy

40
41 Rotational spectroscopy can provide a high degree of molecular specificity, allowing unam-
42 biguous assignment of reaction products that possess at least a modest permanent electric
43 dipole. Traditional cavity-based microwave spectroscopic techniques are not well suited to
44 the measurement of reaction kinetics, due to the need to tune the resonant cavities to the
45 specific rotational lines of the products. This requires knowledge of the expected reaction
46 products and their rotational spectra prior to commencing the measurement. In addition,
47 their high resolution means that scanning between different rotational lines can be very slow.
48
49
50
51
52
53
54
55
56
57
58
59
60

Broadband chirped-pulse Fourier transform microwave (CP-FTMW) spectroscopy, pioneered

1
2
3 by Brooks Pate and colleagues at the University of Virginia,²⁴⁵ has revolutionized the field
4 of microwave spectroscopy and has found applications across a wide range of fields. The
5 technique enables a broadband spectrum (typically ≥ 10 GHz bandwidth) to be collected in
6 a single shot of the spectrometer, allowing high-resolution spectra to be measured several
7 orders of magnitude faster than what was previously possible.
8
9

10
11
12
13 A high bandwidth, frequency stabilized arbitrary waveform generator (AWG) is used to
14 produce a short pulse ($\sim 1 \mu\text{s}$ or less) with a frequency sweep that is linear in time, this chirped
15 pulse is upconverted to the microwave frequency range of interest and, if necessary, amplified
16 for irradiation of the sample. The molecular sample absorbs at all rotational transitions
17 within the frequency range of the chirp and is polarized by the radiation. The emitted free
18 induction decay (FID) radiation is collected, down-converted if necessary, and broadband-
19 shot-by-broadband-shot averaged in the time-domain by a high bandwidth oscilloscope or
20 digitizer card, after which the collected signal is Fourier-transformed to give the rotational
21 spectrum at MHz resolution. The use of the chirped pulse as opposed to the traditional
22 approach of narrowband scanning of the microwave frequency in a resonant cavity has led
23 to several orders of magnitude improvement in the rate of data acquisition, as the power
24 delivered to the sample is decoupled from the bandwidth, and dead time associated with
25 stepping the cavity resonance frequency is eliminated.
26
27
28
29
30
31
32
33
34
35
36
37
38

39 In a recent development, born from a collaboration between the groups of Arthur Suits
40 (Wayne State, now University of Missouri), Robert Field (MIT) and Ian Sims (University of
41 Rennes), the CPMW method has been combined with a pulsed CRESU system.^{22,246} This
42 chirped pulse in uniform flow (CPUF) experiment provides broadband spectra with MHz
43 resolution and allows monitoring, on the μs timescale, of the appearance of transient reaction
44 products. This CPMW apparatus has two main components: a chirped pulse broadband
45 microwave spectrometer and a uniform flow system utilizing a pulsed Laval nozzle. Following
46 laser initiation of the reaction, a frequency chirped microwave pulse is broadcast into the
47 pulsed uniform flow at chosen time intervals. The FID of the polarized sample is collected
48
49
50
51
52
53
54
55
56
57
58
59
60

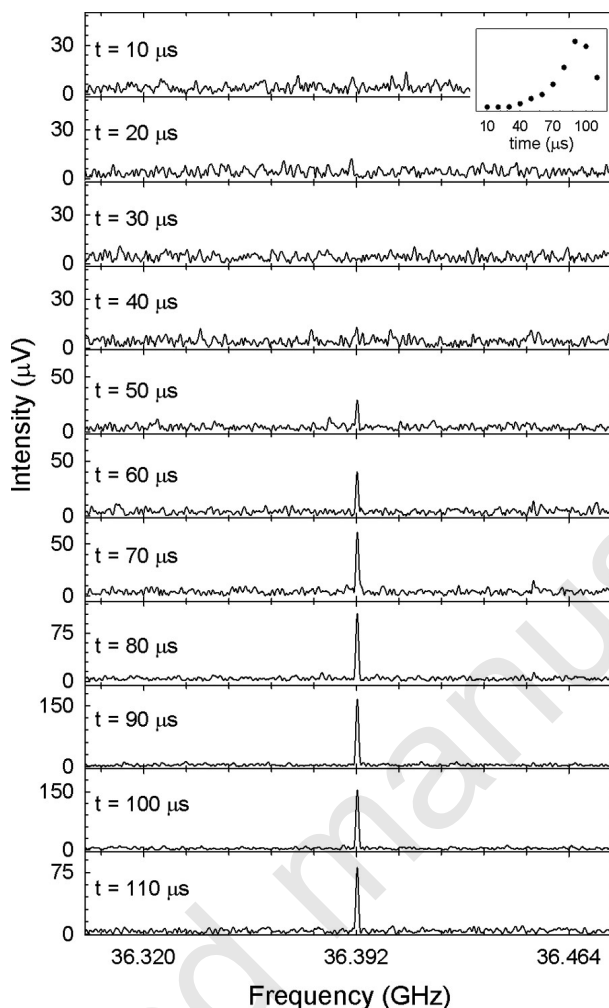


Figure 10: Spectra displaying the time evolution of the $J = 4 - 3$ rotational transition of HC_3N during the reaction of CN with C_2H_2 at 22 K. Reprinted with permission from Abeysekera et al.²⁴⁶ Copyright (2014) AIP.

at each interval through the receiver horn; the signal is then amplified and sent to a digital oscilloscope where the signal is averaged and processed in the time-domain. The FIDs are Fourier transformed to give a series of frequency domain spectra as a function of time.

This technique has been applied thus far to measure the products formed in the reactions of CN with acetylene (C_2H_2) and propyne (C_3H_4) at ~ 22 K..^{81,246} Figure 10 shows the time dependent production of the $J = 4 - 3$ rotational transition for the HC_3N product measured during the reaction of CN with C_2H_2 . The H_3CN product was seen to appear roughly 40 μs after the photolysis laser was fired. The product branching ratios were determined for

the multichannel CN + C₃H₄ reaction and are discussed below. The following pathways are energetically accessible in the reaction between CN and propyne:



Channel 14 occurs via direct abstraction whereas channels 15, 16 and 17 occur by indirect addition/elimination pathways. The potential energy surface was modeled at the CBS-QB3 level of theory, indicating *cis*- and *trans*- barrierless C1 addition complexes as well as a barrierless C2 addition complex, 18.5 kJ mol⁻¹ higher in energy than the *trans*-C1 complex. A low isomerization barrier separating the C1 and C2 complexes facilitates equilibration between these complexes prior to dissociation. The reaction was probed in a uniform flow consisting of 0.5% of the CN precursor BrCN and 1.5% propyne in a helium buffer gas. The reaction was initiated by photolysis of the BrCN at 193 nm. The AWG was used to produce a linear frequency chirp and a phase-locked dielectric resonator oscillator (PDRO) at 8.125 GHz was used to upconvert the pulse via a broadband mixer. The resulting pulse was amplified, passed through a bandpass filter and frequency multiplied 8× by a multiplication chain to obtain the 60-90 GHz frequency output. Spectra were obtained at 10 μs intervals following the laser pulse, resulting in 12 independent spectra per gas pulse, each averaged for ~62500 acquisitions.

The product column densities were calculated from the integrated line intensities and branching ratios of (12 ± 5)%, (66 ± 4)%, (22 ± 6)%, and (0 ± 8)% were determined for the HCN, HCCCN, CH₃CCCN, and CH₂CCHCN channels, respectively. The relatively small branching to the direct abstraction (HCN product) was attributed to the low colli-

1
2
3 sion energy and the strong electrophilic interaction of CN with the propyne π electrons.
4
5 The experimental results were well supported by a series of Rice-Ramsperger-Kassel-Marcus
6 (RRKM) calculations, with 48 or 65% into HCCCN and 33 or 19% into CH₃CCCN when
7
8 initiated at the C1 and C2 minima, respectively.
9
10

11 A remaining challenge in combining CP-FTMW spectroscopy with CRESU flows is the
12 balance between the high-density flows (10^{16} - 10^{17} molecules cm⁻³ buffer gas) required to
13 ensure that the species in the flow are thermalized at a well-defined temperature, and the
14 lower densities required to ensure that the microwave coherence times are long enough to
15 produce detectable signals. We discuss this challenge and the current work being undertaken
16
17 in this area in the future prospects section.
18
19
20
21
22
23

24 Infrared absorption spectroscopy

25
26 The use of infrared absorption spectroscopy for reaction product detection has a number
27 of advantages. Firstly, infrared absorption is nearly universal; that is, with the exception
28 of homonuclear diatomics, all molecules absorb in the infrared. In contrast to LIF, ab-
29 sorption spectroscopy can be used in quenching environments and can be used to detect
30 non-fluorescent species. The absorption signal is a direct and quantitative measure of the
31 absolute concentration without the need for calibration. However, absorption spectroscopy
32 notoriously suffers from inherent low sensitivity, making it difficult to detect low concen-
33 tration products in kinetically isolated reactions. Various methods have been have been
34 employed to enhance the sensitivity by increasing the effective path length (e.g. multipass
35 cells,^{247,248} cavity ring-down spectroscopy²⁴⁹⁻²⁵¹) or by reducing background noise (e.g. fre-
36 quency modulation^{252,253}).
37
38
39
40
41
42
43
44
45
46
47
48

49 These highly sensitive techniques, such as continuous wave cavity ringdown spectroscopy,
50 allow for the detection of trace concentrations at relatively short timescales and with high
51 spectral resolution but do not possess a sufficiently broad bandwidth to capture multiple
52 products. Traditional broadband techniques, for example time-resolved step-scan FTIR,
53
54
55
56
57
58
59
60

1
2
3 provide the time resolution and broad bandwidth required to detect multiple products, but
4 normally use incoherent light sources and thus require long acquisition times to achieve high
5 sensitivity.
6
7
8

9 Cavity-enhanced direct frequency comb spectroscopy (CE-DFCS) possesses a broad band-
10 width that allows detection of multiple species simultaneously, while the signal is enhanced
11 by the increased absorption length afforded by the cavity. The time resolution is limited by
12 the ringdown time of the optical cavity (which can be a few μs) while the spectral resolution
13 is limited only by the linewidth of the comb teeth, i.e. <1 MHz. This high spectral resolution
14 can access narrow rotational features of heavy molecules at low temperatures. Below, we
15 discuss application of this technique to the measurement of product-specific reaction kinetics.
16
17
18
19
20
21
22
23

24 **Infrared frequency comb spectroscopy**

25
26
27 Time-resolved frequency comb spectroscopy (TRFCS) is a promising sensitive and multi-
28 plexed technique for the observation of reactive chemical intermediates on the microsecond
29 timescale.²⁵⁴ Frequency combs are coherent light sources that emit a broad spectrum con-
30 sisting of discrete and evenly spaced narrow lines, each possessing an absolute frequency
31 measurable within the accuracy of an atomic clock. In particular, the development of fre-
32 quency combs in the mid-infrared offers unique sensitivity for the detection of trace species
33 based on fingerprint bands specific to this spectral region.^{255,256}
34
35
36
37
38
39
40

41 Recently, the group of Jun Ye at JILA used the unique sensitive, broadband, and high-
42 resolution capabilities of time-resolved CE-DFCS to probe the OH + CO reaction kinetics
43 and dynamics.²⁵⁷ This reaction is widely believed to involve a transient HOCO intermediate;
44 however, it has eluded direct detection under the thermal conditions required to extract rate
45 coefficients. The OH + CO reaction passes through a pre-reactive weakly bound OHCO
46 complex to form the energized, vibrationally excited HOCO* species. In the low-pressure
47 limit at room temperature, HOCO* primarily dissociates to reform OH + CO, with a small
48 probability of overcoming the low barrier to form H + CO₂ products. In the presence of a
49
50
51
52
53
54
55
56
57
58
59
60

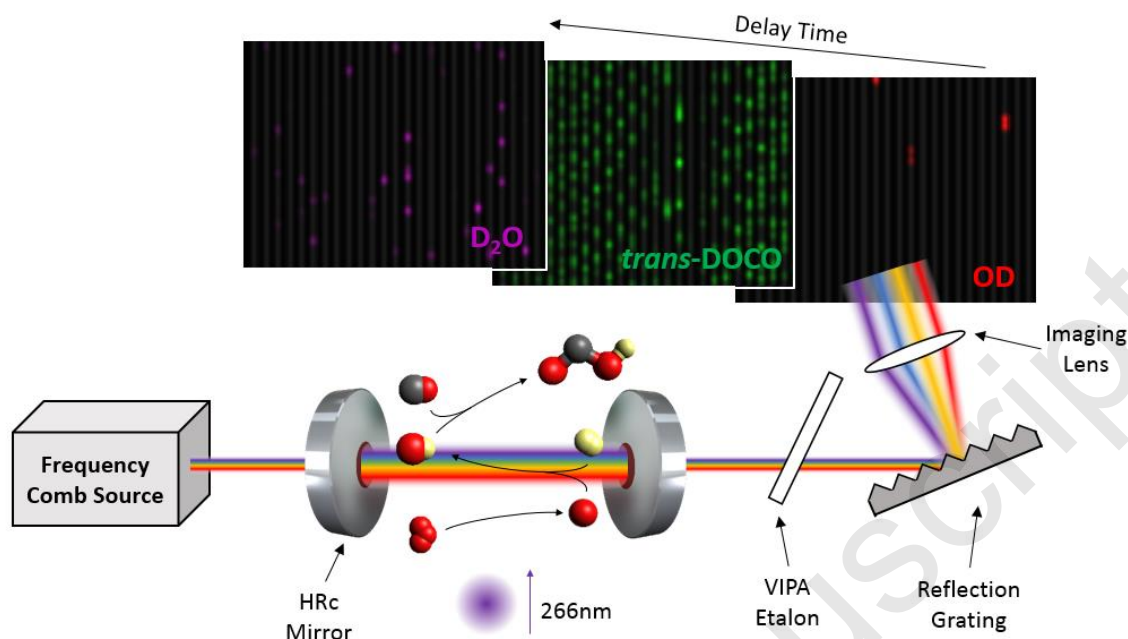


Figure 11: A schematic showing the setup of the time-resolved frequency comb spectroscopy (TRFCS) technique. A mid-IR frequency comb is coupled into an high-finesse optical cavity, consisting of two high reflectivity crystalline (HRC) mirrors. A laser pulse (266 nm) initiates the reaction. The transmitted light from the cavity is spatially dispersed by a virtually imaged phased array (VIPA) etalon and a diffraction grating and is then imaged on an InSb camera. Absorbance intensity is then recorded as a function of wavelength and delay time. The panels shown are simulated cavity absorbance images for OD (red), *trans*-DOCO (green), and D₂O (magenta). Reprinted with permission from Bjork et al.²⁵⁷ Copyright (2016) AAAS.

buffer gas, collisions can stabilize the thermalized HOCO product, diminishing the formation of H + CO₂. In the high-pressure limit, HOCO formation is the dominant channel and H + CO₂ product channel becomes negligible.

Bjork et al.²⁵⁷ observed the formation of the deuterated analogue of HOCO (DOCO), while simultaneously monitoring the OD reactant using an infrared frequency comb. Figure 11 illustrates the experimental setup used to measure the DOCO and OD species. The mid-IR frequency comb was generated using an optical parametric oscillator (OPO) whose spectrum was composed of narrow and evenly spaced comb teeth. The transmitted light covered a bandwidth of $\sim 65 \text{ cm}^{-1}$, corresponding to around 7100 comb teeth. This light was dispersed in two dimensions by a virtually imaged phased array (VIPA) etalon and

1
2
3 a diffraction grating and was imaged using a InSb camera. The absorption spectra were
4 constructed as a function of time, and were used to obtain the absolute concentrations
5 using known line intensities. Using this technique, they observed unambiguous low-pressure
6 dependence of the rate coefficients on the bath gas pressure, and thus were able to confirm
7 the HOCO formation mechanism and determine its yield.
8
9
10
11
12

13 In a complementary study, they measured the kinetics of the $D + CO_2$ channel at room
14 temperature.²⁵⁸ The time-dependence of OD and CO_2 concentrations were used to determine
15 the product channel-specific rates as well as their dependence on pressure and bath gas.
16 These measurements, in combination with the DOCO formation rate, provided the branching
17 channel yields for the DOCO and $D + CO_2$ products of OD + CO reaction in the low-pressure
18 limit. They derived product yields in N_2 bath gas at 75 Torr of $27 \pm 11\%$ for the DOCO
19 channel and $73 \pm 16\%$ for $D + CO_2$; while in a CO bath gas, the product channel yields were
20 roughly equivalent with of $47 \pm 10\%$ and $53 \pm 7\%$ for DOCO and $D + CO_2$, respectively.
21
22
23
24
25
26
27
28
29
30

31 **Conclusions and future prospects for low temperature** 32 **gas-phase kinetics** 33 34 35 36 37

38 In this review, we have discussed laboratory efforts to measure elementary reactions that may
39 play a role in the formation of complex organic molecules in the ISM, with particular empha-
40 sis on experiments to measure directly product branching ratios. Significant advances are
41 being made due to collaborative efforts between observational, computational, and labora-
42 tory astrochemists and it is clear that these will be necessary in order to explain the presence
43 of the increasing number of molecules that are being observed. There are three significant
44 gaps in the available gas-phase laboratory data relevant to COM formation. Firstly, there
45 remain few data for gas-phase reactions measured at the temperatures of cold cores. This
46 is a particular challenge for reactions involving volatile organic species which can condense
47 and dimerize at low temperature and therefore their rate coefficients cannot be measured
48
49
50
51
52
53
54
55
56
57
58
59
60

1
2
3 accurately under pseudo-first order conditions. The second gap is due to difficulties associ-
4 ated with making kinetic measurements for reactions where both species are unstable such
5 as those involving only ions and radicals. This difficulty extends to the solid phase, where
6 laboratory measurements involving radical reactions are particularly sparse. The third major
7 gap in laboratory data involves the measurement of reaction products and their branching
8 ratios at low temperatures, and is particularly pertinent to reactions involving COMs, which
9 are often multichannel. This is an active area of research within the community and large
10 advances are expected to be made in the coming years with new techniques available capable
11 of product detection. Below we discuss some perspectives for the measurement of product-
12 specific reaction kinetics, highlighting new techniques that are currently being developed.
13
14
15
16
17
18
19
20
21
22
23

24 **Ionization-based techniques for measuring product-specific reaction** 25 **kinetics** 26 27 28 29

30 Mass spectrometric methods are particularly promising for the measurement of product-
31 specific reaction kinetics, particularly when combined with photoionization spectroscopy al-
32 lowing one to distinguish between isomers of products. A pulsed version of the CRESU
33 technique has been developed in Rennes in collaboration with the DESIRS beamline group
34 at SOLEIL. This technique, named CRESUSOL, aims to identify the product of reactions
35 below 100 K and estimate their branching ratios. The CRESU chamber is coupled to a
36 photoelectron-photoioncoincidence (PEPICO) mass spectrometer to probe reactants and
37 products of reaction after threshold photoionisation by the VUV beamline of the SOLEIL
38 synchrotron. This technique is currently being used to detect reaction products and derive
39 branching ratios at very low temperatures, down to 20 K.
40
41
42
43
44
45
46
47
48
49
50
51
52
53
54
55
56
57
58
59
60

Spectroscopic techniques for measuring product-specific reaction kinetics

The combination of the CRESU technique with rotational spectroscopy will significantly improve the measurement of product specific reaction kinetics due to its high degree of molecular specificity. In addition to the CPUF technique of the Suits group discussed above, CPUF apparatuses are currently being built in Bordeaux and in Rennes. A key difficulty in studying reaction kinetics using CPUF is the pressure balance required to maintain thermalization through buffer gas collisions while avoiding too severe collisional dephasing and thus reduction in FID signal intensity and duration, which could reduce the sensitivity of the technique to below what is needed to observe low concentration products. One way to mitigate this problem is by sampling the supersonic flow via a second expansion and performing the CPMW detection at lower pressures.

A particular advantage of using rotational spectroscopy to study cold reactions is that the spectral information about reaction products that is obtained during the experiments can be directly compared with spectra obtained from radio telescope observatories operating at the microwave and millimeter-wave frequencies. As a state-specific technique, information on, for example, vibrationally excited products is available.

The use of infrared spectroscopic techniques can likewise provide spectra directly comparable to astronomical observations, for example, spectra taken using space-based infrared observatories. The use of infrared frequency-combs to measure reaction products can provide data that will be of use to the next generation infrared observatories like the *James Webb Space Telescope* (JWST). The CE-DFCS technique has inherent spectral congestion for large molecules at room temperature. This problem could be overcome by implementing CE-DFCS with techniques that produce a continuous source of cooled molecules such as CRESU flows or buffer gas cooling.²⁵⁹ The use of buffer gas cooling has recently been used to great success to rotationally resolve the 8.5 μm band of buckminsterfullerene (C_{60}),²⁶⁰ providing a glimpse of the power of the CE-DFCS technique for the study of cold molecules.

1
2
3 The application of frequency combs to study chemical reaction kinetics will likewise con-
4 tinue to grow with technical developments in higher power combs as well as their extension
5 to longer wavelengths.
6
7
8
9

10 11 Acknowledgement

12
13
14 The authors thank Lucile Rutowski, Olivier Durif, Sébastien Le Picard, Brian Hays, Sophie
15 Carles and Divita Gupta for helpful discussions. The authors thank especially André Canosa
16 for helpful discussion regarding Table 1. The authors also thank two anonymous reviewers for
17 helpful comments that greatly improved the quality of the manuscript. The authors acknowl-
18 edge funding from the European Research Council (ERC) under the European Union’s Hori-
19 zon 2020 research and innovation programme under grant agreement 695724-CRESUCHIRP
20 and under the Marie Skłodowska-Curie grant agreement 845165-MIRAGE.
21
22
23
24
25
26
27
28
29

30 31 References

- 32
33 (1) McGuire, B. A. 2018 Census of Interstellar, Circumstellar, Extragalactic, Protoplan-
34 etary Disk, and Exoplanetary Molecules. *ApJS* **2018**, *239*, 17.
- 35
36 (2) Bacmann, A.; Taquet, V.; Faure, A.; Kahane, C.; Ceccarelli, C. Detection of Complex
37 Organic Molecules in a Prestellar Core: A New Challenge for Astrochemical Models.
38 *Astron. Astrophys.* **2012**, *541*, L12.
- 39
40 (3) van Dishoeck, E. F.; Blake, G. A. Chemical Evolution of Star-forming Regions. *Annu.*
41 *Rev. Astron. Astrophys.* **1998**, *36*, 317–368.
- 42
43 (4) Benson, P. J.; Myers, P. C. A Survey for Dense Cores in Dark Clouds. *ApJS* **1989**,
44 *71*, 89.
- 45
46 (5) Herbst, E.; Klemperer, W. The Formation and Depletion of Molecules in Dense Inter-
47 stellar Clouds. *ApJ* **1973**, *185*, 505.
- 48
49 (6) Garrod, R. T.; Widicus Weaver, S. L. Simulations of Hot-Core Chemistry. *Chem. Rev.*
50 **2013**, *113*, 8939–8960.
- 51
52
53 (7) Herbst, E.; Lee, H.-H.; Howe, D. A.; Millar, T. J. The Effect of Rapid Neutral-Neutral
54 Reactions on Chemical Models of Dense Interstellar Clouds. *MNRAS* **1994**, *268*, 335–
55 344.
56
57
58
59
60

- 1
2
3 (8) Gerlich, D.; Horning, S. Experimental Investigations of Radiative Association Processes As Related to Interstellar Chemistry. *Chem. Rev.* **1992**, *92*, 1509–1539.
- 4
5
6 (9) Qi, C.; Oberg, K. I.; Wilner, D. J.; D'Alessio, P.; Bergin, E.; Andrews, S. M.;
7 Blake, G. A.; Hogerheijde, M. R.; van Dishoeck, E. F. Imaging of the CO Snow
8 Line in a Solar Nebula Analog. *Science* **2013**, *341*, 630–632.
- 9
10 (10) van't Hoff, M. L. R.; Walsh, C.; Kama, M.; Facchini, S.; van Dishoeck, E. F. Robust-
11 ness of N_2H^+ As Tracer of the CO Snowline. *Astron. Astrophys.* **2017**, *599*, A101.
- 12
13 (11) Sims, I. R.; Smith, I. W. M. Rate Constants for the Radical-Radical Reaction between
14 CN and O_2 at Temperatures down to 99 K. *Chem. Phys. Lett.* **1988**, *151*, 481–484.
- 15
16 (12) Frost, M. J.; Sharkey, P.; Smith, I. W. M. Reaction between Hydroxyl (Deuteroxyl)
17 Radicals and Carbon Monoxide at Temperatures down to 80 K: Experiment and The-
18 ory. *J. Phys. Chem.* **1993**, *97*, 12254–12259.
- 19
20 (13) Berteloite, C.; Lara, M.; Bergeat, A.; Le Picard, S. D.; Dayou, F.; Hickson, K. M.;
21 Canosa, A.; Naulin, C.; Launay, J. M.; Sims, I. R.; Costes, M. Kinetics and Dynamics
22 of the $\text{S}(^1\text{D}_2)+\text{H}_2 \rightarrow \text{SH} + \text{H}$ Reaction at Very Low Temperatures and Collision
23 Energies. *Phys. Rev. Lett.* **2010**, *105*, 203201.
- 24
25 (14) Ocaña, A. J.; Blázquez, S.; Potapov, A.; Ballesteros, B.; Canosa, A.; Antiñolo, M.;
26 Vereecken, L.; Albaladejo, J.; Jiménez, E. Gas-phase Reactivity of CH_3OH toward
27 OH at Interstellar Temperatures (11.7–177.5 K): Experimental and Theoretical Study.
28 *PCCP* **2019**, *21*, 6942–6957.
- 29
30 (15) Sims, I. R.; Queffelec, J.-L.; Defrance, A.; Rebrion-Rowe, C.; Travers, D.; Bocherel, P.;
31 Rowe, B. R.; Smith, I. W. M. Ultralow Temperature Kinetics of Neutral-Neutral
32 Reactions. the Technique and Results for the Reactions $\text{CN} + \text{O}_2$ down to 13 K and
33 $\text{CN}+\text{NH}_3$ down to 25 K. *J. Chem. Phys.* **1994**, *100*, 4229–4241.
- 34
35 (16) James, P. L.; Sims, I. R.; Smith, I. W. Total and State-to-state Rate Coefficients for
36 Rotational Energy Transfer in Collisions between $\text{NO}(X^2\Pi)$ and He at Temperatures
37 down to 15 K. *Chem. Phys. Lett.* **1997**, *272*, 412–418.
- 38
39 (17) Daugey, N.; Caubet, P.; Retail, B.; Costes, M.; Bergeat, A.; Dorthe, G. Kinetic Mea-
40 surements on Methylidyne Radical Reactions with Several Hydrocarbons at Low Tem-
41 peratures. *PCCP* **2005**, *7*, 2921–2927.
- 42
43 (18) Atkinson, D. B.; Smith, M. A. Design and Characterization of Pulsed Uniform Super-
44 sonic Expansions for Chemical Applications. *Rev. Sci. Instrum.* **1995**, *66*, 4434–4446.
- 45
46 (19) Lee, S.; Hoobler, R. J.; Leone, S. R. A Pulsed Laval Nozzle Apparatus with Laser
47 Ionization Mass Spectroscopy for Direct Measurements of Rate Coefficients at Low
48 Temperatures with Condensable Gases. *Rev. Sci. Instrum.* **2000**, *71*, 1816–1823.
- 49
50
51
52
53
54
55
56
57
58
59
60

- 1
2
3
4
5
6
7
8
9
10
11
12
13
14
15
16
17
18
19
20
21
22
23
24
25
26
27
28
29
30
31
32
33
34
35
36
37
38
39
40
41
42
43
44
45
46
47
48
49
50
51
52
53
54
55
56
57
58
59
60
- (20) Spangenberg, T.; Köhler, S.; Hansmann, B.; Wachsmuth, U.; Abel, B.; Smith, M. A. Low-temperature Reactions of OH Radicals with Propene and Isoprene in Pulsed Laval Nozzle Expansions. *J. Phys. Chem. A* **2004**, *108*, 7527–7534.
- (21) Taylor, S. E.; Goddard, A.; Blitz, M. A.; Cleary, P. A.; Heard, D. E. Pulsed Laval Nozzle Study of the Kinetics of OH with Unsaturated Hydrocarbons at Very Low Temperatures. *PCCP* **2008**, *10*, 422–437.
- (22) Oldham, J. M.; Abeysekera, C.; Joalland, B.; Zack, L. N.; Prozument, K.; Sims, I. R.; Park, G. B.; Field, R. W.; Suits, A. G. A Chirped-Pulse Fourier-transform Microwave/pulsed Uniform Flow Spectrometer. i. the Low-temperature Flow System. *J. Chem. Phys.* **2014**, *141*, 154202.
- (23) Cheikh Sid Ely, S.; Morales, S. B.; Guillemin, J. C.; Klippenstein, S. J.; Sims, I. R. Low Temperature Rate Coefficients for the Reaction $\text{CN} + \text{HC}_3\text{N}$. *J. Phys. Chem. A* **2013**, *117*, 12155–12164.
- (24) Jiménez, E.; Ballesteros, B.; Canosa, A.; Townsend, T. M.; Maigler, F. J.; Napal, V.; Rowe, B. R.; Albaladejo, J. Development of a Pulsed Uniform Supersonic Gas Expansion System Based on an Aerodynamic Chopper for Gas Phase Reaction Kinetic Studies at Ultra-low Temperatures. *Rev. Sci. Instrum.* **2015**, *86*, 045108.
- (25) Douglas, K.; Blitz, M. A.; Feng, W.; Heard, D. E.; Plane, J. M. C.; Slater, E.; Willacy, K.; Seakins, P. W. Low Temperature Studies of the Removal Reactions of $^1\text{CH}_2$ with Particular Relevance to the Atmosphere of Titan. *Icarus* **2018**, *303*, 10–21.
- (26) Douglas, K. M.; Blitz, M. A.; Feng, W.; Heard, D. E.; Plane, J. M. C.; Rashid, H.; Seakins, P. W. Low Temperature Studies of the Rate Coefficients and Branching Ratios of Reactive Loss vs Quenching for the Reactions of $^1\text{CH}_2$ with C_2H_6 , C_2H_4 , C_2H_2 . *Icarus* **2019**, *321*, 752–766.
- (27) Herbst, E.; Klemperer, W. The Formation and Depletion of Molecules in Dense Interstellar Clouds. *ApJ* **1973**, *185*, 505–534.
- (28) Bohme, D. K.; Rakshit, A. B.; Schiff, H. I. Reactions of $^{12}\text{C}^+$ with Hydrocarbons at 296 K: Carbon-Carbon Bond Formation. *Chem. Phys. Lett.* **1982**, *93*, 592–597.
- (29) Smith, D.; Adams, N. G. A Brief Review of Interstellar Ion Chemistry. *J. Chem. Soc., Faraday Trans. 2* **1989**, *85*, 1613–1630.
- (30) Martinez, O.; Betts, N. B.; Villano, S. M.; Eyet, N.; Snow, T. P.; Bierbaum, V. M. Gas Phase Study of C^+ reactions of Interstellar Relevance. *ApJ* **2008**, *686*, 1486–1492.
- (31) Su, T.; Chesnavich, W. J. Parametrization of the Ion-Polar Molecule Collision Rate Constant by Trajectory Calculations. *J. Chem. Phys.* **1982**, *76*, 5183–5185.
- (32) McMahon, T. B.; Beauchamp, J. L. A Versatile Trapped Ion Cell for Ion Cyclotron Resonance Spectroscopy. *Rev. Sci. Instrum.* **1972**, *43*, 509–512.

- 1
2
3
4
5
6
7
8
9
10
11
12
13
14
15
16
17
18
19
20
21
22
23
24
25
26
27
28
29
30
31
32
33
34
35
36
37
38
39
40
41
42
43
44
45
46
47
48
49
50
51
52
53
54
55
56
57
58
59
60
- (33) Barlow, S. E.; Dunn, G. H.; Schauer, M. Radiative Association of CH_3^+ and H_2 at 13 K. *Phys. Rev. Lett.* **1984**, *52*, 902–905.
- (34) Barlow, S. E.; Luine, J. A.; Dunn, G. H. Measurement of Ion/Molecule Reactions between 10 and 20 K. *Int. J. Mass Spectrom. Ion Process.* **1986**, *74*, 97–128.
- (35) Schauer, M. M.; Jefferts, S. R.; Barlow, S. E.; Dunn, G. H. Reactions of H_2 with He^+ at Temperatures below 40 K. *J. Chem. Phys.* **1989**, *91*, 4593–4596.
- (36) Gerlich, D. Ion-neutral Collisions in a 22-pole Trap at Very Low Energies. *Phys. Scr.* **1995**, *T59*, 256–263.
- (37) Borodi, G.; Luca, A.; Gerlich, D. Reactions of CO_2^+ with H, H_2 and Deuterated Analogues. *Int. J. Mass Spectrom.* **2009**, *280*, 218–225.
- (38) Fehsenfeld, F. C.; Schmeltekopf, A. L.; Goldan, P. D.; Schiff, H. I.; Ferguson, E. E. Thermal Energy Ion-neutral Reaction Rates. i. Some Reactions of Helium Ions. *J. Chem. Phys.* **1966**, *44*, 4087–4094.
- (39) Dunkin, D. B.; Fehsenfeld, F. C.; Schmeltekopf, A. L.; Ferguson, E. E. Ion-Molecule Reaction Studies from 300° to 600°K in a Temperature-controlled Flowing Afterglow System. *J. Chem. Phys.* **1968**, *49*, 1365–1371.
- (40) Adams, N. G.; Smith, D. The Selected Ion Flow Tube (SIFT): A Technique for Studying Ion-Neutral Reactions. *Int. J. Mass Spectrom. Ion Phys.* **1976**, *21*, 349–359.
- (41) Snow, T. P.; Bierbaum, V. M. Ion Chemistry in the Interstellar Medium. *Annu. Rev. Anal. Chem.* **2008**, *1*, 229–259.
- (42) Larsson, M. Atomic and Molecular Physics with Ion Storage Rings. *Reports on Progress in Physics* **1995**, *58*, 1267–1319.
- (43) Geppert, W. D.; Larsson, M. Dissociative Recombination in the Interstellar Medium and Planetary Ionospheres. *Molecular Physics* **2008**, *106*, 2199–2226.
- (44) Rowe, B. R.; Dupeyrat, G.; Marquette, J. B.; Gaucherel, P. Study of the Reactions $\text{N}_2^+ + 2\text{N}_2 \rightarrow \text{N}_4^+ + \text{N}_2$ and $\text{O}_2^+ + 2\text{O}_2 \rightarrow \text{O}_4^+ + \text{O}_2$ from 20 to 160 K by the CRESU Technique. *J. Chem. Phys.* **1984**, *80*, 4915–4921.
- (45) Rowe, B. R.; Marquette, J.-B.; Rebrion, C. Mass-Selected Ion-Molecule Reactions at Very Low Temperatures: The CRESUS Apparatus. *J. Chem. Soc., Faraday Trans. 2* **1989**, *85*, 1631–1641.
- (46) Rowe, B. R.; Dupeyrat, G.; Marquette, J. B.; Smith, D.; Adams, N. G.; Ferguson, E. E. The Reaction $\text{O}_2^+ + \text{CH}_4 \rightarrow \text{CH}_3\text{O}_2^+ + \text{H}$ Studied from 20 to 560 K in a Supersonic Jet and in a SIFT. *J. Chem. Phys.* **1984**, *80*, 241–245.
- (47) Marquette, J.; Rebrion, C.; Rowe, B. Proton Transfer Reactions of H_3^+ with Molecular Neutrals at 30 K. *Astron. Astrophys.* **1989**, *213*, L29–L32.

- 1
2
3
4
5
6
7
8
9
10
11
12
13
14
15
16
17
18
19
20
21
22
23
24
25
26
27
28
29
30
31
32
33
34
35
36
37
38
39
40
41
42
43
44
45
46
47
48
49
50
51
52
53
54
55
56
57
58
59
60
- (48) Rowe, B.; Marquette, J.; Dupeyrat, G.; Ferguson, E. Reactions of He⁺ and N⁺ Ions with Several Molecules at 8 K. *Chem. Phys. Lett.* **1985**, *113*, 403–406.
- (49) Rebrion, C.; Marquette, J.; Rowe, B.; Adams, N.; Smith, D. Low-temperature Reactions of Some Atomic Ions with Molecules of Large Quadrupole Moment: C₆F₆ and c-C₆H₁₂. *Chem. Phys. Lett.* **1987**, *136*, 495–500.
- (50) Rebrion, C.; Marquette, J.; Rowe, B.; Clary, D. Low-temperature Reactions of He⁺ and C⁺ with HCl, SO₂ and H₂S. *Chem. Phys. Lett.* **1988**, *143*, 130–134.
- (51) Marquette, J. B.; Rowe, B. R.; Dupeyrat, G.; Poissant, G.; Rebrion, C. Ion-polar-molecule Reactions: A CRESU Study of He⁺, C⁺, N⁺ + H₂O, NH₃ at 27, 68 and 163 K. *Chem. Phys. Lett.* **1985**, *122*, 431–435.
- (52) Rebrion, C.; Rowe, B. R.; Marquette, J. B. Reactions of Ar⁺ with H₂, N₂, O₂, and CO at 20, 30, and 70 K. *J. Chem. Phys.* **1989**, *91*, 6142–6147.
- (53) Dupeyrat, G.; Marquette, J.; Rowe, B.; Rebrion, C. Reactions of Ar²⁺ (³P) Ions with Some Neutrals at 30 K. *Int. J. Mass Spectrom. Ion Process.* **1991**, *103*, 149–156.
- (54) Gaucherel, P.; Marquette, J. B.; Rebrion, C.; Poissant, G.; Dupeyrat, G.; Rowe, B. R. Temperature Dependence of Slow Charge-Exchange Reactions: N₂⁺+O₂ from 8 to 163 K. *Chem. Phys. Lett.* **1986**, *132*, 63–66.
- (55) Speck, T.; Mostefaoui, T. I.; Travers, D.; Rowe, B. R. Pulsed Injection of Ions into the CRESU Experiment. *Int. J. Mass Spec.* **2001**, *208*, 73–80.
- (56) Le Garrec, J. L.; Lepage, V.; Rowe, B.; Ferguson, E. The Temperature Dependence of the Rate Constant for O⁺ + NO → NO⁺ + O from 23 to 30000 K. *Chem. Phys. Lett.* **1997**, *270*, 66–70.
- (57) Rowe, B. R.; Canosa, A.; Le Page, V. FALP and CRESU Studies of Ionic Reactions. *Int. J. Mass Spectromet. Ion Process.* **1995**, *149-150*, 573–596.
- (58) Hamon, S.; Mitchell, J.; Rowe, B. Low-temperature Measurements of the Atomic Association Reaction Ar⁺ + 2Ar → Ar²⁺ + Ar. *Chem. Phys. Lett.* **1998**, *288*, 523–526.
- (59) Hamon, S.; Speck, T.; Mitchell, J. B. A.; Rowe, B. R.; Troe, J. Experimental and Theoretical Study of the Ion-Molecule Association Reaction NH₄⁺ + NH₃(+M) → N₂H₇⁺(+M). *J. Chem. Phys.* **2002**, *117*, 2557–2567.
- (60) Hamon, S.; Speck, T.; Mitchell, J. B. A.; Rowe, B.; Troe, J. Experimental and Modeling Study of the Ion-Molecule Association Reaction H₃O⁺+H₂O (+M) → H₅O₂⁺(+M). *J. Chem. Phys.* **2005**, *123*, 054303.
- (61) Douglas, A. E.; Herzberg, G. Note on CH⁺ in Interstellar Space and in the Laboratory. *ApJ* **1941**, *94*, 381.
- (62) McCarthy, M. C.; Gottlieb, C. A.; Gupta, H.; Thaddeus, P. Laboratory and Astronomical Identification of the Negative Molecular Ion C₆H⁻. *ApJ* **2006**, *652*, L141–L144.

- 1
2
3
4 (63) Le Garrec, J.-L.; Rowe, B. R.; Queffelec, J. L.; Mitchell, J. B. A.; Clary, D. C. Temperature Dependence of the Rate Constant for the $\text{Cl}^- + \text{CH}_3\text{Br}$ Reaction down to 23 K. *J. Chem. Phys.* **1997**, *107*, 1021.
5
6
7
8 (64) Cernicharo, J.; Guélin, M.; Agúndez, M.; Kawaguchi, K.; McCarthy, M.; Thaddeus, P. Astronomical Detection of C_4H^- , the Second Interstellar Anion. *Astron. Astrophys.* **2007**, *467*, L37–L40.
9
10
11
12 (65) Brünken, S.; Gupta, H.; Gottlieb, C. A.; McCarthy, M. C.; Thaddeus, P. Detection of the Carbon Chain Negative Ion C_8H^- in TMC-1. *ApJ* **2007**, *664*, L43–L46.
13
14
15
16 (66) Thaddeus, P.; Gottlieb, C. A.; Gupta, H.; Brünken, S.; McCarthy, M. C.; Agúndez, M.; Guélin, M.; Cernicharo, J. Laboratory and Astronomical Detection of the Negative Molecular Ion C_3N^- . *ApJ* **2008**, *677*, 1132–1139.
17
18
19
20 (67) Cernicharo, J.; Guélin, M.; Agúndez, M.; McCarthy, M. C.; Thaddeus, P. Detection of C_5N^- and Vibrationally Excited C_6H in IRC +10216. *ApJ* **2008**, *688*, L83–L86.
21
22
23
24 (68) Agúndez, M.; Cernicharo, J.; Guélin, M.; Kahane, C.; Roueff, E.; Klos, J.; Aoziz, F. J.; Lique, F.; Marcelino, N.; Goicoechea, J. R.; González García, M.; Gottlieb, C. A.; McCarthy, M. C.; Thaddeus, P. Astronomical Identification of CN^- , the Smallest Observed Molecular Anion. *Astron. Astrophys.* **2010**, *517*, L2.
25
26
27
28 (69) Biennier, L.; Carles, S.; Cordier, D.; Guillemin, J.-C.; Le Picard, S. D.; Faure, A. Low Temperature Reaction Kinetics of $\text{CN}^- + \text{HC}_3\text{N}$ and Implications for the Growth of Anions in Titan's Atmosphere. *Icarus* **2014**, *227*, 123–131.
29
30
31
32
33 (70) Bourgalais, J.; Jamal-Eddine, N.; Joalland, B.; Capron, M.; Balaganesh, M.; Guillemin, J.-C.; Le Picard, S. D.; Faure, A.; Carles, S.; Biennier, L. Elusive Anion Growth in Titan's Atmosphere: Low Temperature Kinetics of the $\text{C}_3\text{N}^- + \text{HC}_3\text{N}$ Reaction. *Icarus* **2016**, *271*, 194–201.
34
35
36
37
38 (71) Joalland, B.; Jamal-Eddine, N.; Klos, J.; Lique, F.; Trolez, Y.; Guillemin, J.-C.; Carles, S.; Biennier, L. Low-temperature Reactivity of $\text{C}_{2n+1}\text{N}^-$ Anions with Polar Molecules. *J. Phys. Chem. Lett.* **2016**, *7*, 2957–2961.
39
40
41
42
43 (72) Smith, I. W. M.; Rowe, B. R. Reaction Kinetics at Very Low Temperatures: Laboratory Studies and Interstellar Chemistry. *Acc. Chem. Res.* **2000**, *33*, 261–268.
44
45
46
47 (73) Chastaing, D.; James, P. L.; Sims, I. R.; Smith, I. W. M. Neutral-Neutral Reactions at the Temperatures of Interstellar Clouds Rate Coefficients for Reactions of C_2H Radicals with O_2 , C_2H_2 , C_2H_4 and C_3H_6 down to 15 K. *Faraday Discuss.* **1998**, *109*, 165–181.
48
49
50
51
52 (74) Barlow, S. E.; van Doren, J. M.; Depuy, C. H.; Bierbaum, V. M.; Dotan, I.; Ferguson, E. E.; Adams, N. G.; Smith, D.; Rowe, B. R.; Marquette, J. B.; Dupeyrat, G.; Durup-Ferguson, M. Studies of the Reaction of O_2^+ with Deuterated Methanes. *J. Chem. Phys.* **1986**, *85*, 3851–3859.
53
54
55
56
57
58
59
60

- 1
2
3
4 (75) Joalland, B.; Jamal-Eddine, N.; Papanastasiou, D.; Lekkas, A.; Carles, S.; Biennier, L.
5 A Mass-selective Ion Transfer Line Coupled with a Uniform Supersonic Flow for Study-
6 ing Ion-molecule Reactions at Low Temperatures. *J. Chem. Phys.* **2019**, *150*, 164201.
7
8 (76) Marquette, J. B.; Rebrion, C.; Rowe, B. R. Reactions of $N^+(^3P)$ Ions with Normal,
9 Para, and Deuterated Hydrogens at Low Temperatures. *J. Chem. Phys.* **1988**, *89*,
10 2041–2047.
11
12 (77) Rebrion, C.; Marquette, J. B.; Rowe, B. R.; Chakravarty, C.; Clary, D. C.;
13 Adams, N. G.; Smith, D. Reactions of N^+ and H_3^+ with the Structural Isomers of
14 Dichloroethene. *J. Phys. Chem.* **1988**, *92*, 6572–6574.
15
16 (78) Le Garrec, J.-L.; Carles, S.; Speck, T.; Mitchell, J. B. A.; Rowe, B. R.; Ferguson, E. E.
17 The Ion-molecule Reaction of O^+ with N_2 Measured Down to 23 K. *Chem. Phys. Lett.*
18 **2003**, *372*, 485–488.
19
20 (79) Sims, I. R.; Queffelec, J. L.; Defrance, A.; Rebrion-Rowe, C.; Travers, D.; Rowe, B. R.;
21 Smith, I. W. M. Ultra-low Temperature Kinetics of Neutral-Neutral Reactions: The
22 Reaction $CN + O_2$ down to 26 K. *J. Chem. Phys.* **1992**, *97*, 8798–8800.
23
24 (80) Carty, D.; Le Page, V.; Sims, I. R.; Smith, I. W. M. Low Temperature Rate Coefficients
25 for the Reactions of CN and C_2H Radicals with Allene ($CH_2=C=CH_2$) and Methyl
26 Acetylene (CH_3CCH). *Chem. Phys. Lett.* **2001**, *344*, 310–316.
27
28 (81) Abeysekera, C.; Joalland, B.; Ariyasingha, N.; Zack, L. N.; Sims, I. R.; Field, R. W.;
29 Suits, A. G. Product Branching in the Low Temperature Reaction of CN with Propyne
30 by Chirped-Pulse Microwave Spectroscopy in a Uniform Supersonic Flow. *J. Phys.*
31 *Chem. Lett* **2015**, *6*, 1599–1604.
32
33 (82) Morales, S. B.; Le Picard, S. D.; Canosa, A.; Sims, I. R. Experimental Measurements
34 of Low Temperature Rate Coefficients for Neutral-Neutral Reactions of Interest for
35 Atmospheric Chemistry of Titan, Pluto and Triton: Reactions of the CN Radical.
36 *Faraday Discuss.* **2010**, *147*, 155.
37
38 (83) Morales, S. B.; Bennett, C. J.; Le Picard, S. D.; Canosa, A.; Sims, I. R.; Sun, B. J.;
39 Chen, P. H.; Chang, A. H. H.; Kislov, V. V.; Mebel, A. M.; Gu, X.; Zhang, F.;
40 Maksyutenko, P.; Kaiser, R. I. A Crossed Molecular Beam, Low-temperature Ki-
41 netics, and Theoretical Investigation of the Reaction of the Cyano Radical (CN)
42 with 1,3-butadiene (C_4H_6): A Route to Complex Nitrogen-bearing Molecules in Low-
43 temperature Extraterrestrial Environments. *ApJ* **2011**, *742*, 26.
44
45 (84) Sleiman, C.; El Dib, G.; Rosi, M.; Skouteris, D.; Balucani, N.; Canosa, A. Low Tem-
46 perature Kinetics and Theoretical Studies of the Reaction $CN + CH_3NH_2$: A Potential
47 Source of Cyanamide and Methyl Cyanamide in the Interstellar Medium. *PCCP* **2018**,
48 *20*, 5478–5489.
49
50 (85) Sleiman, C.; El Dib, G.; Talbi, D.; Canosa, A. Gas Phase Reactivity of the CN Radical
51 with Methyl Amines at Low Temperatures (23–297 K): A Combined Experimental and
52 Theoretical Investigation. *ACS Earth Sp. Chem.* **2018**, *2*, 1047–1057.
53
54
55
56
57
58
59
60

- 1
2
3
4
5
6
7
8
9
10
11
12
13
14
15
16
17
18
19
20
21
22
23
24
25
26
27
28
29
30
31
32
33
34
35
36
37
38
39
40
41
42
43
44
45
46
47
48
49
50
51
52
53
54
55
56
57
58
59
60
- (86) Sims, I. R.; Queffelec, J.-L.; Travers, D.; Rowe, B. R.; Herbert, L. B.; Karthäuser, J.; Smith, I. W. Rate Constants for the Reactions of CN with Hydrocarbons at Low and Ultra-low Temperatures. *Chem. Phys. Lett.* **1993**, *211*, 461–468.
- (87) Trevitt, A. J.; Goulay, F.; Taatjes, C. A.; Osborn, D. L.; Leone, S. R. Reactions of the CN Radical with Benzene and Toluene: Product Detection and Low-temperature Kinetics. *J. Phys. Chem. A* **2010**, *114*, 1749–1755.
- (88) Bennett, C. J.; Morales, S. B.; Le Picard, S. D.; Canosa, A.; Sims, I. R.; Shih, Y. H.; Chang, A. H. H.; Gu, X.; Zhang, F.; Kaiser, R. I. A Chemical Dynamics, Kinetics, and Theoretical Study on the Reaction of the Cyano Radical (CN; $X^2\Sigma^+$) with Phenylacetylene (C_6H_5CCH ; X^1A_1). *PCCP* **2010**, *12*, 8737–8749.
- (89) Shannon, R. J.; Blitz, M. A.; Goddard, A.; Heard, D. E. Accelerated Chemistry in the Reaction between the Hydroxyl Radical and Methanol at Interstellar Temperatures Facilitated by Tunnelling. *Nat. Chem.* **2013**, *5*, 745–749.
- (90) Gómez-Martín, J. C.; Caravan, R. L.; Blitz, M. A.; Heard, D. E.; Plane, J. M. C. Low Temperature Kinetics of the $CH_3OH + OH$ Reaction. *J. Phys. Chem. A* **2014**, *118*, 2693–2701.
- (91) Antiñolo, M.; Agundez, M.; Jiménez, E.; Ballesteros, B.; Canosa, A.; El Dib, G.; Albaladejo, J.; Cernicharo, J. Reactivity of OH and CH_3OH between 22 and 64 K: Modelling the Gas Phase Production of CH_3O in Barnard 1b. *ApJ* **2016**, *823*.
- (92) Shannon, R. J.; Taylor, S.; Goddard, A.; Blitz, M. A.; Heard, D. E. Observation of a Large Negative Temperature Dependence for Rate Coefficients of Reactions of OH with Oxygenated Volatile Organic Compounds Studied at 86–112 K. *PCCP* **2010**, *12*, 13511–13514.
- (93) Shannon, R. J.; Caravan, R. L.; Blitz, M. A.; Heard, D. E. A Combined Experimental and Theoretical Study of Reactions between the Hydroxyl Radical and Oxygenated Hydrocarbons Relevant to Astrochemical Environments. *PCCP* **2014**, *16*, 3466–3478.
- (94) Caravan, R. L.; Shannon, R. J.; Lewis, T.; Blitz, M. A.; Heard, D. E. Measurements of Rate Coefficients for Reactions of OH with Ethanol and Propan-2-ol at Very Low Temperatures. *J. Phys. Chem. A* **2015**, *119*, 7130–7137.
- (95) Ocaña, A. J.; Blázquez, S.; Ballesteros, B.; Canosa, A.; Antiñolo, M.; Albaladejo, J.; Jiménez, E. Gas Phase Kinetics of the $OH + CH_3CH_2OH$ Reaction at Temperatures of the Interstellar Medium ($T = 21$ –107 K). *PCCP* **2018**, *20*, 5865–5873.
- (96) Jiménez, E.; Antiñolo, M.; Ballesteros, B.; Canosa, A.; Albaladejo, J. First Evidence of the Dramatic Enhancement of the Reactivity of Methyl Formate ($HC(O)OCH_3$) with OH at Temperatures of the Interstellar Medium: A Gas-Phase Kinetic Study between 22 K and 64 K. *PCCP* **2016**, *18*, 2183–2191.

- (97) Ocaña, A. J.; Jiménez, E.; Ballesteros, B.; Canosa, A.; Antiñolo, M.; Albaladejo, J.; Agúndez, M.; Cernicharo, J.; Zanchet, A.; Del Mazo, P.; Roncero, O.; Aguado, A. Is the Gas-phase OH+H₂CO Reaction a Source of HCO in Interstellar Cold Dark Clouds? A Kinetic, Dynamic, and Modeling Study. *ApJ* **2017**, *850*.
- (98) Sims, I. R.; Smith, I. W. M.; Clary, D. C.; Bocherel, P.; Rowe, B. R. Ultra-low Temperature Kinetics of Neutral-Neutral Reactions: New Experimental and Theoretical Results for OH+HBr between 295 and 23 K. *J. Chem. Phys.* **1994**, *101*, 1748–1751.
- (99) Jaramillo, V. I.; Smith, M. A. Temperature-dependent Kinetic Isotope Effects in the Gas-Phase Reaction: OH + HBr. *J. Phys. Chem. A* **2001**, *105*, 5854–5859.
- (100) Jaramillo, V. I.; Gougeon, S.; Le Picard, S. D.; Canosa, A.; Smith, M. A.; Rowe, B. R. A Consensus View of the Temperature Dependence of the Gas Phase Reaction: OH + HBr → H₂O + Br. *Int. J. Chem. Kinet.* **2002**, *34*, 339–344.
- (101) Sims, I. R.; Smith, I. W. M.; Bocherel, P.; Defrance, A.; Travers, D.; Rowe, B. R. Ultra-low Temperature Kinetics of Neutral-Neutral Reactions: Rate Constants for the Reactions of OH Radicals with Butenes between 295 and 23 K. *J. Chem. Soc., Faraday Trans.* **1994**, *90*, 1473–1478.
- (102) Daranlot, J.; Bergeat, A.; Caralp, F.; Caubet, P.; Costes, M.; Forst, W.; Loison, J.-C.; Hickson, K. M. Gas-phase Kinetics of Hydroxyl Radical Reactions with Alkenes: Experiment and Theory. *Chem. Phys. Chem.* **2010**, *11*, 4002–4010.
- (103) Vakhtin, A. B.; Lee, S.; Heard, D. E.; Smith, I. W. M.; Leone, S. R. Low-temperature Kinetics of Reactions of the OH Radical with Propene and 1-butene Studied by a Pulsed Laval Nozzle Apparatus Combined with Laser-induced Fluorescence. *J. Phys. Chem. A* **2001**, *105*, 7889–7895.
- (104) Vakhtin, A. B.; Murphy, J. E.; Leone, S. R. Low-temperature Kinetics of Reactions of OH Radical with Ethene, Propene, and 1-butene. *J. Phys. Chem. A* **2003**, *107*, 10055–10062.
- (105) Carty, D.; Goddard, A.; Köhler, S. P. K.; Sims, I. R.; Smith, I. W. M. Kinetics of the Radical–radical Reaction, O(³P_j) + OH(X²Π_Ω) → O₂ + H, at Temperatures down to 39 K. *J. Phys. Chem. A* **2006**, *110*, 3101–3109.
- (106) Vöhringer-Martinez, E.; Hansmann, B.; Hernandez, H.; Francisco, J. S.; Troe, J.; Abel, B. Water Catalysis of a Radical-molecule Gas-phase Reaction. *Science* **2007**, *315*, 497–501.
- (107) Hansmann, B.; Abel, B. Kinetics in Cold Laval Nozzle Expansions: From Atmospheric Chemistry to Oxidation of Biomolecules in the Gas Phase. *Chem. Phys. Chem.* **2007**, *8*, 343–356.
- (108) Liessmann, M.; Hansmann, B.; Blachly, P. G.; Francisco, J. S.; Abel, B. Primary Steps in the Reaction of OH Radicals with Amino Acids at Low Temperatures in

- Laval Nozzle Expansions: Perspectives from Experiment and Theory. *J. Phys. Chem. A* **2009**, *113*, 7570–7575.
- (109) Vöhringer-Martinez, E.; Tellbach, E.; Liessmann, M.; Abel, B. Role of Water Complexes in the Reaction of Propionaldehyde with OH Radicals. *J. Phys. Chem. A* **2010**, *114*, 9720–9724.
- (110) Vakhtin, A. B.; McCabe, D. C.; Ravishankara, A. R.; Leone, S. R. Low-temperature Kinetics of the Reaction of the OH Radical with Hydrogen Peroxide. *J. Phys. Chem. A* **2003**, *107*, 10642–10647.
- (111) Bocherel, P.; Herbert, L. B.; Rowe, B. R.; Sims, I. R.; Smith, I. W. M.; Travers, D. Ultralow-temperature Kinetics of CH(X²Π) Reactions: Rate Coefficients for Reactions with O₂ and NO (T = 13–708 K), and with NH₃ (T = 23–295 K). *J. Phys. Chem.* **1996**, *100*, 3063–3069.
- (112) Brownsword, R. A.; Canosa, A.; Rowe, B. R.; Sims, I. R.; Smith, I. W. M.; Stewart, D. W. A.; Symonds, A. C.; Travers, D. Kinetics Over a Wide Range of Temperature (13–744 K): Rate Constants for the Reactions of CH($\nu=0$) with H₂ and D₂ and for the Removal of CH($\nu=1$) by H₂ and D₂. *J. Chem. Phys.* **1997**, *106*, 7662–7677.
- (113) Canosa, A.; Sims, I. R.; Travers, D.; Smith, I. W. M.; Rowe, B. R. Reactions of the Methylidene Radical with CH₄, C₂H₂, C₂H₄, C₂H₆, and But-1-ene Studied between 23 and 295 K with a CRESU Apparatus. *Astron. Astrophys.* **1997**, *323*, 644–651.
- (114) Hickson, K. M.; Caubet, P.; Loison, J. C. Unusual Low-temperature Reactivity of Water: The CH + H₂O Reaction as a Source of Interstellar Formaldehyde. *J. Phys. Chem. Lett.* **2013**, *4*, 2843–2846.
- (115) Goulay, F.; Rebrion-Rowe, C.; Biennier, L.; Le Picard, S. D.; Canosa, A.; Rowe, B. R. Reaction of Anthracene with CH Radicals: An Experimental Study of the Kinetics between 58 and 470 K. *J. Phys. Chem. A* **2006**, *110*, 3132–3137.
- (116) Lee, S.; Leone, S. R. Rate Coefficients for the Reaction of C₂H with O₂ at 90 K and 120 K Using a Pulsed Laval Nozzle Apparatus. *Chem. Phys. Lett.* **2000**, *329*, 443–449.
- (117) Vakhtin, A. B.; Heard, D. E.; Smith, I. W. M.; Leone, S. R. Kinetics of Reactions of C₂H Radical with Acetylene, O₂, Methylacetylene, and Allene in a Pulsed Laval Nozzle Apparatus at T=103 K. *Chem. Phys. Lett.* **2001**, *344*, 317–324.
- (118) Soorkia, S.; Liu, C.-L.; Savee, J. D.; Ferrell, S. J.; Leone, S. R.; Wilson, K. R. Air-foil Sampling of a Pulsed Laval Beam with Tunable Vacuum Ultraviolet Synchrotron Ionization Quadrupole Mass Spectrometry: Application to Low-Temperature Kinetics and Product Detection. *Rev. Sci. Instrum.* **2011**, *82*, 124102.
- (119) Lee, S.; Samuels, D. A.; Hoobler, R. J.; Leone, S. R. Direct Measurements of Rate Coefficients for the Reaction of Ethynyl Radical (C₂H) with C₂H₂ at 90 and 120 K Using a Pulsed Laval Nozzle Apparatus. *J. Geophys. Res. Planets* **2000**, *105*, 15085–15090.

- 1
2
3
4
5
6
7
8
9
10
11
12
13
14
15
16
17
18
19
20
21
22
23
24
25
26
27
28
29
30
31
32
33
34
35
36
37
38
39
40
41
42
43
44
45
46
47
48
49
50
51
52
53
54
55
56
57
58
59
60
- (120) Bouwman, J.; Goulay, F.; Leone, S. R.; Wilson, K. R. Bimolecular Rate Constant and Product Branching Ratio Measurements for the Reaction of C_2H with Ethene and Propene at 79 K. *J. Phys. Chem. A* **2012**, *116*, 3907–3917.
- (121) Soorkia, S.; Trevitt, A. J.; Selby, T. M.; Osborn, D. L.; Taatjes, C. A.; Wilson, K. R.; Leone, S. R. Reaction of the C_2H Radical with 1-butyne (C_4H_6): Low-Temperature Kinetics and Isomer-Specific Product Detection. *J. Phys. Chem. A* **2010**, *114*, 3340–3354.
- (122) Vakhtin, A. B.; Heard, D. E.; Smith, I. W. M.; Leone, S. R. Kinetics of C_2H Radical Reactions with Ethene, Propene and 1-Butene Measured in a Pulsed Laval Nozzle Apparatus at $T=103$ and 296 K. *Chem. Phys. Lett.* **2001**, *348*, 21–26.
- (123) Nizamov, B.; Leone, S. R. Kinetics of C_2H Reactions with Hydrocarbons and Nitriles in the 104–296 K Temperature Range. *J. Phys. Chem. A* **2004**, *108*, 1746–1752.
- (124) Bouwman, J.; Fournier, M.; Sims, I. R.; Leone, S. R.; Wilson, K. R. Reaction Rate and Isomer-specific Product Branching Ratios of $C_2H + C_4H_8$: 1-Butene, Cis -2-butene, Trans -2-butene, and Isobutene at 79 K. *J. Phys. Chem. A* **2013**, *117*, 5093–5105.
- (125) Murphy, J. E.; Vakhtin, A. B.; Leone, S. R. Laboratory Kinetics of C_2H Radical Reactions with Ethane, Propane, and n-Butane at $T = 96$ –296 K: Implications for Titan. *Icarus* **2003**, *163*, 175–181.
- (126) Nizamov, B.; Leone, S. R. Rate Coefficients and Kinetic Isotope Effect for the C_2H Reactions with NH_3 and ND_3 in the 104–294 K Temperature Range. *J. Phys. Chem. A* **2004**, *108*, 3766–3771.
- (127) Goulay, F.; Leone, S. R. Low-Temperature Rate Coefficients for the Reaction of Ethynyl Radical (C_2H) with Benzene. *J. Phys. Chem. A* **2006**, *110*, 1875–1880.
- (128) Mullen, C.; Smith, M. A. Low Temperature $NH(X^3\Sigma^-)$ Radical Reactions with NO, Saturated, and Unsaturated Hydrocarbons Studied in a Pulsed Supersonic Laval Nozzle Flow Reactor between 53 and 188 K. *J. Phys. Chem. A* **2005**, *109*, 1391–1399.
- (129) Páramo, A.; Canosa, A.; Le Picard, S. D.; Sims, I. R. An Experimental Study of the Intersystem Crossing and Reactions of $C_2(X^1\Sigma_g^+)$ and $C_2(a^3\Pi_u)$ with O_2 and NO at Very Low Temperature (24–300 K). *J. Phys. Chem. A* **2006**, *110*, 3121–3127.
- (130) Canosa, A.; Páramo, A.; Le Picard, S. D.; Sims, I. R. An Experimental Study of the Reaction Kinetics of $C_2(X^1\Sigma_g^+)$ with Hydrocarbons (CH_4 , C_2H_2 , C_2H_4 , C_2H_6 and C_3H_8) Over the Temperature Range 24–300 K: Implications for the Atmospheres of Titan and the Giant Planets. *Icarus* **2007**, *187*, 558–568.
- (131) Daugey, N.; Caubet, P.; Bergeat, A.; Costes, M.; Hickson, K. M. Reaction Kinetics to Low Temperatures. Dicarbon + Acetylene, Methylacetylene, Allene and Propene from $77 \leq T \leq 296$ K. *PCCP* **2008**, *10*, 729–737.

- 1
2
3
4 (132) Páramo, A.; Canosa, A.; Le Picard, S. D.; Sims, I. R. Rate Coefficients for the Reactions of $C_2(a^3\Pi_u)$ and $C_2(X^1\Sigma_g^+)$ with Various Hydrocarbons (CH_4 , C_2H_2 , C_2H_4 ,
5 C_2H_6 , and C_3H_8): A Gas-Phase Experimental Study over the Temperature Range
6 24300 K. *J. Phys. Chem. A* **2008**, *112*, 9591–9600.
7
8
9 (133) Berteloite, C.; Le Picard, S. D.; Birza, P.; Gazeau, M.-C.; Canosa, A.; Bénilan, Y.;
10 Sims, I. R. Low Temperature (39–298 K) Kinetics Study of the Reactions of the C_4H
11 Radical with Various Hydrocarbons Observed in Titan’s Atmosphere. *Icarus* **2008**,
12 *194*, 746–757.
13
14 (134) Berteloite, C.; Le Picard, S. D.; Balucani, N.; Canosa, A.; Sims, I. R. Low Temper-
15 ature Rate Coefficients for Reactions of the Butadiynyl Radical, C_4H , with Various
16 Hydrocarbons. Part II: Reactions with Alkenes (ethylene, Propene, 1-butene), Dienes
17 (allene, 1,3-butadiene) and Alkynes (acetylene, Propyne and 1-butyne). *PCCP* **2010**,
18 *12*, 3677–3689.
19
20 (135) Berteloite, C.; Le Picard, S. D.; Balucani, N.; Canosa, A.; Sims, I. R. Low Temper-
21 ature Rate Coefficients for Reactions of the Butadiynyl Radical, C_4H , with Various
22 Hydrocarbons. Part I: Reactions with Alkanes (CH_4 , C_2H_6 , C_3H_8 , C_4H_{10}). *PCCP*
23 **2010**, *12*, 3666–3676.
24
25 (136) Chastaing, D.; Le Picard, S. D.; Sims, I. R. Direct Kinetic Measurements on Reactions
26 of Atomic Carbon, $C(^3P)$, with O_2 and NO at Temperatures down to 15 K. *J. Chem.*
27 *Phys.* **2000**, *112*, 8466–8469.
28
29 (137) Geppert, W. D.; Reignier, D.; Stoecklin, T.; Naulin, C.; Costes, M.; Chastaing, D.;
30 Le Picard, S. D.; Sims, I. R.; Smith, I. W. M. Comparison of the Cross-sections and
31 Thermal Rate Constants for the Reactions of $C(^3P_j)$ Atoms with O_2 and NO . *PCCP*
32 **2000**, *2*, 2873–2881.
33
34 (138) Chastaing, D.; James, P. L.; Sims, I. R.; Smith, I. W. M. Neutral-Neutral Reactions
35 at the Temperatures of Interstellar Clouds: Rate Coefficients for Reactions of Atomic
36 Carbon, $C(^3P)$, with O_2 , C_2H_2 , C_2H_4 and C_3H_6 down to 15 K. *PCCP* **1999**, *1*, 2247–
37 2256.
38
39 (139) Hickson, K. M.; Loison, J.-C.; Wakelam, V. Temperature Dependent Product Yields
40 for the Spin Forbidden Singlet Channel of the $C(^3P) + C_2H_2$ Reaction. *Chem. Phys.*
41 *Lett.* **2016**, *659*, 70–75.
42
43 (140) Chastaing, D.; Le Picard, S. D.; Sims, I. R.; Smith, I. W.; Geppert, W. D.; Naulin, C.;
44 Costes, M. Rate Coefficients and Cross-sections for the Reactions of $C(^3P_j)$ Atoms with
45 Methylacetylene and Allene. *Chem. Phys. Lett.* **2000**, *331*, 170–176.
46
47 (141) Hickson, K. M.; Loison, J.-C.; Bourgalais, J.; Capron, M.; Le Picard, S. D.; Goulay, F.;
48 Wakelam, V. The $C(^3P) + NH_3$ Reaction in Interstellar Chemistry. ii. Low Temper-
49 ature Rate Constants and Modeling of NH , NH_2 , and NH_3 Abundances in Dense
50 Interstellar Clouds. *ApJ* **2015**, *812*, 107.
51
52
53
54
55
56
57
58
59
60

- 1
2
3
4
5
6
7
8
9
10
11
12
13
14
15
16
17
18
19
20
21
22
23
24
25
26
27
28
29
30
31
32
33
34
35
36
37
38
39
40
41
42
43
44
45
46
47
48
49
50
51
52
53
54
55
56
57
58
59
60
- (142) Bourgalais, J.; Capron, M.; Kailasanathan, R. K. A.; Osborn, D. L.; Hickson, K. M.; Loison, J. C.; Wakelam, V.; Goulay, F.; Le Picard, S. D. The C(³P) + NH₃ Reaction in Interstellar Chemistry. i. Investigation of the Product Formation Channels. *ApJ* **2015**, *812*, 106.
- (143) Hickson, K. M.; Loison, J.-C.; Nuñez-Reyes, D.; Méreau, R. Quantum Tunneling Enhancement of the C + H₂O and C + D₂O Reactions at Low Temperature. *J. Phys. Chem. Lett.* **2016**, *7*, 3641–3646.
- (144) Shannon, R. J.; Cossou, C.; Loison, J.-C.; Caubet, P.; Balucani, N.; Seakins, P. W.; Wakelam, V.; Hickson, K. M. The Fast C(³P) + CH₃OH Reaction As an Efficient Loss Process for Gas-phase Interstellar Methanol. *R. Soc. Chem. Adv.* **2014**, *4*, 26342–26353.
- (145) Nuñez Reyes, D.; Hickson, K. M. The Reactivity of C(¹D) with Oxygen Bearing Molecules NO and O₂ at Low Temperature. *Chem. Phys. Lett.* **2017**, *687*, 330–335.
- (146) Hickson, K. M.; Loison, J.-C.; Guo, H.; Suleimanov, Y. V. Ring-polymer Molecular Dynamics for the Prediction of Low-temperature Rates: An Investigation of the C(¹D) + H₂ Reaction. *J. Phys. Chem. Lett.* **2015**, *6*, 4194–4199.
- (147) Hickson, K. M.; Suleimanov, Y. V. An Experimental and Theoretical Investigation of the C(¹D) + D₂ Reaction. *PCCP* **2017**, *19*, 480–486.
- (148) Nuñez Reyes, D.; Hickson, K. M. Kinetics of the Gas-Phase O(¹D) + CO₂ and C(¹D) + CO₂ Reactions Over the 50–296 K Range. *J. Phys. Chem. A* **2018**, *122*, 4002–4008.
- (149) Nuñez Reyes, D.; Hickson, K. M. Kinetic and Product Study of the Reactions of C(¹D) with CH₄ and C₂H₆ at Low Temperature. *J. Phys. Chem. A* **2017**, *121*, 3851–3857.
- (150) Le Picard, S. D.; Canosa, A.; Travers, D.; Chastaing, D.; Rowe, B. R.; Stoecklin, T. Experimental and Theoretical Kinetics for the Reaction of Al with O₂ at Temperatures between 23 and 295 K. *J. Chem. Phys.* **1997**, *101*, 1748–1751.
- (151) Canosa, A.; Le Picard, S. D.; Gougeon, S.; Rebrion-Rowe, C.; Travers, D.; Rowe, B. R. Rate Coefficients for the Reactions of Si(³P_{*j*}) with C₂H₂ and C₂H₄: Experimental Results down to 15 K. *J. Chem. Phys.* **2001**, *115*, 6495–6503.
- (152) Le Picard, S. D.; Canosa, A.; Reignier, D.; Stoecklin, T. A Comparative Study of the Reactivity of the Silicon Atom Si(³P_{*j*}) Towards O₂ and NO Molecules at Very Low Temperature. *PCCP* **2002**, *4*, 3659–3664.
- (153) Le Picard, S. D.; Canosa, A.; G. Pineau des Forêts, C.; Rebrion-Rowe, C.; Rowe, B. R. The Si(³P_{*j*}) + O₂ Reaction: A Fast Source of SiO at Very Low Temperature; CRESU Measurements and Interstellar Consequences. *Astron. Astrophys.* **2001**, *372*, 1064–1070.

- 1
2
3
4 (154) Geppert, W. D.; Goulay, F.; Naulin, C.; Costes, M.; Canosa, A.; Le Picard, S. D.;
5 Rowe, B. R. Rate Coefficients and Integral Cross-sections for the Reaction of B(2P_j)
6 Atoms with Acetylene. *PCCP* **2004**, *6*, 566–571.
7
8 (155) Canosa, A.; Le Picard, S. D.; Geppert, W. D. Experimental Kinetics Study of the
9 Reaction of Boron Atoms, B(2P_j), with Ethylene at Very Low Temperatures (23–295
10 K). *J. Phys. Chem. A* **2004**, *108*, 6183–6185.
11
12 (156) Le Picard, S. D.; Canosa, A.; Geppert, W.; Stoecklin, T. Experimental and Theoretical
13 Temperature Dependence of the Rate Coefficient of the B($^2P_{1/2,3/2}$) + O $_2$ ($X^3\Sigma_g^-$)
14 Reaction in the 24–295 K Temperature Range. *Chem. Phys. Lett.* **2004**, *385*, 502–506.
15
16 (157) Sabbah, H.; Biennier, L.; Sims, I. R.; Georgievskii, Y.; Klippenstein, S. J.; Smith, I.
17 W. M. Understanding Reactivity at Very Low Temperatures: The Reactions of Oxygen
18 Atoms with Alkenes. *Science* **2007**, *317*, 102–105.
19
20 (158) Meng, Q.; Hickson, K. M.; Shao, K.; Loison, J.-C.; Zhang, D. H. Theoretical and
21 Experimental Investigations of Rate Coefficients of O(1D) + CH $_4$ at Low Temperature.
22 *PCCP* **2016**, *18*, 29286–29292.
23
24 (159) Hickson, K. M.; Suleimanov, Y. V. Low-temperature Experimental and Theoretical
25 Rate Constants for the O(1D) + H $_2$ Reaction. *J. Phys. Chem. A* **2017**, *121*, 1916–1923.
26
27 (160) Nuñez Reyes, D.; Hickson, K. M. Rate Constants and H-atom Product Yields for the
28 Reactions of O(1D) Atoms with Ethane and Acetylene from 50 to 296 K. *J. Phys.*
29 *Chem. A* **2018**, *122*, 4696–4703.
30
31 (161) Nuñez Reyes, D.; Hickson, K. M.; Larrégaray, P.; Bonnet, L.; González-Lezana, T.;
32 Suleimanov, Y. V. A Combined Theoretical and Experimental Investigation of the
33 Kinetics and Dynamics of the O(1D) + D $_2$ Reaction at Low Temperature. *PCCP*
34 **2018**, *20*, 4404–4414.
35
36 (162) Bergeat, A.; Hickson, K. M.; Daugey, N.; Caubet, P.; Costes, M. A Low Temperature
37 Investigation of the N($^4S^o$) + NO Reaction. *PCCP* **2009**, *11*, 8149–8155.
38
39 (163) Stubbing, J. W.; Vanuzzo, G.; Moudens, A.; Loison, J. C.; Hickson, K. M. Gas-Phase
40 Kinetics of the N + C $_2$ N Reaction at Low Temperature. *J. Phys. Chem. A* **2015**, *119*,
41 3194–3199.
42
43 (164) Daranlot, J.; Jorfi, M.; Xie, C.; Bergeat, A.; Costes, M.; Caubet, P.; Xie, D.; Guo, H.;
44 Honvault, P.; Hickson, K. M. Revealing Atom-Radical Reactivity at Low Temperature
45 through the N + OH Reaction. *Science* **2011**, *334*, 1538–1541.
46
47 (165) Daranlot, J.; Hincelin, U.; Bergeat, A.; Costes, M.; Loison, J.-C.; Wakelam, V.; Hick-
48 son, K. M. Elemental Nitrogen Partitioning in Dense Interstellar Clouds. *PNAS* **2012**,
49 *109*, 10233–10238.
50
51
52
53
54
55
56
57
58
59
60

- 1
2
3 (166) Daranlot, J.; Hu, X.; Xie, C.; Loison, J.-C.; Caubet, P.; Costes, M.; Wakelam, V.;
4 Xie, D.; Guo, H.; Hickson, K. M. Low Temperature Rate Constants for the $N(^4S)$
5 + $CH(X^2\Pi_r)$ Reaction. Implications for N_2 Formation Cycles in Dense Interstellar
6 Clouds. *PCCP* **2013**, *15*, 13888–13896.
7
8
9 (167) Loison, J. C.; Hu, X.; Han, S.; Hickson, K. M.; Guo, H.; Xie, D. An Experimental and
10 Theoretical Investigation of the $N(^4S)$ + $C_2(^1\Sigma_g^+)$ Reaction at Low Temperature.
11 *PCCP* **2014**, *16*, 14212–14219.
12
13 (168) Nuñez Reyes, D.; Hickson, K. M. A Low Temperature Investigation of the Gas-Phase
14 $N(^2D)$ + NO Reaction. Towards a Viable Source of $N(^2D)$ Atoms for Kinetic Studies
15 in Astrochemistry. *PCCP* **2018**, *20*, 17442–17447.
16
17 (169) Nuñez Reyes, D.; Loison, J.-C.; Hickson, K. M.; Dobrijevic, M. A Low Temperature
18 Investigation of the $N(^2D)$ + CH_4 , C_2H_6 and C_3H_8 Reactions. *PCCP* **2019**, *21*, 6574–
19 6581.
20
21
22 (170) Berteloite, C.; Le Picard, S. D.; Sims, I. R.; Rosi, M.; Leonori, F.; Petrucci, R.;
23 Balucani, N.; Wang, X.; Casavecchia, P. Low Temperature Kinetics, Crossed Beam
24 Dynamics and Theoretical Studies of the Reaction $S(^1D)$ + CH_4 and Low Temperature
25 Kinetics of $S(^1D)$ + C_2H_2 . *PCCP* **2011**, *13*, 8485–8501.
26
27
28 (171) Leonori, F.; Petrucci, R.; Balucani, N.; Casavecchia, P.; Rosi, M.; Berteloite, C.; Le
29 Picard, S. D.; Canosa, A.; Sims, I. R. Observation of Organosulfur Products (thiovi-
30 noxy, Thioketene and Thioformyl) in Crossed-beam Experiments and Low Tempera-
31 ture Rate Coefficients for the Reaction $S(^1D)$ + C_2H_4 . *PCCP* **2009**, *11*, 4701–4706.
32
33
34 (172) Leonori, F.; Petrucci, R.; Balucani, N.; Casavecchia, P.; Rosi, M.; Skouteris, D.;
35 Berteloite, C.; Le Picard, S. D.; Canosa, A.; Sims, I. R. Crossed-beam Dynamics,
36 Low-temperature Kinetics, and Theoretical Studies of the Reaction $S(^1D)$ + C_2H_4 . *J.*
37 *Phys. Chem. A* **2009**, *113*, 15328–15345.
38
39
40 (173) Hickson, K. M.; Bergeat, A.; Costes, M. A Low Temperature Study of the Reactions
41 of Atomic Chlorine with Simple Alkanes. *J. Phys. Chem. A* **2010**, *114*, 3038–3044.
42
43 (174) Tizniti, M.; Le Picard, S. D.; Lique, F.; Berteloite, C.; Canosa, A.; Alexander, M. H.;
44 Sims, I. R. The Rate of the F + H_2 Reaction at Very Low Temperatures. *Nature*
45 *Chemistry* **2014**, *6*, 141–145.
46
47 (175) Sharkey, P.; Sims, I. R.; Smith, I. W. M.; Bocherel, P.; Rowe, B. R. Pressure and
48 Temperature Dependence of the Rate Constants for the Association Reaction of OH
49 Radicals with NO between 301 and 23 K. *J. Chem. Soc. Faraday Trans.* **1994**, *90*,
50 3609–3616.
51
52 (176) Atkinson, D. B.; Smith, M. A. Radical-Molecule Kinetics in Pulsed Uniform Supersonic
53 Flows: Termolecular Association of OH + NO between 90 and 220 K. *J. Phys. Chem.*
54 **1994**, *98*, 5797–5800.
55
56
57
58
59
60

- 1
2
3
4 (177) Liessmann, M.; Miller, Y.; Gerber, R. B.; Abel, B. Reaction of OH and NO at Low
5 Temperatures in the Presence of Water: the Role of Clusters. *Z. Phys. Chem.* **2011**,
6 *225*, 1129–1144.
7
8 (178) Daranlot, J.; Hickson, K. M.; Loison, J.-C.; Méreau, R.; Caralp, F.; Forst, W.;
9 Bergeat, A. Gas-phase Kinetics of the Hydroxyl Radical Reaction with Allene: Abso-
10 lute Rate Measurements at Low Temperature, Product Determinations, and Calcula-
11 tions. *J. Phys. Chem. A* **2012**, *116*, 10871–10881.
12
13 (179) Le Picard, S. D.; Tizniti, M.; Canosa, A.; Sims, I. R.; Smith, I. W. M. The Thermo-
14 dynamics of the Elusive HO₃ Radical. *Science* **2010**, *328*, 1258–1262.
15
16 (180) Tizniti, M.; Le Picard, S. D.; Canosa, A.; Sims, I. R.; Smith, I. W. M. Low Tempera-
17 ture Kinetics: The Association of OH Radicals with O₂. *PCCP* **2010**, *12*, 12702–12710.
18
19 (181) Smith, I. W. M.; Le Picard, S. D.; Tizniti, M.; Canosa, A.; Sims, I. R. The Quest for
20 the Hydroxyl-peroxy Radical. *Z. Phys. Chem.* **2010**, *224*, 949–965.
21
22 (182) Goulay, F.; Rebrion-Rowe, C.; Le Garrec, J. L.; Le Picard, S. D.; Canosa, A.;
23 Rowe, B. R. The Reaction of Anthracene with OH Radicals: An Experimental Study
24 of the Kinetics between 58 and 470 K. *J. Chem. Phys.* **2005**, *122*, 104308.
25
26 (183) Hamon, S.; Le Picard, S. D.; Canosa, A.; Rowe, B. R.; Smith, I. W. M. Low Tem-
27 perature Measurements of the Rate of Association to Benzene Dimers in Helium. *J.*
28 *Chem. Phys.* **2000**, *112*, 4506–4516.
29
30 (184) Brownsword, R. A.; Sims, I. R.; Smith, I. W. M.; Stewart, D. W. A.; Canosa, A.;
31 Rowe, B. R. The Radiative Association of CH with H₂: A Mechanism for Formation
32 of CH₃ in Interstellar Clouds. *ApJ* **1997**, *485*, 195–202.
33
34 (185) Le Picard, S. D.; Canosa, A.; Rowe, B. R.; Brownsword, R. A.; Smith, I. W. M.
35 Determination of the Limiting Low Pressure Rate Constants of the Reactions of CH
36 with N₂ and CO: A CRESU Measurement at 53 K. *J. Chem. Soc. Faraday Trans.*
37 **1998**, *94*, 2889–2893.
38
39 (186) Le Picard, S. D.; Canosa, A. Measurement of the Rate Constant for the Association
40 Reaction CH + N₂ at 53 K and its Relevance to Triton’s Atmosphere. *Geophys. Res.*
41 *Lett.* **1998**, *25*, 485–488.
42
43 (187) Sleiman, C.; González, S.; Klippenstein, S. J.; Talbi, D.; El Dib, G.; Canosa, A.
44 Pressure Dependent Low Temperature Kinetics for CN + CH₃CN: Competition be-
45 tween Chemical Reaction and van der Waals Complex Formation. *PCCP* **2016**, *18*,
46 15118–15132.
47
48 (188) Biennier, L.; Sabbah, H.; Chandrasekaran, V.; Klippenstein, S. J.; Sims, I. R.;
49 Rowe, B. R. Insights into the Role of Polycyclic Aromatic Hydrocarbon Condensa-
50 tion in Haze Formation in Jupiter’s Atmosphere. *Astron. Astrophys.* **2011**, *532*, A40.
51
52
53
54
55
56
57
58
59
60

- 1
2
3
4 (189) Sabbah, H.; Biennier, L.; Klippenstein, S. J.; Sims, I. R.; Rowe, B. R. Exploring the
5 Role of PAHs in the Formation of Soot: Pyrene Dimerization. *J. Phys. Chem. Lett.*
6 **2010**, *1*, 2962–2967.
7
8 (190) Bourgalais, J.; Roussel, V.; Capron, M.; Benidar, A.; Jasper, A. W.; Klippen-
9 stein, S. J.; Biennier, L.; Le Picard, S. D. Low Temperature Kinetics of the First
10 Steps of Water Cluster Formation. *Phys. Rev. Lett.* **2016**, *116*, 113401.
11
12 (191) Sánchez-González, R.; Eveland, W. D.; West, N. A.; Mai, C. L. N.; Bowersox, R.
13 D. W.; North, S. W. Low-temperature Collisional Quenching of NO $A^2\Sigma^+(v' = 0)$ by
14 NO($X^2\Pi$) and O₂ between 34 and 109 K. *J. Chem. Phys.* **2014**, *141*, 074313.
15
16 (192) James, P. L.; Sims, I. R.; Smith, I. W. Rate Coefficients for the Vibrational Self-
17 relaxation of NO($X^2\Pi$, $\nu = 3$) at Temperatures down to 7 K. *Chem. Phys. Lett.* **1997**,
18 *276*, 423–429.
19
20 (193) James, P. L.; Sims, I. R.; Smith, I. W. M.; Alexander, M. H.; Yang, M. A Combined
21 Experimental and Theoretical Study of Rotational Energy Transfer in Collisions be-
22 tween NO($X^2\Pi_{1/2}$, $v=3,j$) and He, Ar and N₂ at Temperatures down to 7 K. *J. Chem.*
23 *Phys.* **1998**, *109*, 3882–3897.
24
25 (194) Wright, S. M.; Sims, I. R.; Smith, L. W. Vibrational Relaxation of Highly Excited
26 Toluene in Collisions with He, Ar, and N₂ at Temperatures down to 38 K. *J. Phys.*
27 *Chem. A* **2000**, *104*, 10347–10355.
28
29 (195) Carty, D.; Goddard, A.; Sims, I. R.; Smith, I. W. M. Rotational Energy Transfer in
30 Collisions between CO($X^1\Sigma^+$, $v=2$, $J=0, 1, 4$, and 6) and He at Temperatures from
31 294 to 15 K. *J. Chem. Phys.* **2004**, *121*, 4671–4683.
32
33 (196) Mertens, L. A.; Labiad, H.; Denis-Alpizar, O.; Fournier, M.; Carty, D.; Le Pi-
34 card, S. D.; Stoecklin, T.; Sims, I. R. Rotational Energy Transfer in Collisions between
35 CO and Ar at Temperatures from 293 to 30 K. *Chem. Phys. Lett.* **2017**, *683*, 521–528.
36
37 (197) Herbert, L. B.; Sims, I. R.; Smith, I. W. M.; Stewart, D. W. A.; Symonds, A. C.;
38 Canosa, A.; Rowe, B. R. Rate Constants for the Relaxation of CH($X^2\Pi, \nu=1$) by CO
39 and N₂ at Temperatures from 23 to 584 K. *J. Phys. Chem.* **1996**, *100*, 14928–14935.
40
41 (198) Le Picard, S. D.; Bussery-Honvault, B.; Rebrion-Rowe, C.; Honvault, P.; Canosa, A.;
42 Launay, J. M.; Rowe, B. R. Fine Structure Relaxation of Aluminum by Atomic Argon
43 between 30 and 300 K: An Experimental and Theoretical Study. *J. Chem. Phys.* **1998**,
44 *108*, 10319–10326.
45
46 (199) Le Picard, S. D.; Honvault, P.; Bussery-Honvault, B.; Canosa, A.; Laubé, S.; Lau-
47 nay, J.-M.; Rowe, B.; Chastaing, D.; Sims, I. R. Experimental and Theoretical Study
48 of Intramultiplet Transitions in Collisions of C(3P) and Si(3P) with He. *J. Chem.*
49 *Phys.* **2002**, *117*, 10109–10120.
50
51 (200) Grondin, R.; Loison, J.-C.; Hickson, K. M. Low Temperature Rate Constants for the
52 Reactions of O(1D) with N₂, O₂, and Ar. *J. Phys. Chem. A* **2016**, *120*, 4838–4844.
53
54
55
56
57
58
59
60

- 1
2
3 (201) Nuñez Reyes, D.; Klos, J.; Alexander, M. H.; Dagdigian, P. J.; Hickson, K. M. Ex-
4 perimental and Theoretical Investigation of the Temperature Dependent Electronic
5 Quenching of O(¹D) Atoms in Collisions with Kr. *J. Chem. Phys.* **2018**, *148*, 124311.
6
7 (202) Hickson, K. M.; Loison, J.-C.; Lique, F.; Klos, J. An Experimental and Theoretical
8 Investigation of the C(¹D) + N₂ → C(³P) + N₂ Quenching Reaction at Low Temper-
9 ature. *J. Phys. Chem. A* **2016**, *120*, 2504–2513.
10
11 (203) Lara, M.; Berteloite, C.; Paniagua, M.; Dayou, F.; Le Picard, S. D.; Launay, J.-M.
12 Experimental and Theoretical Study of the Collisional Quenching of S(¹D) by Ar.
13 *PCCP* **2017**, *19*, 28555–28571.
14
15 (204) Le Garrec, J. L.; Sidko, O.; Queffelec, J. L.; Hamon, S.; Mitchell, J. B. A.; Rowe, B. R.
16 Experimental Studies of Cold Electron Attachment to SF₆, CF₃Br, and CCl₂F₂. *J.*
17 *Chem. Phys.* **1997**, *107*, 54–63.
18
19 (205) Moustefaoui, T.; Rebrion-Rowe, C.; Le Garrec, J.-L.; Rowe, B. R.; Brian
20 A. Mitchell, J. Low Temperature Electron Attachment to Polycyclic Aromatic Hy-
21 drocarbons. *Faraday Discuss.* **1998**, *109*, 71–82.
22
23 (206) Speck, T.; Mostefaoui, T.; Rebrion-Rowe, C.; Mitchell, J. B. A.; Rowe, B. R. Low-
24 temperature Electron Attachment to CH₃I. *J. Phys. B At. Mol. Opt. Phys.* **2000**, *33*,
25 3575–3582.
26
27 (207) Goulay, F.; Rebrion-Rowe, C.; Carles, S.; Le Garrec, J. L.; Rowe, B. R. Electron
28 Attachment on HI and DI in a Uniform Supersonic Flow: Thermalization of the
29 Electrons. *J. Chem. Phys.* **2004**, *121*, 1303–1308.
30
31 (208) Speck, T.; Le Garrec, J. L.; Le Picard, S.; Canosa, A.; Mitchell, J. B. A.; Rowe, B. R.
32 Electron Attachment in HBr and HCl. *J. Chem. Phys.* **2001**, *114*, 8303–8309.
33
34 (209) Carles, S.; Saidani, G.; Le Garrec, J.-L.; Guen, N.; Mitchell, J. B.; Viggiano, A. A.;
35 Shuman, N. S. Demonstration of the Branching Ratio Inversion for the Electron At-
36 tachment to Phosphoryl Chloride POCl₃ in the Gas Phase between 300 and 200 K.
37 *Chem. Phys. Lett.* **2016**, *650*, 144–147.
38
39 (210) Smith, I. W. M.; Sage, A. M.; Donahue, N. M.; Herbst, E.; Quan, D. The Temperature-
40 dependence of Rapid Low Temperature Reactions: Experiment, Understanding and
41 Prediction. *Faraday Discuss.* **2006**, *133*, 137.
42
43 (211) Herbert, L.; Smith, I. W. M.; Spencer-Smith, R. D. Rate Constants for the Elementary
44 Reactions between CN Radicals and CH₄, C₂H₆, C₂H₄, C₃H₆, and C₂H₂ in the Range:
45 295 ≤ T/K ≤ 700. *Int. J. Chem. Kinet.* **1992**, *24*, 791–802.
46
47 (212) Huang, L. C. L.; Balucani, N.; Lee, Y. T.; Kaiser, R. I.; Osamura, Y. Crossed Beam
48 Reaction of the Cyano Radical, CN(X²Σ⁺), with Methylacetylene, CH₃CCH (X¹A₁):
49 Observation of Cyanopropyne, CH₃CCCN (X¹A₁), and Cyanoallene, H₂CCCHCN
50 (X¹A₁). *J. Chem. Phys.* **1999**, *111*, 2857–2860.
51
52
53
54
55
56
57
58
59
60

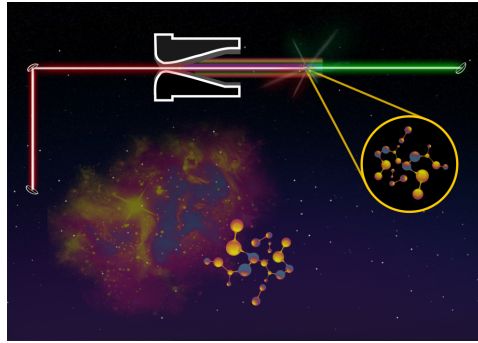
- 1
2
3 (213) Balucani, N.; Asvany, O.; Huang, L. C. L.; Lee, Y. T.; Kaiser, R. I.; Osamura, Y.;
4 Bettinger, H. F. Formation of Nitriles in the Interstellar Medium via Reactions of
5 Cyano Radicals, $CN(X^2\Sigma^+)$, with Unsaturated Hydrocarbons. *ApJ* **2000**, *545*, 892–
6 906.
7
8
9 (214) Roncero, O.; Zanchet, A.; Aguado, A. Low Temperature Reaction Dynamics for
10 $CH_3OH + OH$ Collisions on a New Full Dimensional Potential Energy Surface. *PCCP*
11 **2018**, *20*, 25951–25958.
12
13 (215) Gao, L. G.; Zheng, J.; Fernández-Ramos, A.; Truhlar, D. G.; Xu, X. Kinetics of the
14 Methanol Reaction with OH at Interstellar, Atmospheric, and Combustion Tempera-
15 tures. *J. Am. Chem. Soc.* **2018**, *140*, 2906–2918.
16
17 (216) Nguyen, T. L.; Ruscic, B.; Stanton, J. F. A Master Equation Simulation for the $\bullet OH$
18 + CH_3OH Reaction. *J. Chem. Phys.* **2019**, *150*, 084105.
19
20 (217) del Mazo-Sevillano, P.; Aguado, A.; Jiménez, E.; Suleimanov, Y. V.; Roncero, O.
21 Quantum Roaming in the Complex-forming Mechanism of the Reactions of OH with
22 Formaldehyde and Methanol at Low Temperature and Zero Pressure: A Ring Polymer
23 Molecular Dynamics Approach. *J. Phys. Chem. Lett.* **2019**, *10*, 1900–1907.
24
25 (218) Dillon, T. J.; Hölscher, D.; Sivakumaran, V.; Horowitz, A.; Crowley, J. N. Kinetics
26 of the Reactions of HO with Methanol (210–351 K) and with Ethanol (216–368 K).
27 *PCCP* **2005**, *7*, 349–355.
28
29 (219) Heard, D. E. Rapid Acceleration of Hydrogen Atom Abstraction Reactions of OH
30 at Very Low Temperatures through Weakly Bound Complexes and Tunneling. *Acc.*
31 *Chem. Res.* **2018**, *51*, 2620–2627.
32
33 (220) Seakins, P. W. Product Branching Ratios in Simple Gas Phase Reactions. *Annu.*
34 *Reports Sect. C* **2007**, *103*, 173.
35
36 (221) Choi, N.; Blitz, M. A.; Mckee, K.; Pilling, M. J.; Seakins, P. W. H Atom Branching
37 Ratios from the Reactions of CN Radicals with C_2H_2 and C_2H_4 . *Chem. Phys. Lett.*
38 **2004**, *384*, 68–72.
39
40 (222) Gannon, K. L.; Blitz, M. A.; Liang, C.-H.; Pilling, M. J.; Seakins, P. W.;
41 Glowacki, D. R.; Harvey, J. N. An Experimental and Theoretical Investigation of the
42 Competition between Chemical Reaction and Relaxation for the Reactions of 1CH_2
43 with Acetylene and Ethene: Implications for the Chemistry of the Giant Planets.
44 *Faraday Discuss.* **2010**, *147*, 173–188.
45
46 (223) Blitz, M. A.; Choi, N.; Kovács, T.; Seakins, P. W.; Pilling, M. J. The Effect of Tem-
47 perature on Collision Induced Intersystem Crossing in the Reaction of 1CH_2 with H_2 .
48 *Proceedings of the Combustion Institute* **2005**, *30*, 927–933.
49
50 (224) Gannon, K. L.; Blitz, M. A.; Pilling, M. J.; Seakins, P. W.; Klippenstein, S. J.;
51 Harding, L. B. Kinetics and Product Branching Ratios of the Reaction of 1CH_2 with
52 H_2 and D_2 . *J. Phys. Chem. A* **2008**, *112*, 9575–9583.
53
54
55
56
57
58
59
60

- 1
2
3 (225) Bergeat, A.; Loison, J.-C. Reaction of Carbon Atoms, C($2p^2$, 3P) with C₂H₂, C₂H₄
4 and C₆H₆: Overall Rate Constant and Relative Atomic Hydrogen Production. *PCCP*
5 **2001**, *3*, 2038–2042.
6
7 (226) Glowacki, D. R.; Liang, C. H.; Morley, C.; Pilling, M. J.; Robertson, S. H. MESMER:
8 An Open-source Master Equation Solver for Multi-Energy Well Reactions. *J. Phys.*
9 *Chem. A* **2012**, *116*, 9545–9560.
10
11 (227) Osborn, D. L.; Zou, P.; Johnsen, H.; Hayden, C. C.; Taatjes, C. A.; Knyazev, V. D.;
12 North, S. W.; Peterka, D. S.; Ahmed, M.; Leone, S. R. The Multiplexed Chemical
13 Kinetic Photoionization Mass Spectrometer: A New Approach to Isomer-resolved
14 Chemical Kinetics. *Rev. Sci. Instrum.* **2008**, *79*, 104103.
15
16 (228) Slagle, I. R.; Yamada, F.; Gutman, D. Kinetics of Free Radicals Produced by Infrared
17 Multiphoton-induced Decompositions. 1. Reactions of Allyl Radicals with Nitrogen
18 Dioxide and Bromine. *J. Am. Chem. Soc.* **1981**, *103*, 149–153.
19
20 (229) Slagle, I. R.; Gutman, D. Kinetics of Polyatomic Free Radicals Produced by Laser
21 Photolysis. 5. Study of the Equilibrium Methyl + Oxygen \rightleftharpoons CH₃O₂ between 421 and
22 538 degree Celsius. *J. Am. Chem. Soc.* **1985**, *107*, 5342–5347.
23
24 (230) Soorkia, S.; Taatjes, C. A.; Osborn, D. L.; Selby, T. M.; Trevitt, A. J.; Wilson, K. R.;
25 Leone, S. R. Direct Detection of Pyridine Formation by the Reaction of CH (CD) with
26 Pyrrole: A Ring Expansion Reaction. *PCCP* **2010**, *12*, 8750–8758.
27
28 (231) Goulay, F.; Soorkia, S.; Meloni, G.; Osborn, D. L.; Taatjes, C. A.; Leone, S. R.
29 Detection of Pentatetraene by Reaction of the Ethynyl Radical (C₂H) with Allene
30 (CH₂=C=CH₂) at Room Temperature. *PCCP* **2011**, *13*, 20820–20827.
31
32 (232) Welz, O.; Savee, J. D.; Osborn, D. L.; Vasu, S. S.; Percival, C. J.; Shallcross, D. E.;
33 Taatjes, C. A. Direct Kinetic Measurements of Criegee Intermediate (CH₂OO) Formed
34 by Reaction of CH₂I with O₂. *Science* **2012**, *335*, 204–207.
35
36 (233) Savee, J. D.; Papajak, E.; Rotavera, B.; Huang, H.; Eskola, A. J.; Welz, O.; Sheps, L.;
37 Taatjes, C.; Zádor, J.; Osborn, D. L. Direct Observation and Kinetics of a Hydroper-
38 oxyalkyl Radical (QOOH). *Science* **2015**, *347*, 643–645.
39
40 (234) McGuire, B. A.; Burkhardt, A. M.; Kalenskii, S.; Shingledecker, C. N.; Remijan, A. J.;
41 Herbst, E.; McCarthy, M. C. Detection of the Aromatic Molecule Benzonitrile (c-
42 C₆H₅CN) in the Interstellar Medium. *Science* **2018**, *359*, 202–205.
43
44 (235) Lockyear, J. F.; Fournier, M.; Sims, I. R.; Guillemin, J.-c.; Taatjes, C. A.; Os-
45 born, D. L.; Leone, S. R. Formation of Fulvene in the Reaction of C₂H with 1,3-
46 butadiene. *Int. J. Mass Spectrom.* **2015**, *378*, 232–245.
47
48 (236) Jones, B. M.; Zhang, F.; Kaiser, R. I.; Jamal, A.; Mebel, A. M.; Cordiner, M. A.;
49 Charnley, S. B. Formation of Benzene in the Interstellar Medium. *PNAS* **2011**, *108*,
50 452–457.
51
52
53
54
55
56
57
58
59
60

- 1
2
3
4
5
6
7
8
9
10
11
12
13
14
15
16
17
18
19
20
21
22
23
24
25
26
27
28
29
30
31
32
33
34
35
36
37
38
39
40
41
42
43
44
45
46
47
48
49
50
51
52
53
54
55
56
57
58
59
60
- (237) Taatjes, C. A. How Does the Molecular Velocity Distribution Affect Kinetics Measurements by Time-resolved Mass Spectrometry? *Int. J. Chem. Kinet.* **2007**, *39*, 565–570.
- (238) Lee, Y. T.; McDonald, J. D.; Lebreton, P. R.; Herschbach, D. R. Molecular Beam Reactive Scattering Apparatus with Electron Bombardment Detector. *Rev. Sci. Instrum.* **1969**, *40*, 1402–1408.
- (239) Lai, L.-H.; Wang, J.-H.; Che, D.-C.; Liu, K. Direct Mapping of Vibrational-specific Angular Distributions of the Polyatomic Reaction Product: $\text{CN} + \text{D}_2 \rightarrow \text{DCN} + \text{D}$. *J. Chem. Phys.* **1996**, *105*, 3332–3335.
- (240) Lin, J. J.; Zhou, J.; Shiu, W.; Liu, K. Application of Time-sliced Ion Velocity Imaging to Crossed Molecular Beam Experiments. *Review of Scientific Instruments* **2003**, *74*, 2495–2500.
- (241) Schnieder, L.; Meier, W.; Welge, K. H.; Ashfold, M. N. R.; Western, C. M. Photodissociation Dynamics of H_2S at 121.6 nm and a Determination of the Potential Energy Function of $\text{SH}(\text{A}^2\Sigma^+)$. *J. Chem. Phys.* **1990**, *92*, 7027–7037.
- (242) Pan, H.; Liu, K.; Caracciolo, A.; Casavecchia, P. Crossed Beam Polyatomic Reaction Dynamics: Recent Advances and New Insights. *Chem. Soc. Rev.* **2017**, *46*, 7517–7547.
- (243) Naulin, C.; Costes, M. Crossed-beam Study of the $\text{Al}(\text{}^2\text{P}_{1/2,3/2}) + \text{O}_2(\text{X}^3\Sigma^-g) \rightarrow \text{AlO}(\text{X}^2\Sigma^+) + \text{O}(\text{}^3\text{P}_J)$ Reaction at Low and Very Low Kinetic Energies. *Chem. Phys. Lett.* **1999**, *310*, 231–239.
- (244) Naulin, C.; Daugey, N.; Hickson, K. M.; Costes, M. Dynamics of the Reactions of $\text{C}(\text{}^3\text{P}_J)$ Atoms with Ethylene, Allene, and Methylacetylene at Low Energy Revealed by Doppler–Fizeau Spectroscopy. *J. Phys. Chem. A* **2009**, *113*, 14447–14457.
- (245) Brown, G. G.; Dian, B. C.; Douglass, K. O.; Geyer, S. M.; Shipman, S. T.; Pate, B. H. A Broadband Fourier Transform Microwave Spectrometer Based on Chirped Pulse Excitation. *Rev. Sci. Instrum.* **2008**, *79*, 053103.
- (246) Abeysekera, C.; Zack, L. N.; Park, G. B.; Joalland, B.; Oldham, J. M.; Prozument, K.; Ariyasingha, N. M.; Sims, I. R.; Field, R. W.; Suits, A. G. A Chirped-pulse Fourier-transform Microwave/pulsed Uniform Flow Spectrometer. II. Performance and Applications for Reaction Dynamics. *J. Chem. Phys.* **2014**, *141*, 214203.
- (247) Pilgrim, J. S.; McIlroy, A.; Taatjes, C. A. Kinetics of Cl Atom Reactions with Methane, Ethane, and Propane from 292 to 800 K. *J. Phys. Chem. A* **1997**, *101*, 1873–1880.
- (248) Taatjes, C. A.; Hershberger, J. F. Recent Progress in Infrared Absorption Techniques for Elementary Gas-phase Reaction Kinetics. *Annu. Rev. Phys. Chem.* **2001**, *52*, 41–70.
- (249) Yu, T.; Lin, M. C. Kinetics of the $\text{C}_6\text{H}_5 + \text{O}_2$ Reaction at Low Temperatures. *J. Am. Chem. Soc.* **1994**, *116*, 9571–9576.

- 1
2
3
4 (250) Friedrichs, G. Sensitive Absorption Methods for Quantitative Gas Phase Kinetic Measurements. Part 2: Cavity Ringdown Spectroscopy. *Z. Phys. Chem.* **2008**, *222*, 31–61.
5
6
7 (251) Sprague, M. K.; Mertens, L. A.; Widgren, H. N.; Okumura, M.; Sander, S. P.; McCoy, A. B. Cavity Ringdown Spectroscopy of the Hydroxy-methyl-peroxy Radical. *J. Phys. Chem. A* **2013**, *117*, 10006–10017.
8
9
10
11 (252) North, S. W.; Fei, R.; Sears, T. J.; Hall, G. E. CN Radical Reaction Rate Measurements by Time-resolved FM Spectroscopy. *Int. J. Chem. Kinet.* **1997**, *29*, 127–129.
12
13
14 (253) Friedrichs, G. Sensitive Absorption Methods for Quantitative Gas Phase Kinetic Measurements. Part 1: Frequency Modulation Spectroscopy. *Z. Phys. Chem.* **2008**, *222*, 1–30.
15
16
17
18 (254) Fleisher, A. J.; Bjork, B. J.; Bui, T. Q.; Cossel, K. C.; Okumura, M.; Ye, J. Mid-infrared Time-resolved Frequency Comb Spectroscopy of Transient Free Radicals. *J. Phys. Chem. Lett.* **2014**, *5*, 2241–2246.
19
20
21
22
23 (255) Schliesser, A.; Brehm, M.; Keilmann, F.; van der Weide, D. W. Frequency-comb Infrared Spectrometer for Rapid, Remote Chemical Sensing. *Opt. Express* **2005**, *13*, 9029–9038.
24
25
26
27 (256) Adler, F.; Masłowski, P.; Foltynowicz, A.; Cossel, K. C.; Briles, T. C.; Hartl, I.; Ye, J. Mid-infrared Fourier Transform Spectroscopy with a Broadband Frequency Comb. *Opt. Express* **2010**, *18*, 21861–21872.
28
29
30
31
32 (257) Bjork, B. J.; Bui, T. Q.; Heckl, O. H.; Changala, P. B.; Spaun, B.; Heu, P.; Follman, D.; Deutsch, C.; Cole, G. D.; Aspelmeyer, M.; Okumura, M.; Ye, J. Direct Frequency Comb Measurement of $\text{OD} + \text{CO} \rightarrow \text{DOC O}$ Kinetics. *Science* **2016**, *354*, 444–448.
33
34
35
36 (258) Bui, T. Q.; Bjork, B. J.; Changala, P. B.; Heckl, O. H.; Spaun, B.; Ye, J. $\text{OD} + \text{CO} \rightarrow \text{D} + \text{CO}_2$ Branching Kinetics Probed with Time-resolved Frequency Comb Spectroscopy. *Chem. Phys. Lett.* **2017**, *683*, 91–95.
37
38
39
40
41 (259) Spaun, B.; Changala, P. B.; Patterson, D.; Bjork, B. J.; Heckl, O. H.; Doyle, J. M.; Ye, J. Continuous Probing of Cold Complex Molecules with Infrared Frequency Comb Spectroscopy. *Nature* **2016**, *533*, 517–520.
42
43
44
45 (260) Changala, P. B.; Weichman, M. L.; Lee, K. F.; Fermann, M. E.; Ye, J. Rovibrational Quantum State Resolution of the C_{60} Fullerene. *Science* **2019**, *363*, 49–54.
46
47
48
49
50
51
52
53
54
55
56
57
58
59
60

For TOC Only



Accepted manuscript